NASA/TM-20205011704

NASA Electronic Parts and Packaging (NEPP) Program

Breakdown and Self-healing in MnO2 and Polymer Tantalum Capacitors

Alexander Teverovsky

February 2021

NASA STI Program ... in Profile

Since its founding, NASA has been dedicated to the advancement of aeronautics and space science. The NASA scientific and technical information (STI) program plays a key part in helping NASA maintain this important role.

The NASA STI program operates under the auspices of the Agency Chief Information Officer. It collects, organizes, provides for archiving, and disseminates NASA's STI. The NASA STI program provides access to the NTRS Registered and its public interface, the NASA Technical Reports Server, thus providing one of the largest collections of aeronautical and space science STI in the world. Results are published in both non-NASA channels and by NASA in the NASA STI Report Series, which includes the following report types:

- TECHNICAL PUBLICATION. Reports of completed research or a major significant phase of research that present the results of NASA Programs and include extensive data or theoretical analysis. Includes compilations of significant scientific and technical data and information deemed to be of continuing reference value. NASA counterpart of peer-reviewed formal professional papers but has less stringent limitations on manuscript length and extent of graphic presentations.

- TECHNICAL MEMORANDUM. Scientific and technical findings that are preliminary or of specialized interest, e.g., quick release reports, working papers, and bibliographies that contain minimal annotation. Does not contain extensive analysis.

- CONTRACTOR REPORT. Scientific and technical findings by NASA-sponsored contractors and grantees.

- CONFERENCE PUBLICATION. Collected papers from scientific and technical conferences, symposia, seminars, or other meetings sponsored or co-sponsored by NASA.

- SPECIAL PUBLICATION. Scientific, technical, or historical information from NASA programs, projects, and missions, often concerned with subjects having substantial public interest.

- TECHNICAL TRANSLATION. English-language translations of foreign scientific and technical material pertinent to NASA's mission.

Specialized services also include organizing and publishing research results, distributing specialized research announcements and feeds, providing information desk and personal search support, and enabling data exchange services.

For more information about the NASA STI program, see the following:

- Access the NASA STI program home page at http://www.sti.nasa.gov

- E-mail your question to help@sti.nasa.gov

- Phone the NASA STI Information Desk at 757-864-9658

- Write to:
  NASA STI Information Desk
  Mail Stop 148
  NASA Langley Research Center
  Hampton, VA 23681-2199

NASA/TM-20205011704

NASA Electronic Parts and Packaging (NEPP) Program

Breakdown and Self-healing in MnO2 and Polymer Tantalum Capacitors

Alexander Teverovsky
Jacobs Technology Inc., Greenbelt, MD

National Aeronautics and
Space Administration

Goddard Space Flight Center
Greenbelt, Maryland 20771

February 2021

Level of Review: This material has been technically reviewed by technical management.

Available from

NASA STI Program
Mail Stop 148
NASA's Langley Research
Center Hampton, VA
23681-2199

National Technical Information
Service 5285 Port Royal Road
Springfield, VA 22161
703-605-6000

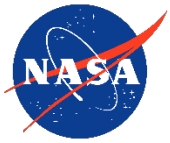

NASA Electronic Parts and Packaging (NEPP) Program

NEPP Task: Evaluation of Polymer Tantalum Capacitors for Space Applications

Breakdown and Self-healing in MnO2 and Polymer Tantalum Capacitors

Alexander Teverovsky
Jacobs Technology Inc.
Alexander.A.Teverovsky@nasa.gov

Worked performed at NASA Goddard Space Flight Center

10/27/2020

Breakdown and Self-healing in MnO2 and Polymer Tantalum Capacitors

Contents

I. Introduction

Dielectric layers in tantalum capacitors are formed by anodic electrolytic oxidation of porous tantalum pellets. The thickness of the dielectric is proportional to the formation voltage, $d = \alpha \times V_f$, where the coefficient α is typically ~2 nm/V, and V_f is from 2.5 to 4 times greater than the voltage rating (VR). Estimations based on these data show that for capacitors rated from 6 to 50 V the thickness of the dielectric is from 30 to 450 nm and at rated voltages tantalum capacitors are operating at high electric fields, in the range from 100 to 200 V/μm. These fields are only 2-3 times below the breakdown fields in Ta2O5 dielectrics that are in the range from 320 to 420 V/μm [1]. Thermochemical processes in the dielectric operating under high electric fields can cause failures at voltages substantially lower than the breakdown voltage (VBR). These processes can be modeled as time-dependent dielectric breakdown (TDDB) in tantalum capacitors [2], and indicate that VBR is an important characteristic directly related to the quality and reliability of the parts.

Thin tantalum pentoxide dielectric layers in capacitors are grown on the pellets made of sintered tantalum powder, have a rather large, in the range from 100 to 500 cm^2, and irregular surface area. Considering condition on the surface of the pellet and stresses during manufacturing and assembly, it is reasonable to assume that Ta2O5 dielectrics have a certain concentration of structural defects reducing VBR, and hence reliability of the parts. These defects are responsible for the infant mortality failures, and to reduce the probability of failures, special screening tests to remove defective samples with low values of VBR have been suggested. KEMET is using a simulated breakdown testing,

SBDS, during manufacturing of their high-quality commercial capacitors [3]. A margin verification test had been suggested for the users to cut-off low-voltage tails of VBR distributions as an additional screen for space-quality capacitors [4].

In spite of the presence of defects, tantalum capacitors can assure long-term operations in variety of reliability demanding applications, including space instruments. To a large degree, this is due to the self-healing processes that allow for a fast termination of breakdown and prevention of significant damage to the dielectric. In this case, a momentary scintillation current spike occurs instead of a catastrophic short circuit failure of the capacitor.

A mechanism of self-healing in MnO2 capacitors is associated with oxygen reduction in the cathode layer caused by local overheating and isolation of the breakdown site with high-resistive Mn2O3/Mn3O4 compositions. The process of the manganese oxide conversion occurs with time and when sufficient power supply current is instantly available, the joule heating might trig exothermic reactions of tantalum oxidation by oxygen generated in MnO2. This situation might happen when the damage to the dielectric is large enough, for example due to pop-corning associated with soldering of parts containing moisture [5]. In low impedance circuits, this damage can result in significant inrush currents and so-called first turn-on failures that in the worst case can cause ignition of the part and damage the whole assembly.

To prevent post-soldering catastrophic failures, proofing, or controlled, slow powering up of capacitors had been suggested by J. Prymak and co-workers [6]. This process supposed to activate the self-healing mechanisms in tantalum capacitors and thus prevent short circuit failures. In a later work by CALCE, it has been shown that scintillation conditioning does not degrade reliability of capacitors, but can increase surge current breakdown voltages up to 25% [7]. However, this conclusion was made based on testing of two lots only. Our data showed that in general, proofing might not guarantee reliability of the parts, be damaging, and has rather limited applications [8].

Although the mechanism of self-healing in MnO2 capacitors is commonly accepted, its details have not been sufficiently analyzed yet and the effect of scintillations on performance and reliability of the parts has not been fully understood. In particular, there is practically no data regarding durations and amplitudes of the scintillation spikes and the degree to which they can change characteristics of the capacitors. More analysis is necessary to reveal possible lot-to lot variations of the self-healing efficiency of capacitors. Also, there is only limited information regarding location and appearance of the damaged sites.

Even less is known about self-healing in chip polymer tantalum capacitors, CPTCs. Prymak and co-workers assumed that for these devices, the self-healing activity involves changes in the conductivity to the fault site, or a break in the contact by evaporating the polymer. It was suggested that this activity requires much less energy than for MnO2 capacitors [9]. T.Zednicek [10] also explained self-healing in CPTCs by formation of voids caused by evaporation or peeling-off the conductive polymer at the breakdown site. Y.Freeman [11] attributed self-healing in polymer capacitors to separation between the PEDOT and PSS molecules in the vicinity of defect sites in the dielectric caused by high current density and rising temperature. It was assumed that this separation increases resistance of the polymer and decreases leakage currents in the parts. Moisture, working as a plasticizer enhances self-healing and thus is beneficial for performance of capacitors.

In spite of the importance of self-healing for assuring reliable operation of tantalum capacitors, the associated processes and mechanisms have not been studied sufficiently and need more analysis. In this work, different types of polymer and MnO2 capacitors have been tested for scintillation breakdown using a constant current stress (CCS) technique modified to allow detection of current spikes during breakdown. Characteristics of the parts and in particular leakage currents were measured to assess the efficiency of self-healing and suggest better screening procedures. Damaged sites were localized using infrared camera and their appearance analyzed after deprocessing and cross-sectioning. Thermal processes during scintillations have been modeled to better understand mechanisms of self-healing and post-scintillation behavior of tantalum capacitors.

II. Experiment

Measurements of breakdown voltages in capacitors in this study were carried out using a constant current stress, CCS, technique [2] that has been modified to detect voltage variations during scintillation events and the shape of the power supply (PS) current spikes. Figure II.1.a shows a schematic of the test set-up. A source measurement unit (SMU), typically Keithley 2400, in a constant current mode was used to charge a capacitor under test that had a 10 ohm current sense resistor connected in series. An oscilloscope that was trigged by the breakdown event was used to monitor

voltage across the capacitor and PS currents by voltage measurements across the sense resistor. Test parameters, including the level of charging current and duration of the test were controlled by a PC that was also used to record variations of voltage with time of charging and oscilloscope data. The level of charging currents was selected to charge capacitors to the rated voltage within a few seconds.

When a charging current, I_{ch}, is applied to a capacitor, having a leakage current $I_L(t,V)$, that depends on voltage and time under bias, the voltage across the part increases with time:

$$V(t) = \frac{1}{C_{DC}} \int_0^t [I_{ch} - I_L(t,V)]\, dt\,, \qquad \text{(II.1)}$$

where C_{DC} is the capacitance measured at quasi-static conditions. This capacitance is a sum of an AC capacitance measured at 120 Hz, C_{AC}, and absorption capacitance, C_{ab}, that is typically 5 to 20% of C_{AC} [12]:

$$C_{DC} = C_{AC} + C_{ab}. \qquad \text{(II.2)}$$

When $I_{ch} >> I_L$, the voltage increases with time linearly, $V(t) = I_{ch} \times t/C_{DC}$ and the slope of the *V-t* curve can be used to calculate the value of C_{DC}. The breakdown voltage is determined as maximum on the *V-t* curves.

At high enough voltages, the charging current might be comparable with the leakage current and the *V-t* curve becomes sublinear as shown in Fig II.1.b. At this condition, the leakage current can be calculated as:

$$I_L(t,V) = I_{ch} - C_{DC} \frac{dV(t)}{dt} \qquad \text{(II.3)}$$

Obviously, when I_{ch} is not sufficient, breakdown cannot be reached, the voltage is stabilizing at a certain level $V <$ *VBR* as shown in Fig.II.1.c, and larger charging currents should be applied to cause breakdown.

Due to self-healing, the voltage across the part that drops during a scintillation starts increasing again and the process can be repeated (Fig. II.1.b). If self-healing does not occur or is not sufficient for voltage to increase again, the part remains shorted after breakdown as shown in Fig. II.1.d. In this case, voltage is stabilizing at a relatively low level $V_{st} = I_{ch} \times R_{sc}$, where R_{sc} is the short circuit resistance. These types of scintillation events are defined as damaging scintillations.

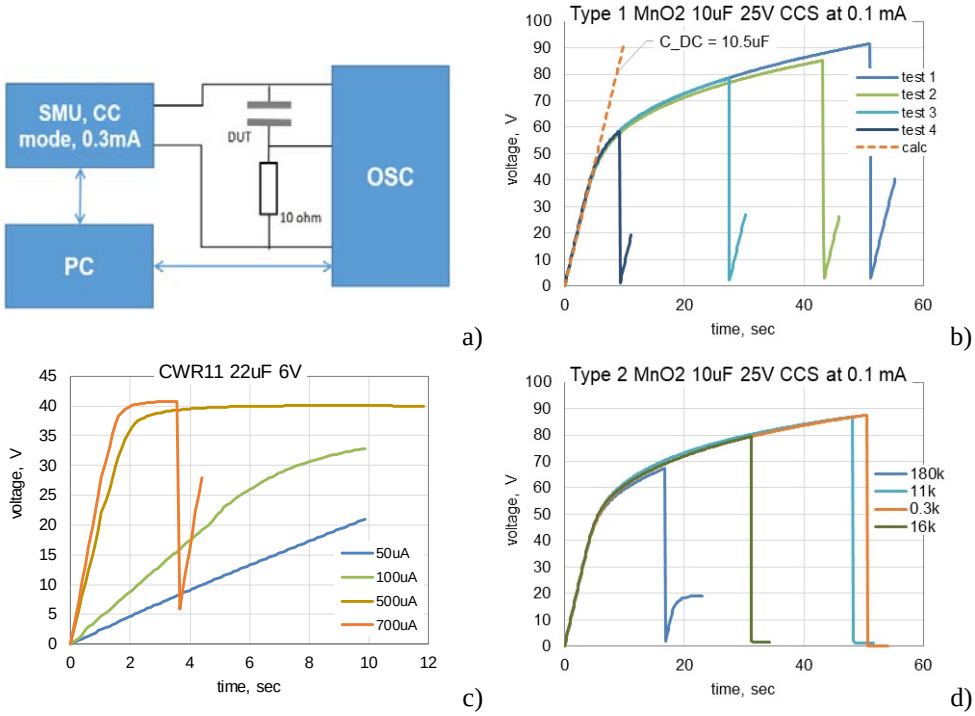

Figure II.1. Schematic of the test set-up (a) and typical CCS data recorded during self-healing (a) and damaging (d) scintillation events in 10 uF 25 V MnO2 capacitors. Fig. (c) shows an example of CCS testing that required increasing charging currents to reach breakdown. Dashed line in Fig.1.b was calculated at C_{DC} = 10.5 uF.

A total current flowing through a capacitor during a scintillation event is a sum of the PS current, I_{PS}, and internal current caused by discharging of the capacitors, I_{disch}: $I_{sc} = I_{PS} + I_{disch}$. The discharge current can be calculated as a derivative of the voltage variations during breakdown:

$$I_{disch}(t) = C_{AC} \times {}^{dV(t)}/_{dt}. \qquad \text{(II.4)}$$

Examples of voltage variations, discharge currents calculated per Eq.(II.4), and measured power supply currents during scintillation events for two types of MnO2 capacitors are shown in Fig.II.2. The discharge current spikes are sharp, have a width of ~ 10 μsec and can reach dozens of amperes. Spikes of the currents provided by the power supply have a trapezoid shape with the width from ~100 μsec to ~200 μsec and much lower amplitudes, ~ 0.22 A. The width of PS spikes increases practically linearly with the breakdown voltage (Fig. II.2.c), whereas the width of discharge spike have a tendency of decreasing with VBR.

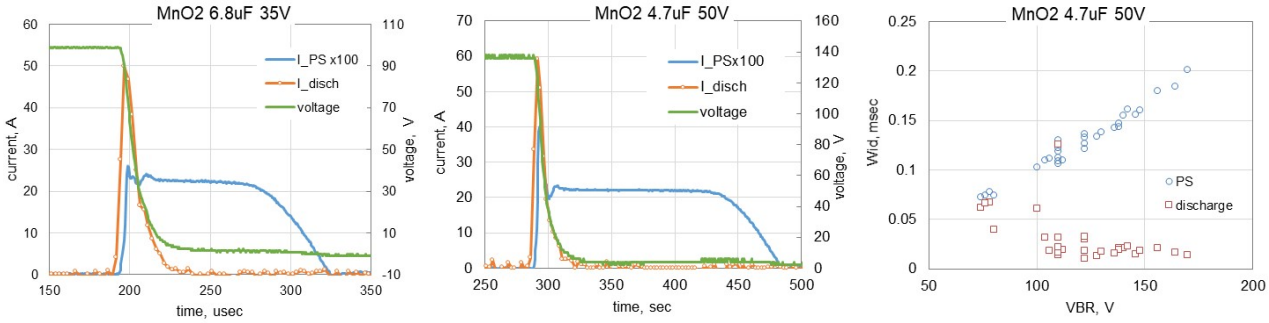

a) b) c)

Fig.II.2. Variations of voltages, discharge currents, and power supply currents during scintillation events in two types of MnO2 capacitors, 6.8 μF/35 V (a) and 4.7 μF/50 V (b). Figure (c) shows correlation between the widths of the PS and discharge current spikes and breakdown voltages for different samples of 4.7 μF 50 V capacitors.

To determine whether results of CCS testing reflect processes during scintillations or they depend on the power source, breakdown voltages and shapes of PS spikes have been measured for several groups of capacitors with 10 to 20 samples each group using different power supplies. In one group, CCS testing was carried out using SMU Agilent K2400 that has maximum current of 200 mA and another group was tested using a less compliance current SMU, Keithley K237, that is capable to provide maximum current of 10 mA.

Results of VBR measurements for five types of MnO2 capacitors are shown in Table II.1. Analysis of the data using Student's t-test show that at 95% confidence level the distributions of breakdown voltages in both cases are similar. However, amplitudes and widths of PS current spikes were substantially less for SMU K237 as evident also from Fig. II.3.

Table II.1. Average values and standard deviations (in brackets) of breakdown voltages measured using different power supplies.

Part	QTY	K2400	K237
CWR06 10uF 25V	20	101.3 (6.1)	102.5 (8.6)
CWR09 6.8uF 35V	10	108.6 (11.8)	103.6 (12.1)
Commercial 6.8uF 35V	10	84.1 (3.2)	84.4 (4.7)
CWR09 4.7uF 50V	13	120.7 (13)	135.4 (19)
CWR11 22uF 6V	13	33.3 (6.7)	27.6 (6.3)

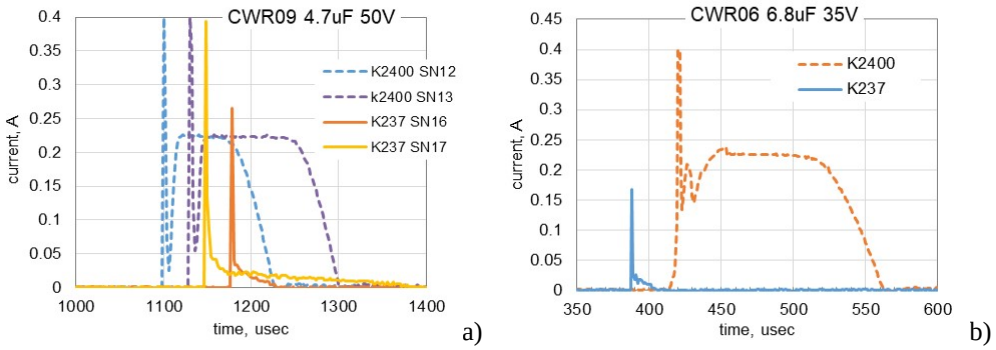

Fig.II.3. Typical power supply current spikes during scintillation events tested using different power supplies (K2400 and K237) in CWR09 4.7 μF 50 V (a) and CWR06 6.8 μF 35 V (b) types of capacitors.

An additional prove that the shape of PS spikes does not reflect processes during scintillations was obtained by the breakdown simulation experiments. A short circuit condition in the part was simulated by a power N- FET connected to MnO2 4.7 μF 50 V capacitors in parallel. At a certain moment before breakdown of the part, the switch was closed and maximum reached voltage simulating breakdown voltage and the shape of PS spike were detected by an oscilloscope. Results of these tests are shown in Fig. II.4. The amplitudes and shapes of PS spikes during these simulations were comparable to actual breakdown events, and similar to results shown in Fig.II.2.c, the width of the spikes increased linearly with the simulated breakdown voltage.

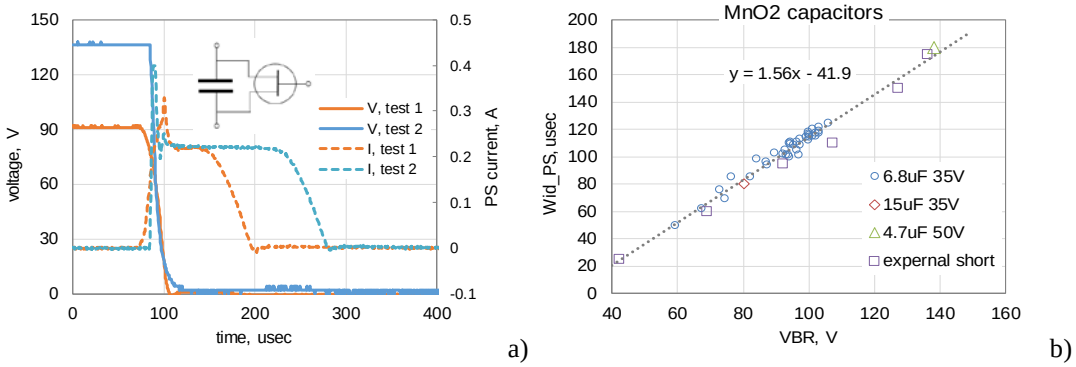

Fig. II.4. Examples of voltage and power supply current variations during breakdown simulation by external shorting of the parts (a) and correlation between the width of the power supply current spikes and breakdown voltage in 4.7 μF 50 V capacitors during simulations (b). The red marks in figure (b) correspond to results of actual scintillation tests.

Results show that the shape and amplitude of PS current spikes depend on the dynamic characteristics of the power supply used and do not reflect self-healing processes in the parts. The duration of the self-healing process is apparently greater than the width of the PS current spike.

Scintillation events were characterized by the shape of discharge, including breakdown voltage, minimal voltage before increasing caused by self-healing, V_{min}, and the width of the discharge, *Wid*, determined as shown in Fig. II.5. The value of *Wid* allows for estimations of the average discharge current as follows:

$$I_{disch} = C_{AC} \times 0.8 \times (\mathrm{VBR} - V_{min})/Wid \qquad \text{(II.5)}$$

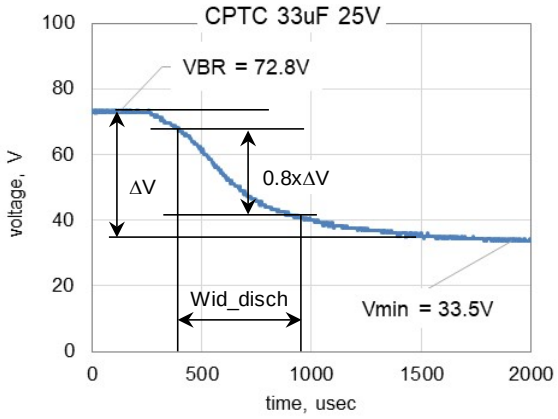

Fig. II.5. An example of a discharge process for a scintillation event in a polymer 33 μF 25 V capacitor illustrating parameters calculated based on V-t curves.

III. Breakdown voltages and scintillation times in MnO2 and polymer capacitors

III.1. Distributions of VBR and Wid.

Various groups of MnO2 and polymer capacitors rated at voltages from 6.3 V to 35 V were used to evaluate the effect of the type of cathode materials on scintillation breakdowns. Each group had typically from 10 to 20 samples. Weibull distributions of VBR were characterized by two parameters: the characteristic breakdown voltage, η, and slope, or shape factor, β. The durations of scintillation events, or scintillation times, *Wid*, were approximated by log-normal distributions and characterized by the median values. The spread of *Wid* was evaluated using 25th and 75th percentiles of the distributions.

Examples of VBR distributions for two types of polymer and MnO2 capacitors rated to 6.3 V and 35 V are shown in Fig. III.1.a. Distributions for 35 V capacitors were practically identical, whereas 6.3 V polymer capacitors had somewhat lower values of VBR compared to MnO2 parts. Polymer and MnO2 35 V capacitors in this chart had the same cases and were produced by the same manufacturer, which might explain the similarity of the distributions.

PAQ style polymer capacitors with different ratings had the same slopes of VBR distributions (Fig. III.1.c) indicating similar concentration of defects and similar mechanisms of breakdown. The median value of the breakdown voltage normalized to VR increased from 2.6 for 35 V capacitors to 3 for 10 V and to 3.8 for 6.3 V ratings. This behavior is similar to MnO2 capacitors [2] and indicates a greater breakdown margin for low voltage capacitors for both types of technologies.

Distributions of scintillation times, *Wid*, for 4 lots of MnO2 and 5 lots of polymer capacitors rated to 35 V are shown in Fig. III.1.b. In spite of a relatively wide spread of the data, on average, the duration of scintillation events in MnO2 capacitors (~90 μsec) is almost an order of magnitude shorter than for polymer cathode parts (~700 μsec). For some lots, the distributions were bimodal indicating the presence of faster and longer scintillation events.

Fig. III.1.d illustrates the effect of voltage rating on the width of scintillation spikes for PAQ type capacitors. Same type polymer capacitors had similar *Wid* distributions for 10 μF and 33 μF capacitors indicating that the value of capacitance does not affect significantly the duration of scintillation events. Approximately 20% of 35 V capacitors had several times greater *Wid* values comparted to the rest of the group. At lower voltage ratings, the median of the *Wid* distributions increased from 0.36 msec at 35 V to 0.6 msec at 10 V and 0.75 msec at 6.3 V and contrary to 35 V capacitors the distributions had no outliers.

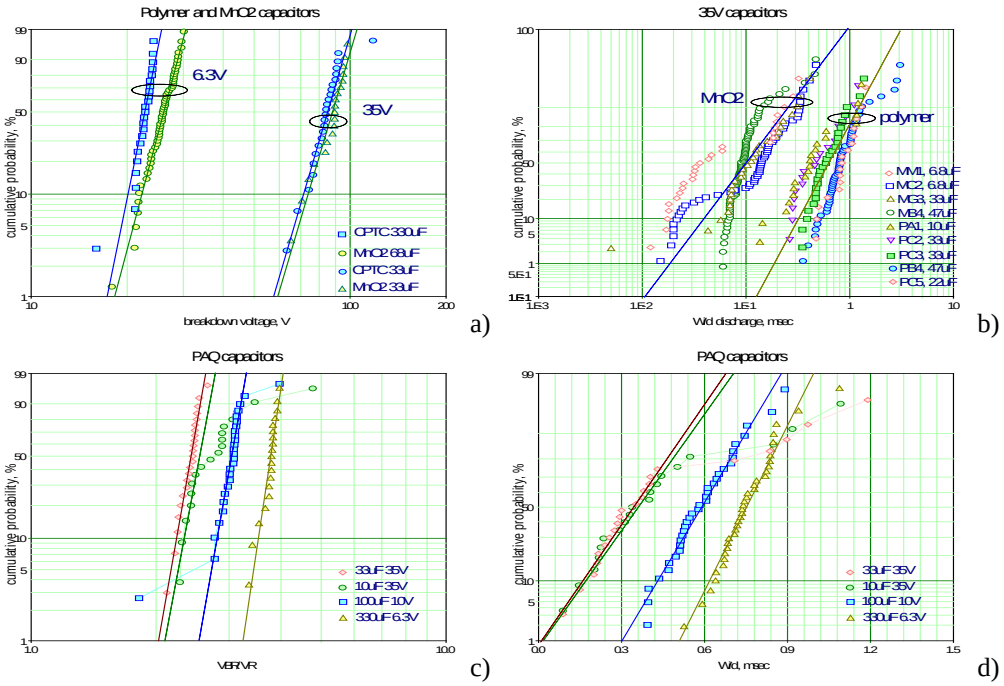

Fig.III.1. Weibull distributions of breakdown voltages for polymer (CPTC) and MnO2 capacitors rated to 6.3 V and 35 V (a) and lognormal distributions of the width of scintillation spikes for different lots of capacitors rated to 35 V (b). Figures (c and d) show distributions of breakdown voltages and durations of scintillation events for the same types of capacitors but with different ratings. Here and below different lots of capacitors are marked by three letters indicating type of the cathode material (M for MnO2 and P for polymer), manufacturer (A, B, or C), and the last letter or number reflects the type of capacitors.

Due to some variations of manufacturing processes, used materials, and the level of quality of the capacitors, one can expect differences in VBR distributions for lots rated to the same voltage. However, in spite of the spread of data, the voltage rating correlated well with breakdown voltages in the parts. Fig. III.2.a shows variation of the average values of VBR calculated for several lots of MnO2 and polymer capacitors with the voltage rating. Considering the spread of the data, there is no significant difference in breakdown voltages between CPTC and MnO2 capacitors with similar ratings. On average, VBR is 2.7 times greater than VR for both type of capacitors, which is in agreement with results described by Y.Freeman [11] showing that at formation voltages below 200 V, MnO2 and polymer capacitors have similar breakdown voltages. However, the ratio VBR/VR is greater than the average, ~3.5 for 6.3 V capacitors and lower, ~2.5 for 35 V capacitors, which is likely related to a greater concentration of defects in thicker Ta2O5 dielectrics [11].

The chart on Fig. III.2.a also shows variations of average values of V_{min} for both types of capacitors. Discharging during scintillation events in MnO2 capacitors results in voltage dropping practically to zero before it starts increasing again as a result of self-healing. For polymer capacitors, V_{min} increases linearly with VR, V_{min} ~ 0.5VR, reaching ~ 18 V for capacitors rated to 35 V. Considering that the discharge energy is proportional to V^2, this implies that the difference in the discharge energy is only slightly, by ~ 4%, greater for MnO2 compared to polymer capacitors.

On average, the slopes of Weibull distributions of breakdown voltages, β, are substantially larger for polymer than for MnO2 capacitors (see Fig. III.2.b). This indicates tighter distributions for CPTCs that is likely related to a lesser probability of having defects in the dielectric, therefore smaller low-voltage tails of the distributions. Apparently, polymer technology allows for softer and less stressful conditions of the cathode formation compared to MnO2 technology.

Average scintillation times, are varying from ~0.25 ±0.2 msec for 35 V to ~1.25 ±1 msec for 6.3 V MnO2 capacitors (see Figure 2c). For polymer capacitors rated to 16 V and above, these values are 2 to 7 times greater. Discharge times are similar for both types of capacitors rated to 6.3 and 10 V, but the spread of *Wid* values is large, ~ 1 msec for 6.3 V to ~ 0.5 msec for 10 V capacitors. (see Fig. III.2.c). There is a tendency of decreasing *Wid* with the rated voltage.

A trend of decreasing breakdown voltages with the value of capacitance was observed for the non-solid electrolyte tantalum [13] and ceramic [14] capacitors. The effect was attributed to a greater probability of having defects in the

dielectric for the larger surface area parts. However, no correlation between VBR and capacitance was found for solid electrolyte capacitors used in this study (see Fig. III.2.c). This might indicate a relatively even distribution of concentration of defects along the surface of the pellet.

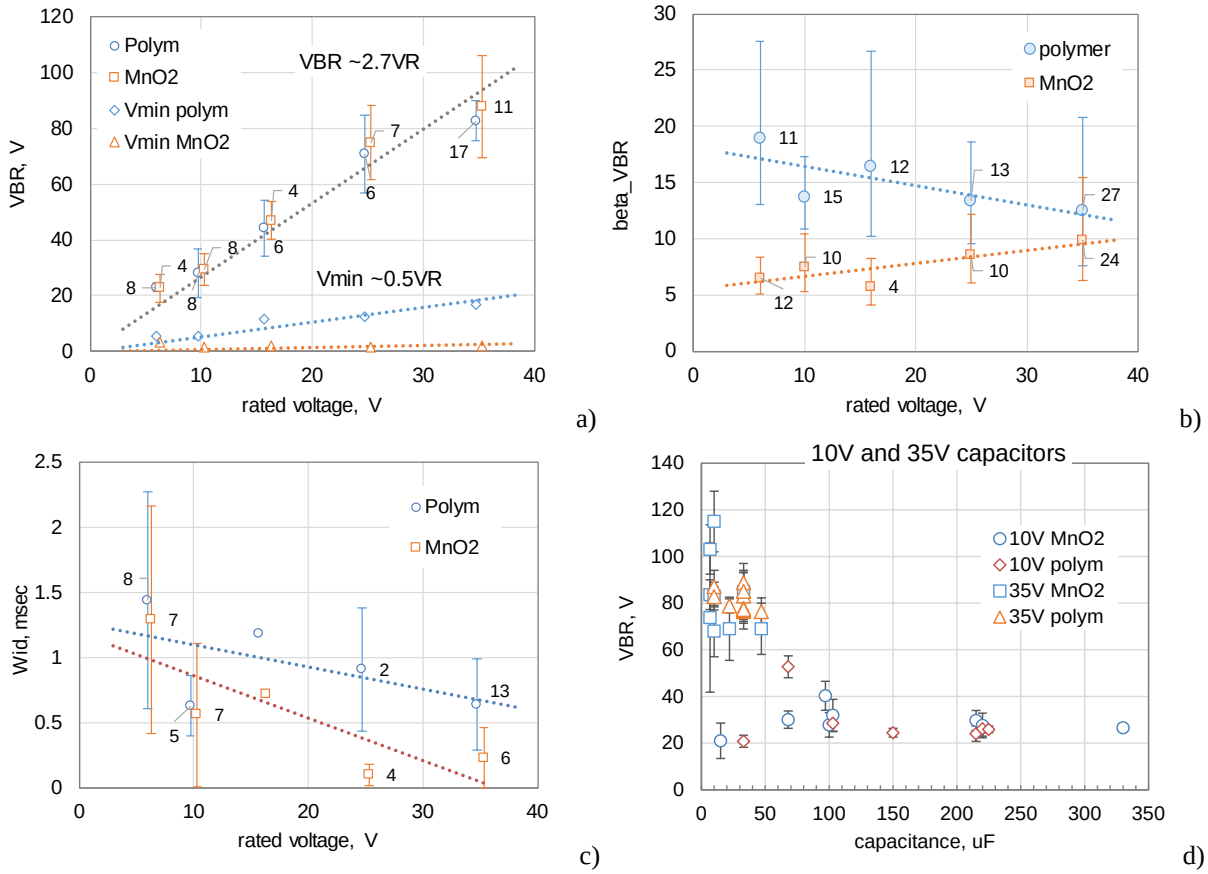

Fig. III.2. Variations of average breakdown voltages (a), median values of the slopes of breakdown distributions (b), and scintillation times (c) for MnO2 and polymer capacitors with the rated voltage. Figure (c) illustrates the lack of correlation between VBR and capacitance values for 10 V and 35 V capacitors. Digits at the marks correspond to the number of tested lots.

III.2. Effect of moisture.

It is known that performance of tantalum capacitors can change substantially [15-17] in humid environments, but there is no sufficient information on the effect of moisture on breakdown voltages, especially for CPTCs. To assess this effect, capacitors from several lots before CCS testing were split into three groups. The first group was tested in "as received" condition, the second after bake at 125 ºC for 120 hours (marked below as "dry" capacitors), and the third after storage in humidity chamber at 85 ºC, 85% RH for 1 week (marked below as "wet" capacitors).

An example of results of CCS testing for polymer and MnO2 47 µF 35 V capacitors is shown in Fig. III.3.a. Breakdown voltages in "as received" and baked polymer capacitors were similar (η = 78.8 and 75.8 V respectively). However, wet capacitors had η = 90.2 V, which is substantially, by ~ 20% greater than for dry parts. No statistically significant difference in VBR distributions was observed for MnO2 capacitors. At all conditions, the slopes of distributions were greater for polymer than for MnO2 capacitors. Distributions of VBR for the "as received" and dry CPTCs were close indicating a low moisture content in the "as received" capacitors.

Majority of the samples in both types of capacitors had similar distributions of scintillation times in wet and dry conditions (see Fig. III.3.b). However, for approximately 10% of the parts the proportion of samples with large *Wid* values was greater for dry capacitors (an increase from ~ 0.1 msec to 0.5 msec for MnO2 and from 1 msec up to ~3 msec for polymer capacitors). Overall, the difference in *Wid* values between MnO2 and polymer capacitors was consistent with results shown in Fig. III.2.c.

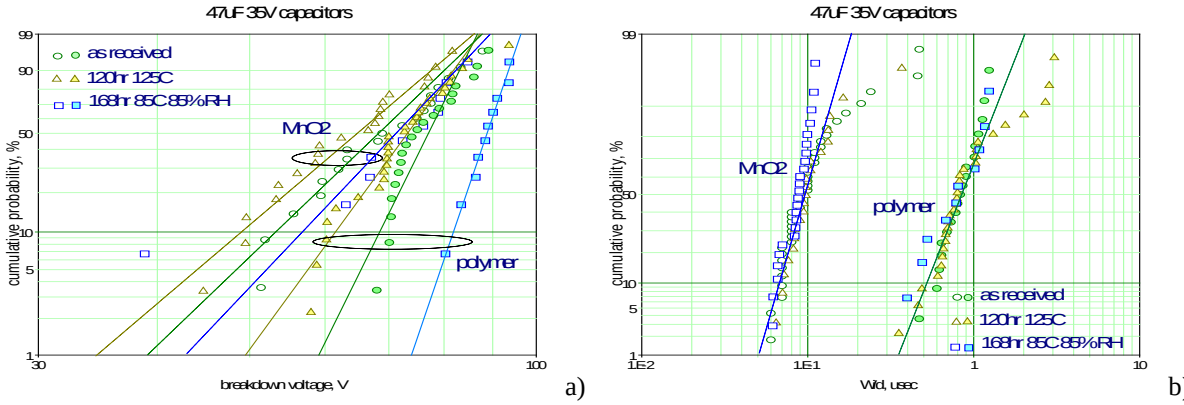

Fig. III.3. Distributions of breakdown voltages (a) and times of scintillations (b) for polymer and MnO2 47 μF 35 V capacitors. Open marks correspond to MnO2 and filled marks to polymer capacitors.

Results of CCS testing for 5 lots of MnO2 and 14 lots of polymer capacitors in wet and dry conditions are displayed in Fig. III.4. MnO2 capacitors had close breakdown voltages for wet and dry samples: the average ratio of breakdown voltages was 1.03 at a standard deviation of 0.07. This result is consistent with results of our previous study where storage in humidity chamber at 85 ºC/85% RH for 240 hours for 10 lots of MnO2 capacitors did not change distributions of VBR [18] substantially. However, moisture has a much stronger effect on breakdown voltages for polymer capacitors: an average increase of VBR for 14 lots was 21% at a standard deviation of 14% (see Fig. III.4.a). Although there is a tendency of decreasing *Wid* for some wet compared to dry capacitors (see Fig.III.4.b), the effect is not as strong as for breakdown voltages.

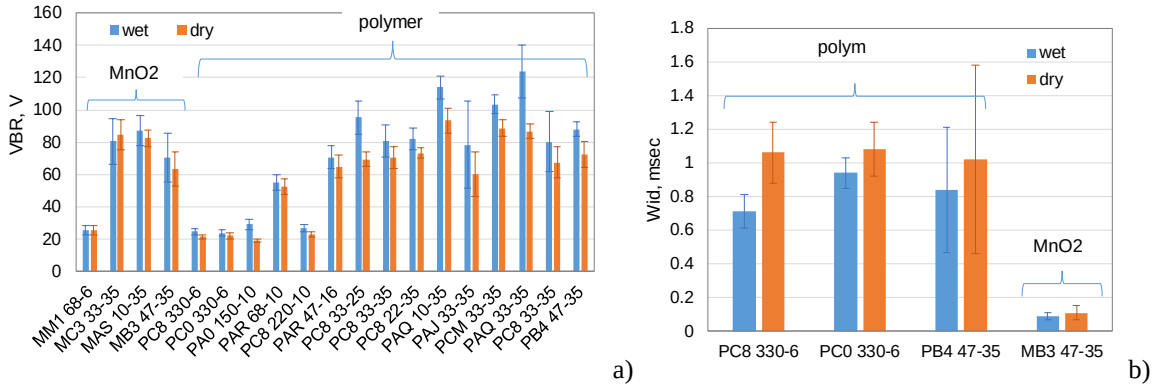

Fig. III.4. Average values of breakdown voltages (a) and scintillation times (b) for different types of wet and dry tantalum capacitors. Error bars correspond to the values of standard deviations.

IV. Damaging scintillations

IV.1. Effectiveness of self-healing.

Due to self-healing, capacitors during CCS testing can recover after the first scintillation so the voltage across the part continue increasing at the same rate as initially as shown for MnO2 capacitors in Fig. IV.1.a. However, in some cases, the voltage after scintillations does not increase, but remains constant indicating a short circuit in the part as shown for polymer tantalum capacitors in Fig IV.1.b. Similar scintillation events indicate that the part is not self-healed and damage site is not isolated. CCS testing of different lots of MnO2 and polymer capacitors showed that the proportion of samples that are damaged by the first scintillation might vary from lot to lot substantially. In this study, the proportion of damaging scintillations was used as a metric to assess the self-healing capability of the bunch.

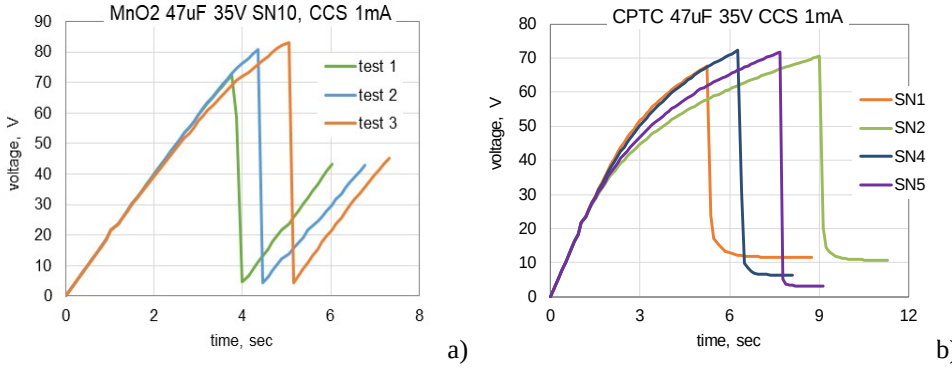

Fig. IV.1. Results of CCS testing at 1 mA for MnO2 (a) and polymer (b) 47 µF 35 V capacitors from the same manufacturer. A sample of MnO2 capacitors (SN10) experienced non-damaging scintillations during three consecutive tests and five samples of polymer capacitors were damaged by the scintillation that resulted in short circuit failures with resistances in the kiloohm range.

A proportion of the first damaging scintillation events, *d*, was calculated for 5 lots of MnO2 and 11 lots of polymer capacitors rated to 35 V. Results of these calculations are shown in Fig. IV.2.a. On average, the value of *d* is much less for MnO2 (d_{avr} = 11.5% at a standard deviation of 14.6%) than for polymer capacitors (d_{avr} = 88.3% at a standard deviation of 14.3%).

Average values of *d* for 41 lots of polymer and 34 lots of MnO2 capacitors with different VR are plotted in Fig. IV.2.b. For capacitors rated to ≥16 V, the proportion of damaged parts is much greater for polymer than for MnO2 parts, but for lower voltages, the spread of data increases, so the difference is not significant. This might be due to different cathode materials used for high- and low-voltage polymer capacitors. In the first case, pre-polymerized PEDOT:PSS compositions are used, whereas low-voltage capacitors are typically manufactured using in-situ polymerized PEDOT polymers. Based on results in Fig. IV.2.b, self-healing processes in high-voltage CPTCs are much less effective than in MnO2 capacitors.

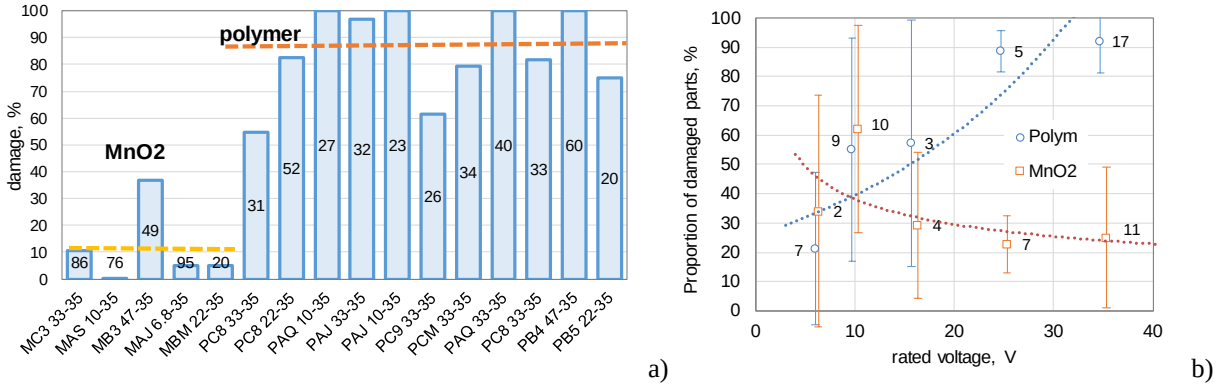

Fig. IV.2. Proportion of damaging scintillations in different lots of MnO2 and polymer capacitors rated to 35 V (a) and variations of average values of *d* with the rated voltage (b). Digits in (a) indicate the number of tested samples in a lot, and dashed lines correspond to average values of damaged polymer and MnO2 capacitors. Digits in (b) indicate the number of tested lots and the error bars correspond to the standard deviations.

IV.2. Damaging scintillations in MnO2 capacitors.

To assess the reproducibility of self-healing in similar types of capacitors, 5 types of 6.8 µF 35 V MnO2 capacitors were tested at the same conditions. Results of these tests are shown in Table IV.1. The value of *d* varied from 5% to almost 90% indicating that the probability of damage, hence the self-healing capability is lot-related.

A snapping sound that indicates formation of cracks in the parts can be often heard during CCS testing, and in some cases, scintillations resulted in formation of chip-outs as shown in Fig. IV.3. However, severe damage to the part that destructed a portion of the cathode layers and exposed tantalum pellets, did not result in a short circuit. These parts behaved similar to capacitors with non-damaging scintillations and could sustain several consecutive scintillation breakdowns. Apparently, self-healing in MnO2 capacitors can be effective enough to assure functioning of capacitors

even after severe mechanical damage. Also, as can be seen from Fig. VI.3.c, consecutive scintillations can cause damage at different sites of the same part.

Table IV.1. Proportion of 6.8 μF 35 V capacitors shorted after the first scintillation test.

Part	QTY	Damage, %
CWR06	14	7.1
Commercial 1	44	20.5
Commercial 2	95	5.0
CWR09 DC1	31	87.1
CWR09 DC2	20	65

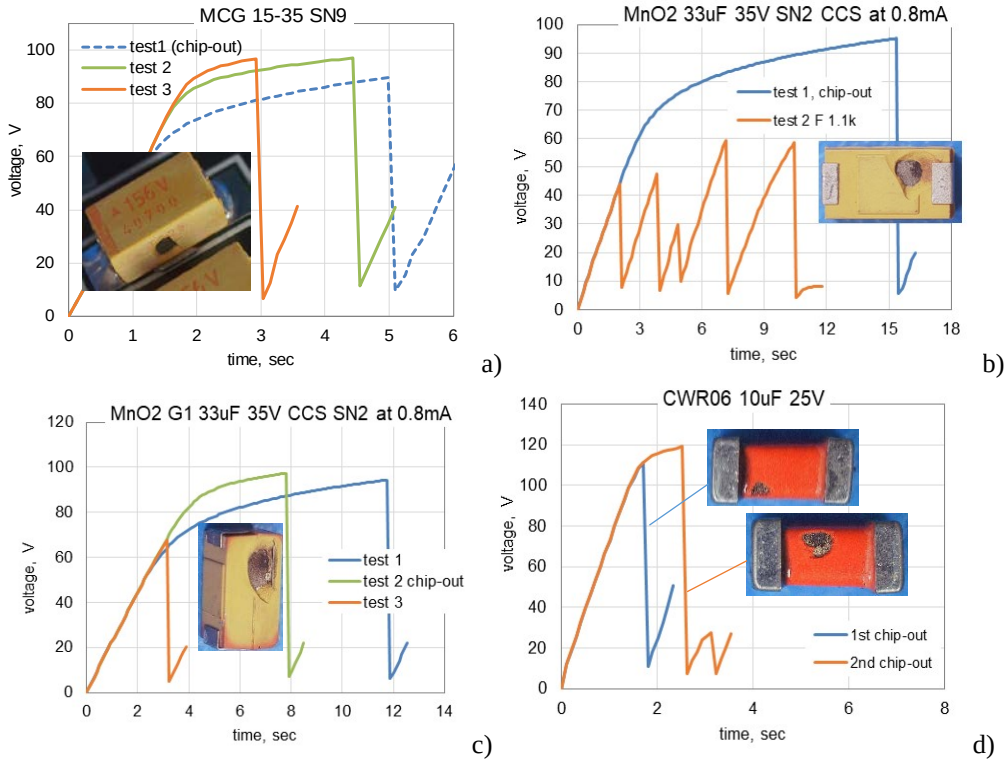

Fig. IV.3. Examples of scintillation events in different types of MnO2 capacitors that caused visual damage in the parts without short circuit. A 15 μF 35 V capacitor in (a) had a chip-out after the first scintillation event, but then sustained two more events at higher voltages. A 33 μF 35 V capacitor (b) also had a chip-out after the first scintillation, but then sustained 5 more breakdowns before failing at 1.1 kohm. Another type of 33 μF 35 V capacitor had a chip-out after the second CCS test, but passed the third one (c). A CWR06 10 μF 25 V capacitor (d) had two chip-outs at different locations during two consecutive CCS tests.

Some samples of CWR06 capacitors that are encapsulated with a relatively thin conformal coating had damage that could be seen even without chip-outs. Fig. IV.4 shows results of testing of a 10 μF 25 V capacitor using a power supply capable of providing high dynamic currents. During this test, the current spike happened at 19 V, had a width of several milliseconds and reached 9 A. After breakdown, the current stabilized at 3 A by the PS and the power was turned off after ~ 1 sec. Although this part did not ignite, the burning area under the coating spread along the surface of the slug approximately half of the distance between anode and cathode terminals. Apparently, when high enough currents are available after breakdown, the damaged area spreads along the surface of the slug. This and other experiments confirm that if not terminated, the damaging process can continue for a few seconds until the whole surface of a capacitor is burned-out.

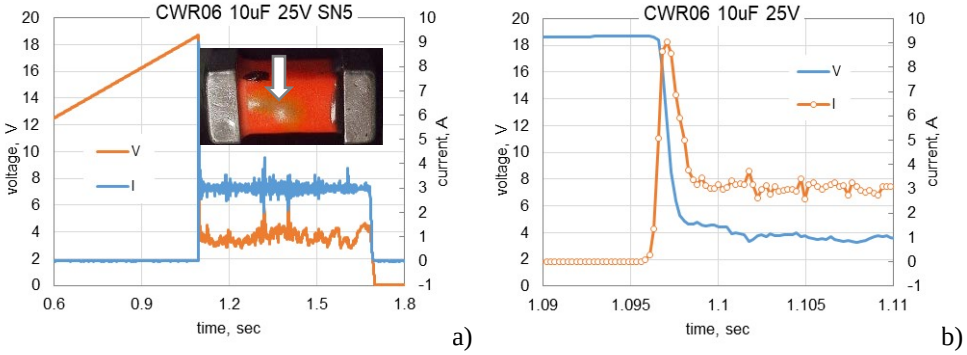

Fig. IV.4. Variations of voltage (a, b) and current (b) during a scintillation event in a 10 µF 25 V MnO2 capacitor that resulted in extensive burning area under the coating on the surface of the pellet.

Consecutive scintillation in MnO2 capacitors often result in increasing breakdown voltages (see Fig. IV.5. a, b). Capacitors in these lots can sustain multiple breakdown events without short circuit. However, in some lots VBR changes erratically (see Fig.IV.5. c, d). The first case is more probable for lots with low proportion of damaging scintillations, whereas lots with large values of *d* are more likely to have decreasing breakdown voltages. Apparently, in the first case, self-healing isolates damage reliably, and the next breakdown happens at a new site and at higher voltages, whereas in the latter case, repeat breakdowns occur likely at the same damage site.

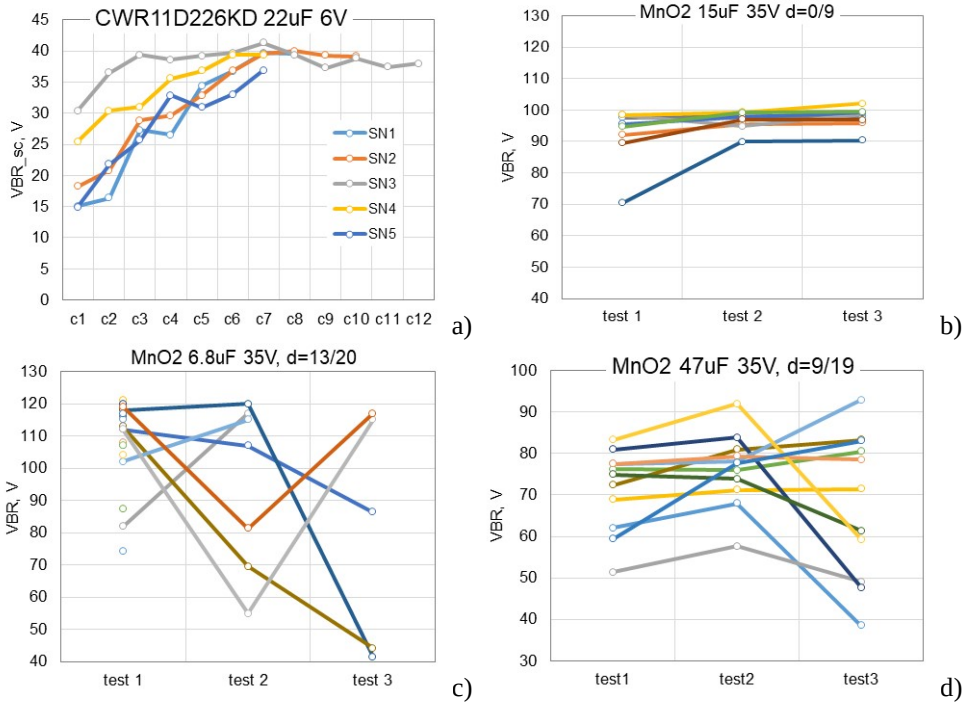

Fig. IV.5. Variations of VBR during consecutive CCS tests for MnO2 capacitors with low (a, b) and large (c, d) proportion of damaging scintillations. The values of *d* are 2/42, 0/9, 13/20, and 9/19 for figures (a to d) respectively.

In many cases, faster and more powerful discharges increased the probability of damage as it is shown for MnO2 100 µF 10 V capacitors in Fig. IV.6.a, b. For SN8, SN9, and SN10 discharge of capacitors during scintillations occurred smoothly but the values of *Wid* varied substantially, from 1.3 for SN8 to 0.1 msec for SN10. Sorting in the kiloohm range happened for SN9 and SN10 that had minimal *Wid* values.

During scintillation events in 47 µF and 6.8 µF capacitors rated to 35 V (see Fig.IV.7.c to f) the rate of discharge was changing with time substantially. Samples SN18 and SN19 of 47 µF capacitors had similar breakdown voltages and width of scintillation spikes ~ 80 µsec. However, discharging of SN18 occurred smoothly, the current spike was ~ 70 A and did not damage the part. Discharging of SN19 occurred much faster, mostly during first 10 µsec and resulted in a current spike of ~ 220 A that caused shorting with a 10 kohm resistance.

A similar increase in the rate of discharge occurred for SN5 of 6.8 μF capacitors at the end of the discharging process during the third CCS test. Two first tests had smooth discharges with current spikes ~ 5 A and were not damaging. During the third test, the current spike increased to ~18 A and resulted in a 0.8 kohm short.

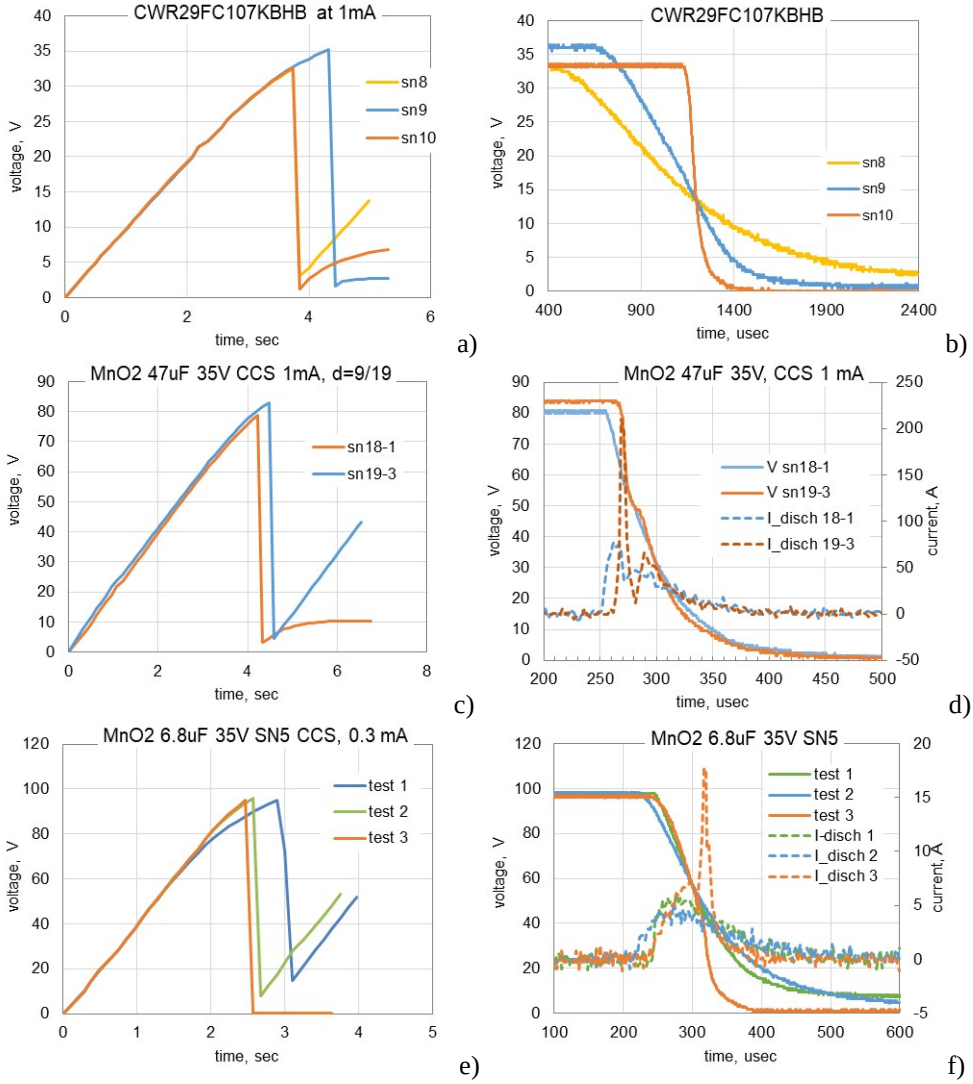

Fig. VI.6. Results of scintillation testing in different MnO2 capacitors: 100 μF 10 V (a, b), 47 μF 35 V (c, d), and 6.8 μF 35 V (e, f) illustrating that faster and more powerful discharges are more likely to cause damage.

However, in some cases the rate of discharge appeared similar for damaging and non-damaging scintillations during consecutive CCS testing (see Fig. VI.7.a, b) and increasing of the rate of discharge did not cause damage (Fig. IV.7.c, d and e, f). Apparently, the power of discharge is only one of the factors affecting the probability of damaging.

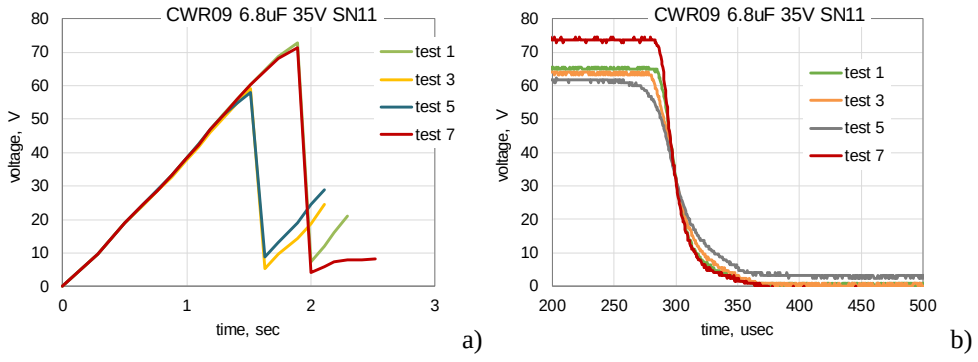

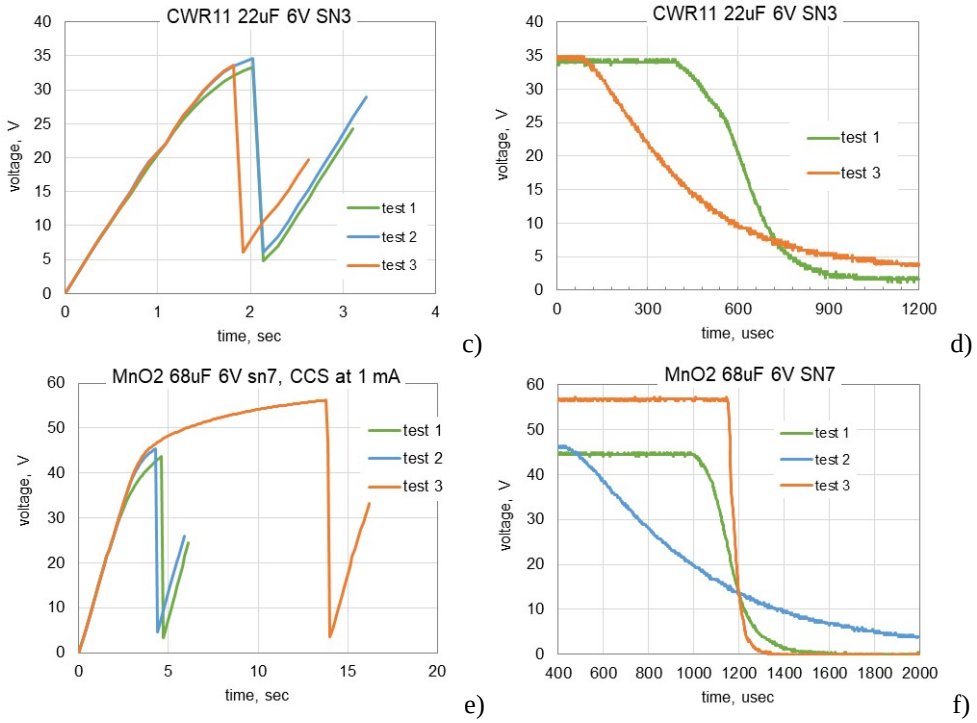

Fig. IV.7. Results of CCS testing (a, c, e) and variations of discharge voltages with time (b, d, f) during consecutive scintillation tests for 6.8 µF 35 V (a, b), 22 µF 6 V (c, d), and 68 µF 6 V capacitors. Note that the 7th test of the 6.8 µF capacitor resulted in a short circuit whereas the rate of discharge was similar to the non-damaging tests. In the 22 µF and 68 µF capacitors, the discharge during one of the tests was much faster than in others, but all scintillations were not damaging. The rate of discharging during consecutive testing of 68 µF capacitors changed almost an order of magnitude, but the part did not fail short circuit.

Large value MnO2 capacitors are often burning during CCS testing that contrary to surge current test is carried out at relatively low charging currents. Examples of similar tests for 330 µF 10 V and 470 µF 6.3 V tantalum capacitors are shown in Fig. IV.8. Note that the discharge was completed in ~200 µsec for both types of capacitors, whereas the burning lasted a few seconds after the power supply was disconnected. This indicates that the ignition in large value capacitors might be trigged by a scintillation event even when capacitors are used in high impedance circuits with a limited current from the power supply.

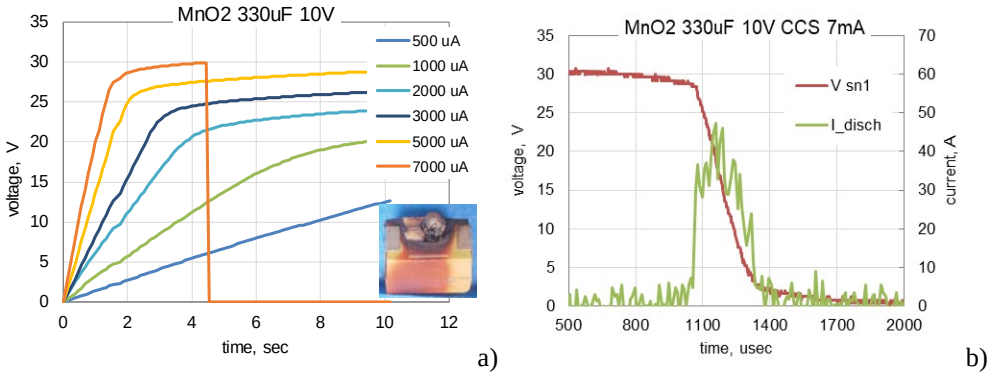

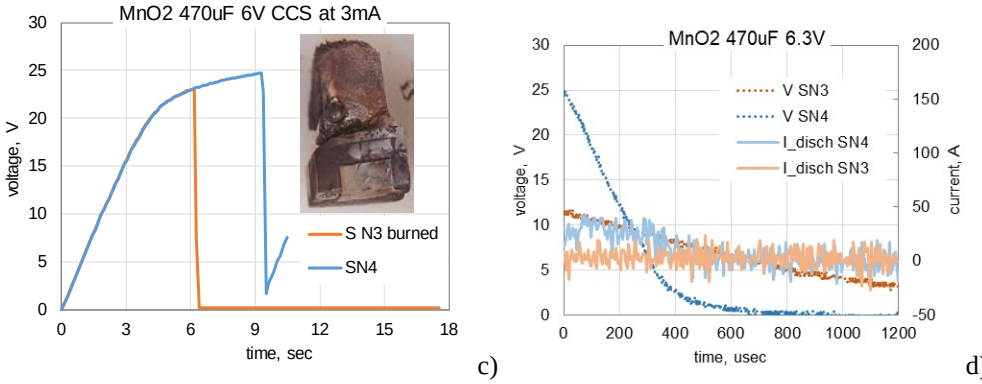

Fig. IV.8. Results of CCS testing for large-value MnO2 capacitors, 330 µF 10 V (a, b) and 470 µF 6.3 V (c, d). Inserts show burned capacitors after the testing.

IV.3. Damaging scintillations in polymer capacitors.

Durations of scintillation events in 25 and 35 V polymer capacitors are 4 to 7 times larger compared to MnO2 capacitors. For this reason, the average discharge power in CPTCs is lower, and the probability of damaging should have been less than in MnO2 capacitors. However, majority of polymer capacitors fail the first scintillation test. These failures are due to substantial variations of the discharge power with time during scintillations. Examples of such events for PB4 47 µF 35 V capacitors are shown in Fig. IV.9.

CCS testing of SN18 resulted in a rapid increase of the discharge current up to 20 A initially and exponential decrease with time after breakdown (Fig. IV.9.b). Eventually, the voltage after breakdown stabilizes after hundreds of miliseconds at a level that corresponds to 6.8 k of the short circuit resistance. However, the characteristic time of the exponentially decreasing current spike was 180 µsec. Sample SN8 from this group of capacitors also had maximum discharge rate at the beginning of the process that resulted in a 100 µsec, 30 A current spike and short circuit failure at 4.6k after hundredths of milliseconds (Fig. IV.9 c, d). For SN13, the increase of the discharge rate occurred twice, at the beginning and at the end and of the scintilation resulting in a relatively small spike of 10 A, 100 µsec, initially and another, a more powerful spike of 88 A, 50 µsec, at the end of the process that lasted ~ 1 msec. Apparently, the second spike resulted in a 0.4k short circuit.

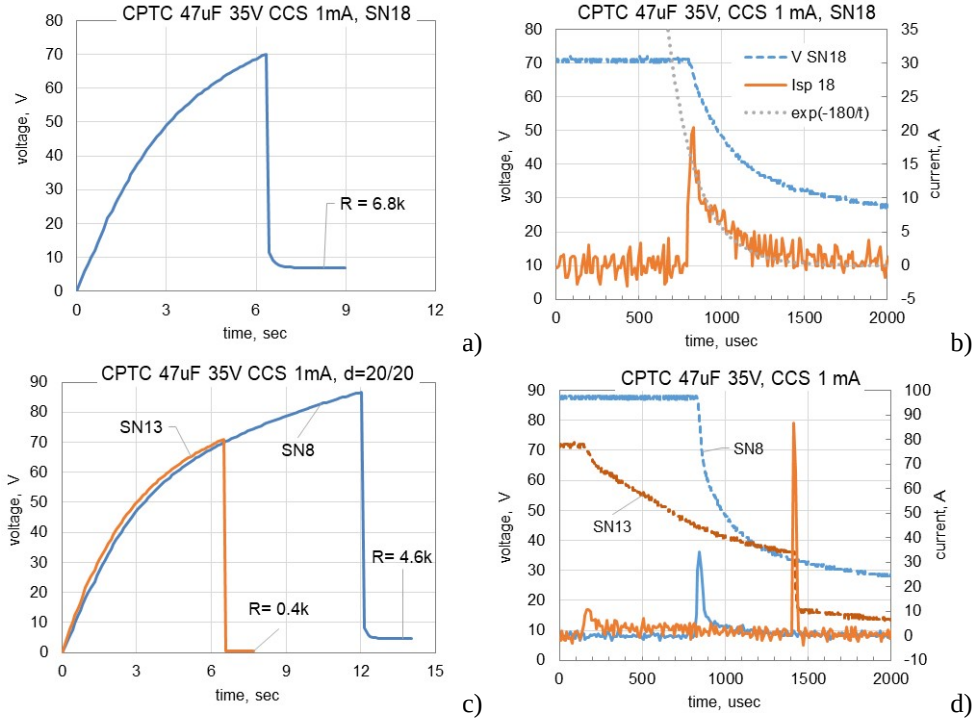

Fig. IV.9. Variations of voltage with time during CCS testing (a, c) and discharge current spikes (b, d) for different samples of polymer 47 µF 35 V capacitors.

Results of CCS testing for three types of polymer 33 μF 35 V capacitors are shown in Fig.IV.10. In all cases, the scintillations appeared to be damaging, but to the different degree. PAQ capacitors (Fig.IV.10.a) failed mostly with short circuits at the ohms level, whereas PC8 capacitors (Fig. IV.10.b) failed at dozens of kiloohms. Voltages across PC9 capacitors (Fig. IV.10.c) increased with time after scintillations, but at a slower rate than initially. Calculations showed that this corresponds to increasing of leakage currents from below 1 μA initially to 350 – 400 μA after scintillations. The rate of discharge, hence discharge currents, in all parts was changing with time substantially. PC8 and PC9 capacitors had maximal rates initially, during first 100 μsec of the discharge period, which resulted in current spikes reaching from 8 to 18 A (Fig.IV.10.h, i). For PAQ capacitors, similar spikes occurred towards the end of the scintillation events (Fig.IV.10.g).

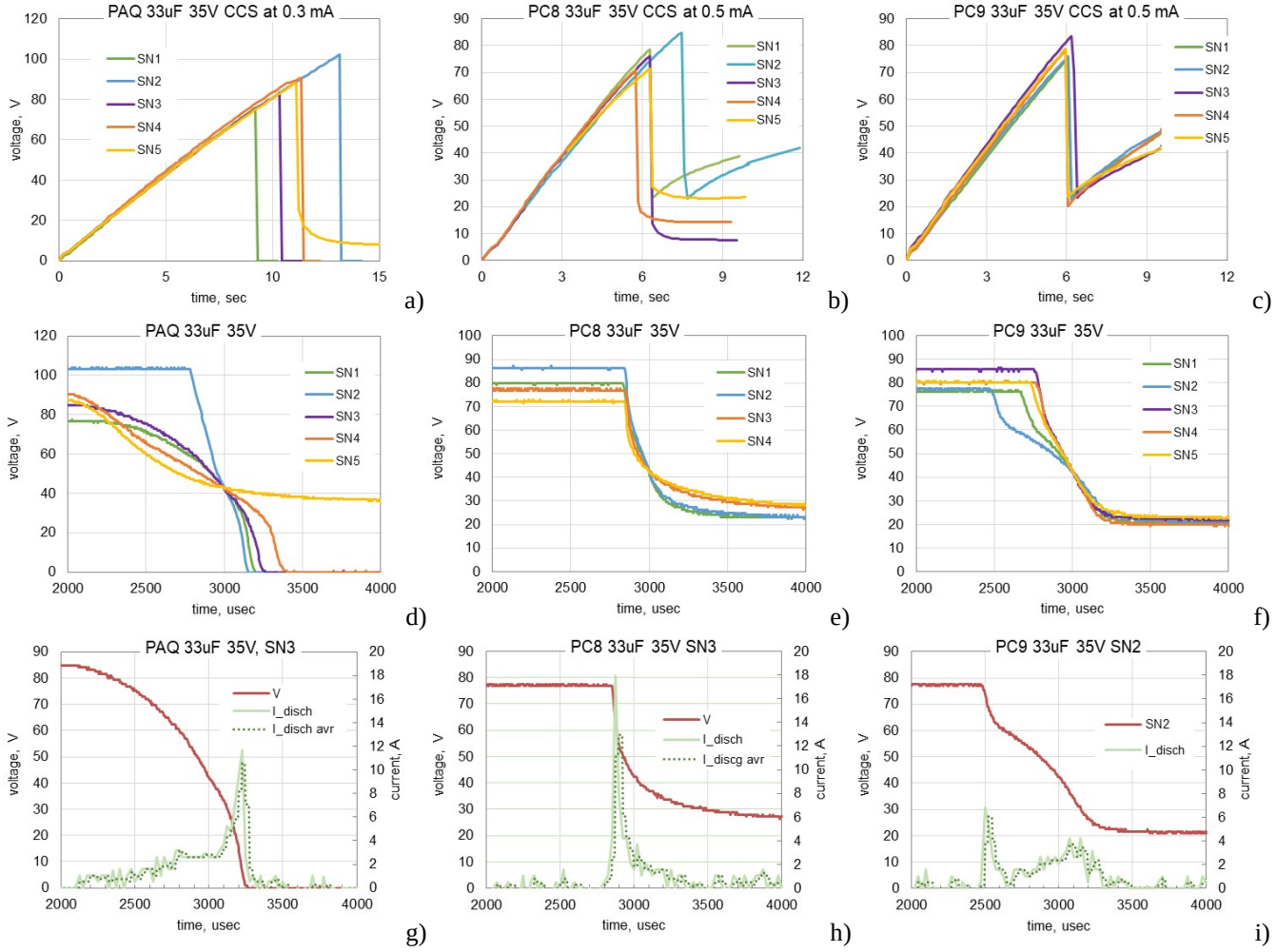

Fig. IV.10. Results of scintillation testing for three types of 33 μF 35 V polymer capacitors: PAQ (a, d, g), PC8 (b, e, h), and PC9 (c, f, i). Figures (d, e, f) show variations of discharge voltages for 4 to 5 samples in each group, and figures (g, h, i) display examples of discharge currents calculated based on *V-t* curves for one of the samples in the group.

Proportions of damaged capacitors after CCS testing for 4 lots of MnO2 and 18 lots of polymer capacitors in dry and wet conditions are shown in Fig. IV.11. Average values of *d* and the relevant standard deviations for wet and dry MnO2 and polymer capacitors are shown in Table IV.2. Similar to results discussed above, polymer capacitors are much more susceptible to damage caused by scintillation breakdowns. However, due to a wide spread of *d*, no significant effect of moisture on the probability of damaging during scintillations was revealed.

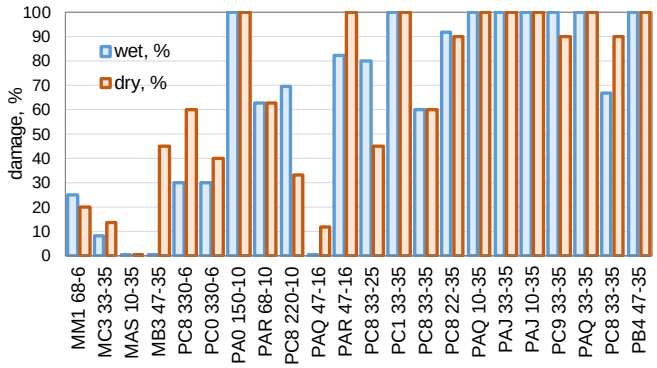

Fig. IV.11. Proportion of damaged capacitors in different lots of wet and dry polymer and MnO2 capacitors.

Table IV.2. Effect of moisture on the proportion of damaging scintillations.

Part	QTY of lots	d_{avr}, %	STD, %
MnO2 dry	4	8.3	11.7
MnO2 wet	4	19.6	18.8
Polymer dry	18	76.3	30.2
Polymer wet	18	76.8	28.8

It is important to note that evaluation of whether a CPTC is damaged or not for capacitors in dry condition is complicated by the anomalous transient effect [16]. Dry polymer capacitors require high charging currents to reach breakdown. When this current exceeds the leakage current caused by the damage, the part can continue charging and appears as not damaged even if leakage current is above the specified limit. Fig. IV.12.a shows an example of CCS testing for dry 100 µF 10 V polymer capacitors that required 100 mA charging currents to reach breakdown. At this condition, damaged capacitors with leakage currents in milliampere range would be able to pass the testing. Measurements of I-V characteristics of the parts after the testing (see Fig.IV.12.b) were close to linear indicating that the parts were shorted with resistances in the range from 2.5 to 5 kiloohm.

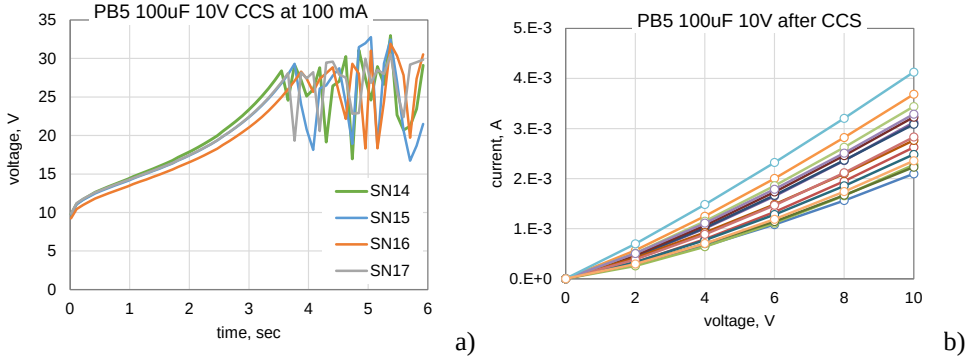

a) b)

Fig. IV.12. An example of CCS testing at a charging current of 100 mA for dry PB5 100 µF 10 V capacitors (a) and post-testing I-V characteristics (b) indicating short circuit resistances in the range from 2.5 to 5 kiloohms.

IV.4. Resistance of damaged capacitors.

Distributions of post-scintillation resistances in most types of polymer capacitors rated to 35 V stretched widely, from ohms to hundreds of kiloohms (see Fig. IV.13.a). Different lots of CPTCs have different distributions and the median value of the resistance varies from ~10 ohm for PAQ 33 µF 35 V capacitors to 20 kohm for PC1 33 µF 35 V capacitors. Capacitors rated to voltages below 35 V had a similar wide range of resistances as shown in Fig. IV.13.b to d. All voltage ratings MnO2 capacitors damaged by scintillations had typically higher resistances than polymer capacitors. In some cases, distributions of resistances were bimodal suggesting presence of at least two groups of with different severity of damage.

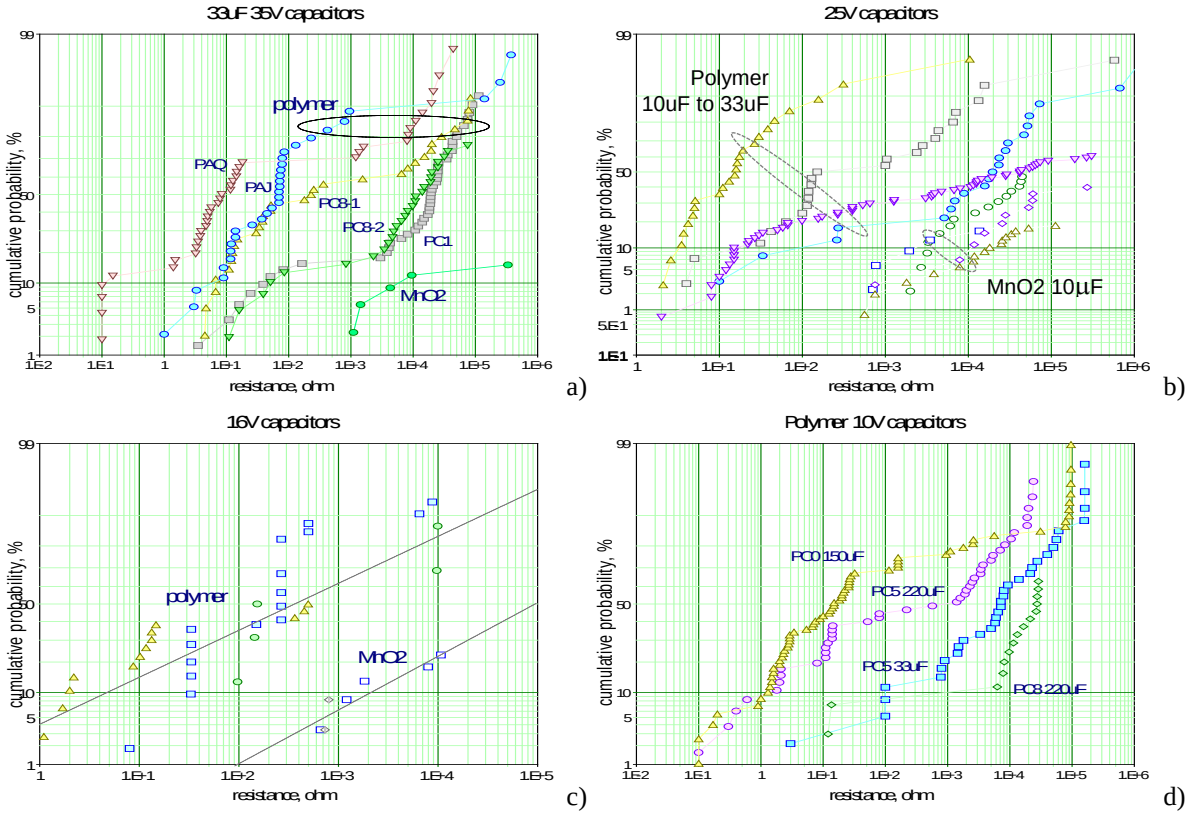

Fig. IV.13. Distribution of resistances after scintillation testing in capacitors rated to 35 V (a), 25 V (b), 16 V (c), and 10 V (d).

IV.5. Stability of resistance in damaged capacitors.

The resistance of capacitors after damaging scintillations is often unstable for both, MnO2 and polymer parts and can be changed by repeat scintillation events. In some cases, shorted MnO2 capacitors could be healed at relatively low voltages after a powerful enough current surge. However, these parts have a greater chance to turn into shorts with even lower resistance.

To simulate the effect of low-voltage operating conditions, 6.8 µF 35 V MnO2 capacitors having shorts after scintillation testing were tested using a dynamic power SMU (Keysight N7973A). During this test, the voltage was increasing to 15 V at a rate of 5V/sec and voltages and power supply currents were recorded every millisecond. Test results for 4 samples that recovered at a voltage of ~ 5 V are shown in Fig. IV.14.

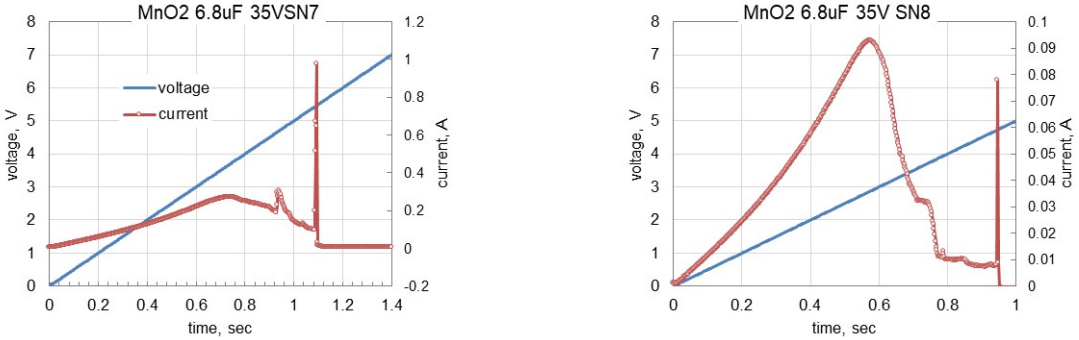

a) SN7 failed at 284 ohm after the 3rd CCS test.

b) SN8 failed at 42 ohm after the initial scintillation testing.

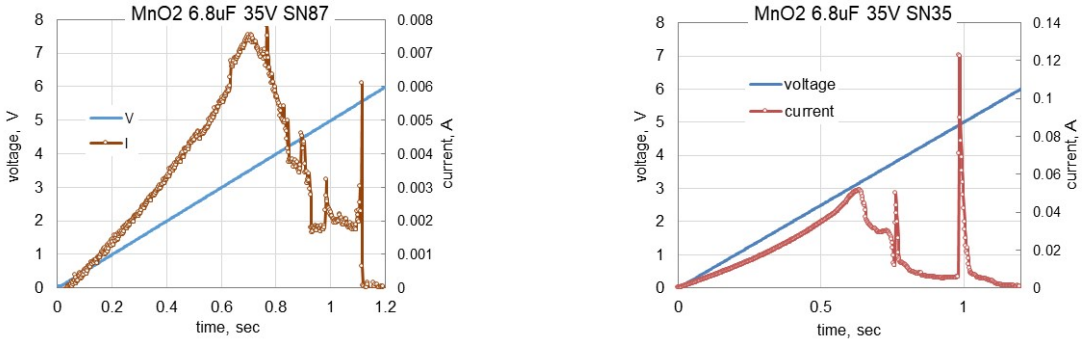

c) SN87 failed CCS at 680 ohm. d) SN35 failed CCS at 95 ohm

Fig. IV.14. Low-voltage testing of 6.8 μF 35 V MnO2 capacitors that have been damaged by CCS testing. In all cases, samples recovered at ~ 5 V as a result of additional scintillations that produced a few millisecond power supply current spikes with amplitudes from 0.1 to 1 A.

Recovery of polymer capacitors that have been damaged by scintillations can also happen but occurs differently compared to MnO2 capacitors. Fig. IV.15 shows results of four consecutive CCS tests for a sample of PC8 22 μF 35 V capacitors. This part failed at 54 kohm after the first scintillation with voltage stabilizing at ~ 27 V (Fig. IV.15.a). However, voltage continued increasing above 30 V during the second and the third tests, although at a lower rate than initially thus indicating high, but decreasing with consecutive tests leakage currents. During the fourth test, the rate of voltage increase was similar to the initial suggesting that the leakage currents decreased to the microampere range, and the part reached voltages higher than the initial breakdown. After that, the part failed at ~ 6k. The rate of voltage discharge during the fourth test was greater than during the first one (see Fig. IV.15.b) indicating a more powerful breakdown.

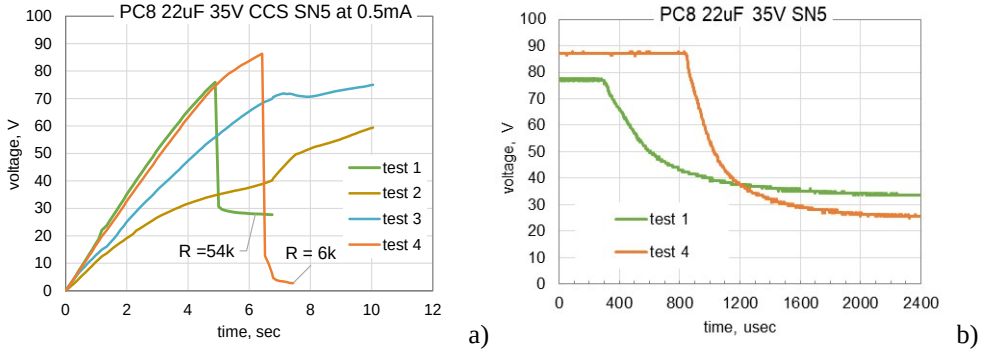

a) b)

Fig. IV.15. Four consecutive CCS tests at 0.5 mA for SN5 of 22 μF 35 V capacitors (a) and kinetics of the voltage discharge process for the initial and final tests (b).

The first scintillation test did not cause short circuit during testing of 33 μF PC8 type capacitors rated to 25 V and 35 V, but increased leakage currents from less than 1 μA initially to ~ 650 - 850 uA after scintillations (see Fig. IV.16.a, c). Both parts had lower leakage currents during the second test, but breakdown voltages did not change substantially. The 25 V capacitor failed hard short circuit at 8 ohm during the third CCS testing at apparently lower rate of the discharge than initially (Fig. IV.16.b). However, the final *V-t* curve indicated presence of power spikes. The 35 V capacitor passed two additional CCS tests at higher charging currents (1.2 and 1.6 mA) and breakdown voltages close to the initial. This capacitor failed short circuit at 29 ohm after the fifth test following a sharp, 2 μsec and 95 A discharge current spike that occurred at the end of the discharging process (see Fig.IV.16.d).

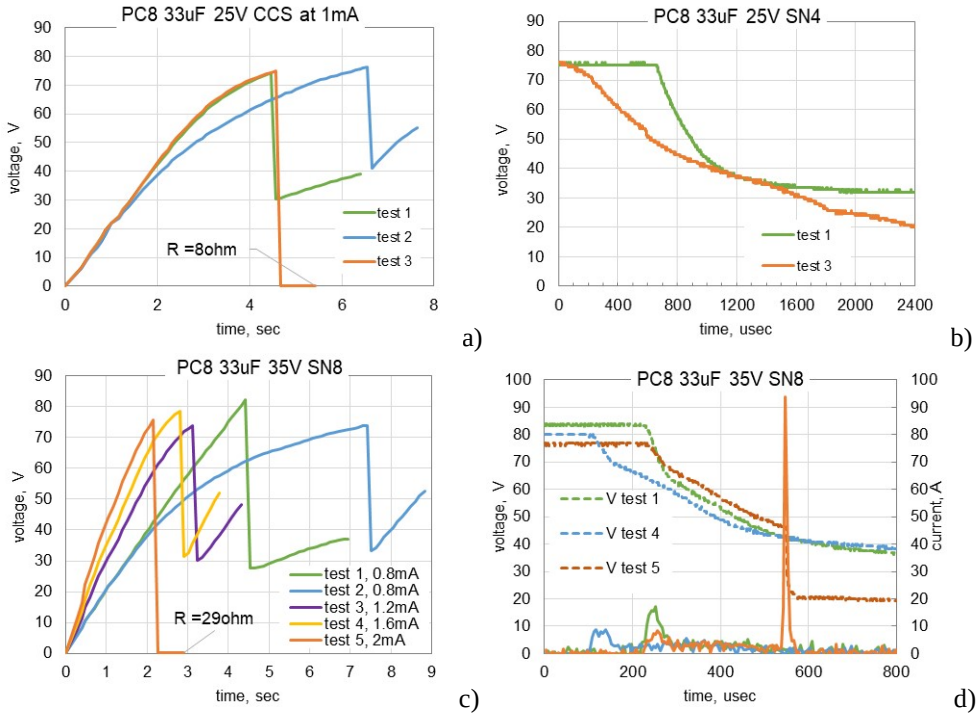

Fig. IV.16. Results of CCS testing for 33 µF 25 V SN4 (a, b) and 33 µF 35 V SN8 (c, d) PC8 capacitors.

A similar behavior was observed in other types of CPTCs (see Fig. IV.17). Sample SN4 of PC1 33 µF 35 V capacitors that had a substantially increased leakage current (~25k resistive short) as a result of a 30 A, 10 µsec current spike at the beginning of the scintillation (Fig. IV.17.b). The part appeared normal during the second test, but failed at 6 ohm after a short, 2 µsec 300 A current spike in the middle of the discharge process. Sample SN3 of PC9 capacitors (Fig. IV.17.c) was damaged by the first scintillation associated with a 15 A, 20 usec current spike at the beginning of the process that resulted in leakage currents increased up to ~ 350 µA. Leakage currents during the second test remained large, although somewhat lower than after the first scintillation. During the third test at a larger charging current, the part appeared normal and sustained ten scintillations at breakdown voltages between 63 to 70 V.

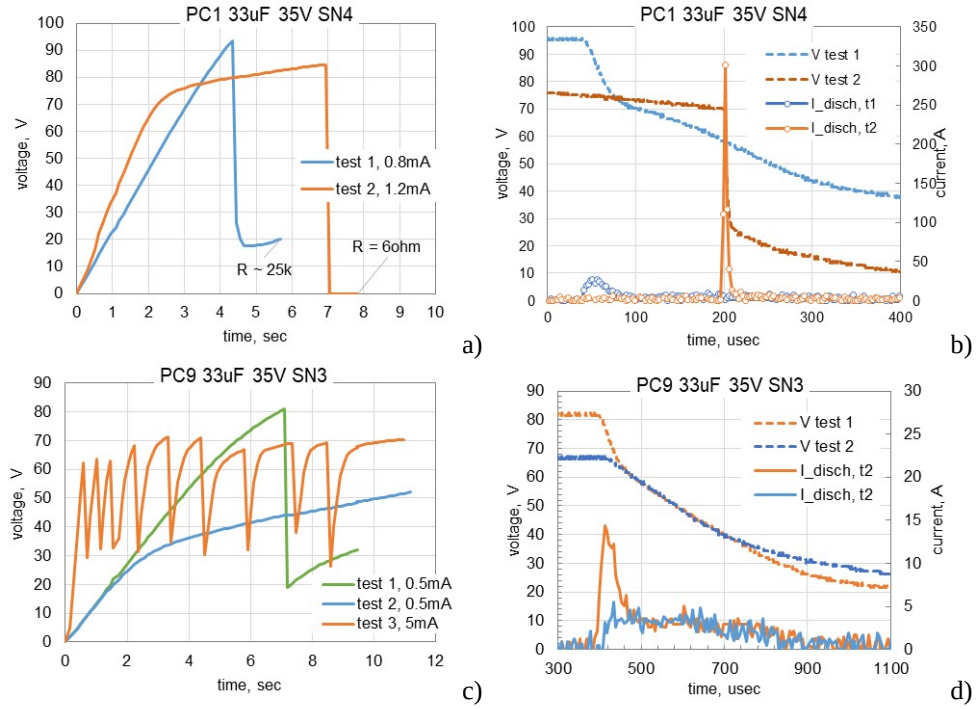

Fig. IV.17. CCS testing of 33 µF 35 V PC1 (a, b) and PC9 (c, d) capacitors.

V. Effect of scintillations on characteristics of capacitors

Capacitors damaged by scintillation breakdown are revealed based on analysis of results of CCS testing as it is described in section IV. According to this method, if voltage can increase above VR after breakdown at the same rate as initially, the part considered self-healed. In other words, the part considered self-healed if leakage current caused by a possible damage is well below the charging current. Obviously, this technique might be not sensitive enough to reveal degradation in parts with low leakage currents. Determination of self-healing based on results of CCS testing might be acceptable for practical reasons, because in many applications excessive leakage currents will not cause failures of the system. However, for a better understanding of the mechanisms of breakdown and self-heling, more information related to the effect of scintillations on performance of the parts is necessary. In this section, we compare AC and DC characteristics of different types of capacitors before and after CCS testing.

V.1. AC characteristics.

Correlations between capacitance, DF, and ESR for different types of MnO2 capacitors before and after scintillation breakdowns are shown in Fig. V.1. Figures (a) to (c) correspond to non-damaging scintillations, whereas (d) to (f) show results for both, damaging and non-damaging scintillations. Majority of the 130 tested capacitors after scintillation events had practically the same values of capacitance as initially (Fig.V.1.a, d) and only ~20% of the samples that have been damaged during CCS testing had capacitance decreased by a few percent. These samples had the most significant damage after scintillation breakdowns and failed with resistances in the range of dozens of ohms. Stability of capacitance indicates that the damaged area is at least two orders of magnitude less than the total area of the part. Equivalent series resistances (ESR) also did not change significantly after CCS even for capacitors severely damaged by scintillations, see Fig.V.1.c and V.1.f. Obviously, this is due to the high frequency of measurements, 100 kHz, when the impedance is sensitive to shorting resistances that have values comparable to ESR, which is typically below ~ 1 ohm.

Approximately 10% of self-healed capacitors had substantially increased DF values after CCS testing (Fig. V.1.b). Damaged capacitors had the most significant increase in DF (Fig.V.1.e) that is due to a direct effect of the shorting resistance on DF. Note that the limit for DF is typically in the range from 8% to 12%, whereas actual values are almost an order of magnitude below. Because of the substantial DF margin, capacitors damaged by scintillations might have “out-of-family”, but still acceptable characteristics and thus pass the screening. To select the best quality parts for space applications, the out-of-family parts should be screened out, for example, using the 3-sigma criterion.

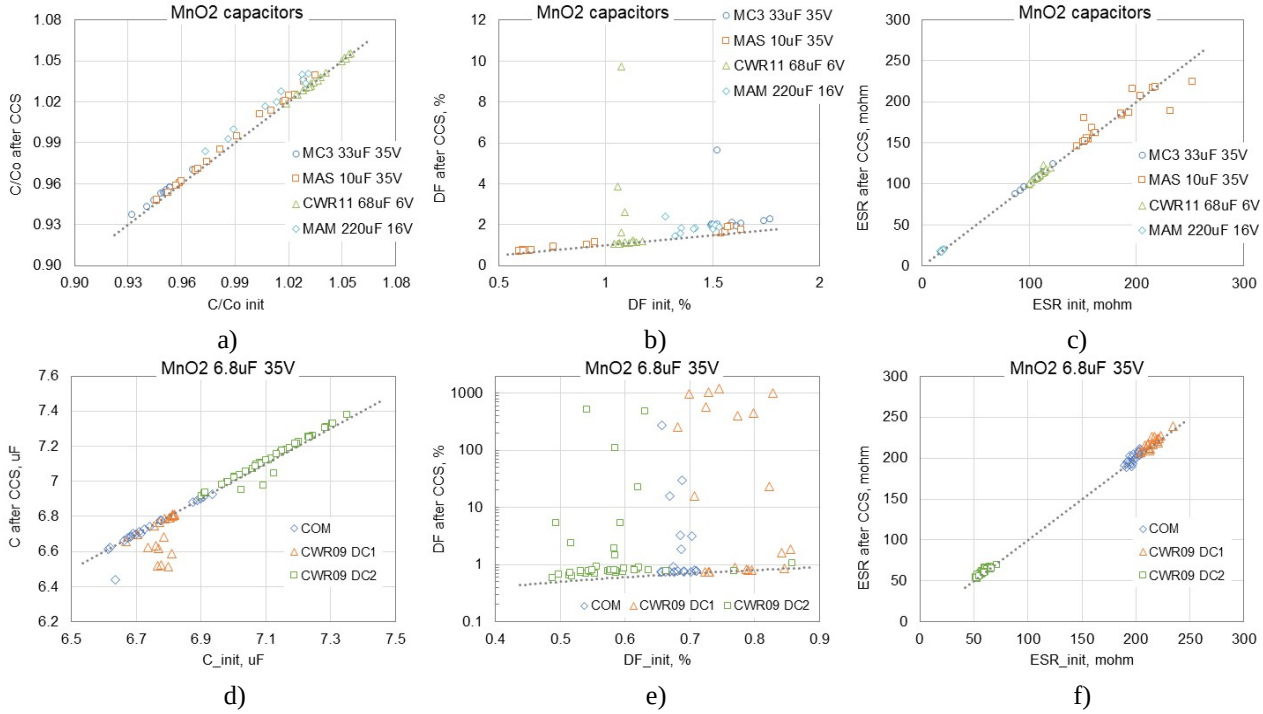

Fig. V.1. Correlation between the initial and post scintillation values of capacitance (a, d), dissipation factor (b, e), and ESR (c, f) for different types of MnO2 capacitors. Dotted lines here and below correspond to no change values.

Similar to MnO2 capacitors, capacitance and ESR in polymer tantalum capacitors did not change much after CCS testing, but dissipation factors increased significantly (see Fig. V.2). The values of DF in PC8 and PC9 capacitors increased on average 2 to 4 times, but remained within the specified limits. However, for PAQ capacitors, the increase was more substantial, and ~80% of the parts failed DF.

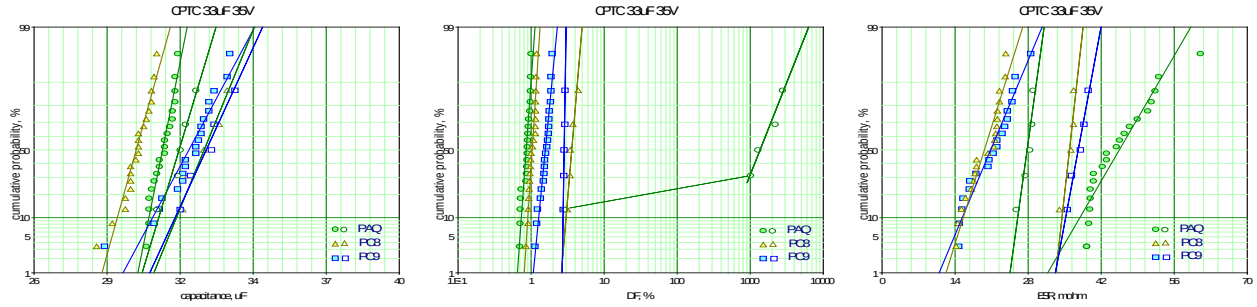

a) b) c)

Fig. V.2. Distributions of capacitance (a), dissipation factor (b), and ESR (c) in "as received" condition (dark marks) and after CCS testing (empty marks) for three types of 33 µF 35 V polymer capacitors.

As was shown in section III, breakdown voltages in tantalum capacitors might change in the presence of moisture. The effect of moisture content on variations of AC characteristics caused by scintillation breakdown for three types of tantalum capacitors is illustrated in Fig.V.3. Similar to results in Fig.V.1 and Fig.V.2, values of DF experienced the most significant changes, but these changes were comparable for wet, dry, and virgin MnO2 capacitors. Polymer 47 µF 35 V capacitors appear to have a more serious degradation in wet condition. This might be partially due to higher breakdown voltages for wet compared to dry polymer capacitors.

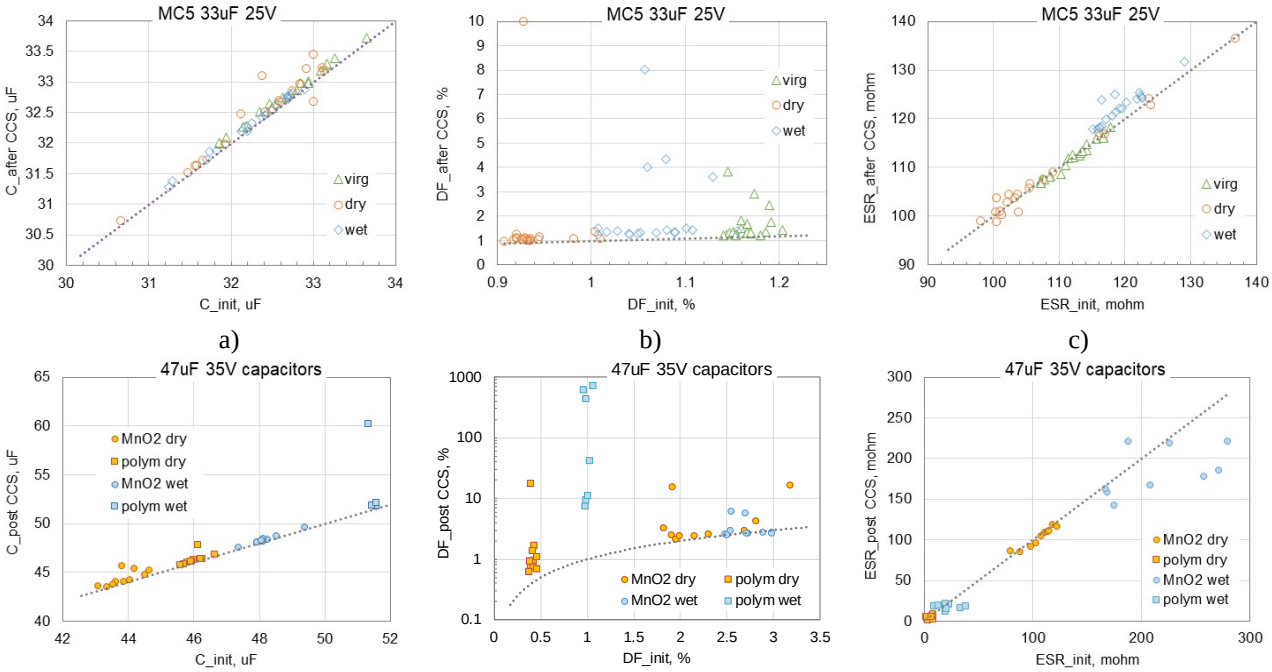

a) b) c)

d) e) f)

Fig.V.3. Effect of moisture on variations of AC characteristics after CCS testing for MnO2 33 µF 25 V (a, b, c) and polymer 47 µF 35 V (d, e, f) capacitors.

V.2. Leakage currents.

Fig. V.4 shows examples of the effect of CCS testing on leakage currents in different types of MnO2 and polymer capacitors. Increasing DCL for polymer capacitors was expected because majority of these parts have been damaged during scintillation events. However, results show that leakage currents increased significantly even for capacitors that considered self-healed (majority of MnO2 and some polymer capacitors). Due to a large (orders of magnitude) margin between the actual and specified leakage currents, majority of capacitors that could have been damaged by

scintillation events, for example, during Weibull grading test would be considered acceptable. Revealing and screening-out capacitors with the out-of-family DCL values, similar to requirements of M55365 for T-grade parts (3-sigma test), will help to select best quality capacitors for space systems.

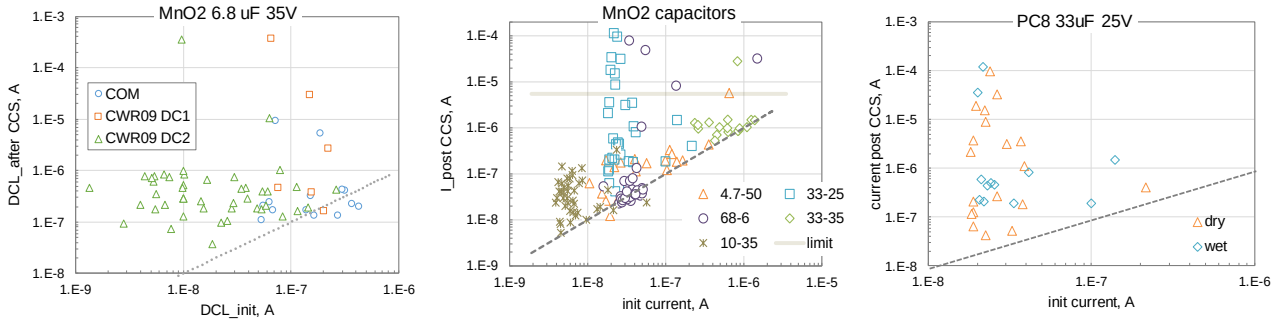

a) b) c)

Fig. V.4. Effect of scintillation breakdowns during CCS testing on leakage currents in MnO2 (a, b) and polymer (c) capacitors.

Variations of leakage currents with time under bias before and after CCS testing for different types of MnO2 capacitors are shown in Fig. V.5. Scintillation breakdowns increased leakage currents from several times to several orders of magnitude for all samples, including parts that appeared self-healed during CCS testing. In cases when currents increased more than 2 orders of magnitude, their behavior was erratic indicating that scintillation events can happen with time under bias at rated voltages. In some cases, currents decreased gradually with time similar to virgin samples and although the level of currents was much larger than for non-stressed samples, they remained below the specified limits. These results indicate that some capacitors damaged by scintillation breakdowns during manufacturing might still have acceptable leakage currents. However, the reliability of these parts might be compromised, and for space applications these parts should be screened out by monitoring leakage currents and revealing the out-of-family samples.

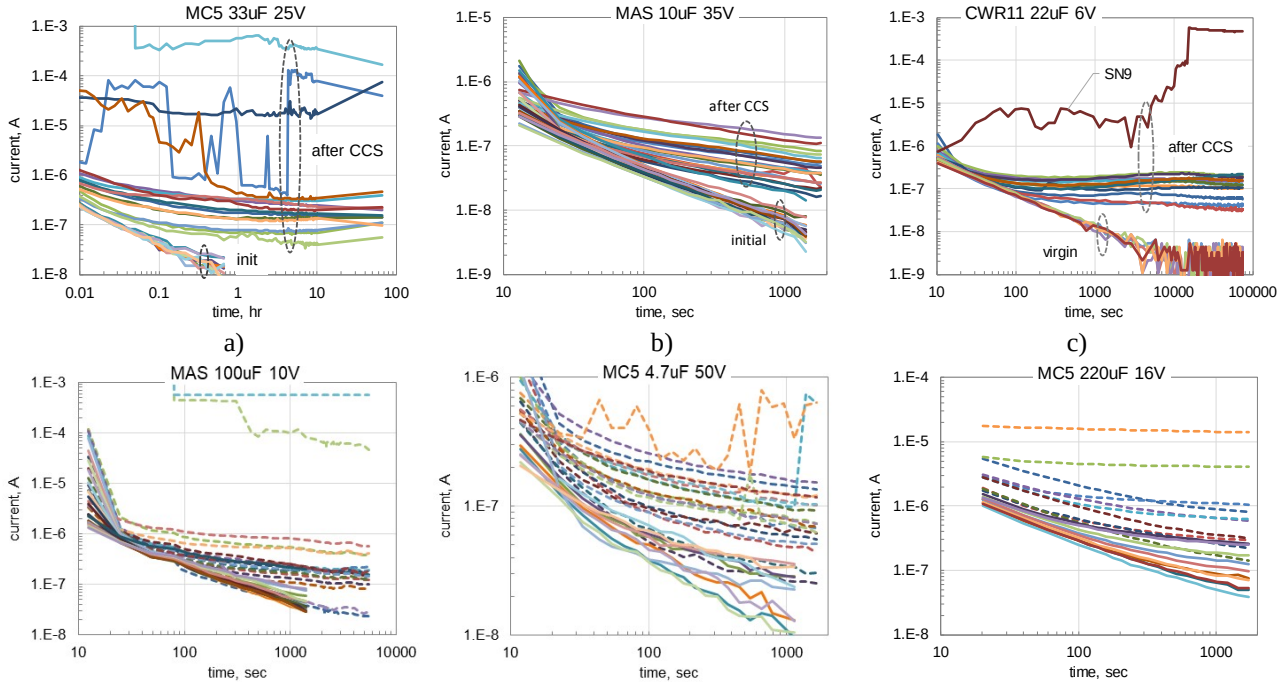

a) b) c)

d) e) f)

Fig. V.5. Variations of leakage currents with time at room temperature and rated voltages for different types of MnO2 capacitors before and after scintillation breakdown testing. Solid lines in figures (d, e, f) correspond to virgin parts and dashed lines to the parts after scintillation breakdown. Note that the specified leakage current in μA for MnO2 capacitors can be calculated as 0.01×VR×C, where VR is in volts and C is in microfarads.

The effect of scintillations on long-term variations of leakage currents for 6.8 μF 35 V MnO2 capacitor is shown in Fig. V.6. At room conditions, currents in virgin capacitors (15 pcs) do not exceed 0.1 uA and remained stable for 100 hours of testing (Fig. V.6.a). After CCS (Fig. V.6.b), currents in all parts (55 pcs) increased up to an order of magnitude. Four samples, SN9, 10, 51 and 54, had even greater currents, were unstable and had scintillation-like spikes. Note, that SN9 failed CCS at 8 kohm and SN51 failed at 3.6 kohm, but no damage was detected during CCS testing for other samples. Anomalies in leakage currents for samples SN9 and SN54 appeared after a few hours of electrification and would have not been detected by regular screening procedures. Apparently, excessive currents and anomalies might develop in damaged capacitors with time under bias.

Fig. V.6.c displays result of 800 hours life testing at 85 ºC 35 V for a group of 15 non-stressed samples and capacitors stressed by three non-damaging scintillation breakdowns (47 samples). For this test, the parts with anomalies shown in Fig. V.6.b were removed from the population. All non-stressed capacitors at 85 ºC had leakage currents well below 1 uA, whereas capacitors that experienced scintillation breakdowns had more than two orders of magnitude greater and increasing with time currents. Approximately 40% of capacitors after scintillation testing increased leakage currents by the end of life testing above the specified limit of 24 μA, whereas leakage currents in non-stressed parts remained below 0.5 μA.

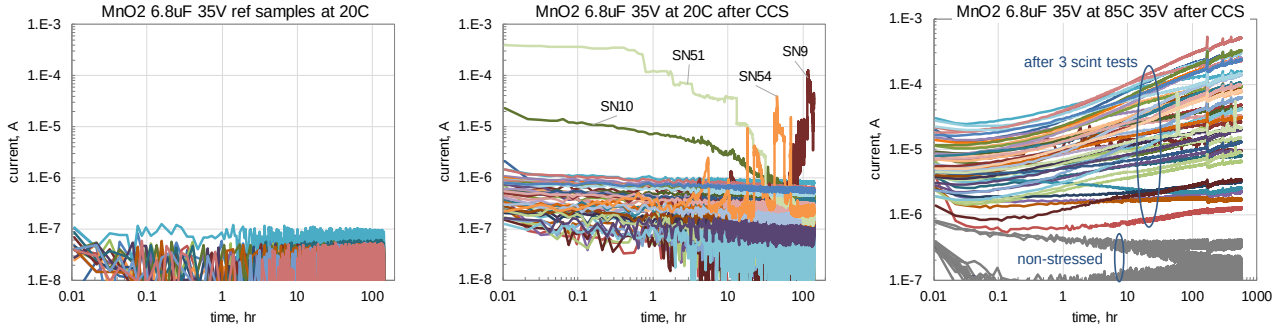

a) b) c)

Fig. V.6. Variations of leakage currents in CWR09 6.8 μF 35 V with time at 35 V and room temperature before (a) and after (b) CCS testing. Figure (c) shows results of life testing during 800 hours at 85C, 35V for non-stressed and capacitors stressed by 3 non-damaging scintillation tests.

Relaxation of leakage currents with time under bias for polymer 47 μF 35 V capacitors before and after CCS testing is shown in Fig. V.7. Based on CCS results, scintillation breakdowns in all these parts were damaging and as shown in Fig. V.7.b resulted in increased leakage currents by 2 to 3 orders of magnitude. However, the currents decreased gradually with time and reduced by more than an order of magnitude after 100 hours of testing. Baking of the parts at 125 ºC for 1 hour decreased currents even more (Fig. V.7.c); however, they still remained approximately 10 times greater than initially.

Testing at 85 ºC and 35 V for 100 hours (Fig. V.7.d) resulted in further decreasing of leakage currents that apparently stabilized by the end of testing at levels from 4 to 40 μA, that is close to the level of currents at room temperature. This behavior is likely associated with anomalous transients in dry polymer capacitors when leakage currents are decreasing at higher temperatures [19]. Some samples at 85 ºC had relatively shallow current spikes, and the maximum spike when the current increased more than 3 times was detected in SN7 (Fig. V.7e). Considering that the time between the current reading was 10 min, most likely the actual amplitude of the spike was much greater. After the spike, the currents decreased gradually, in about 1 hour, to the initial level.

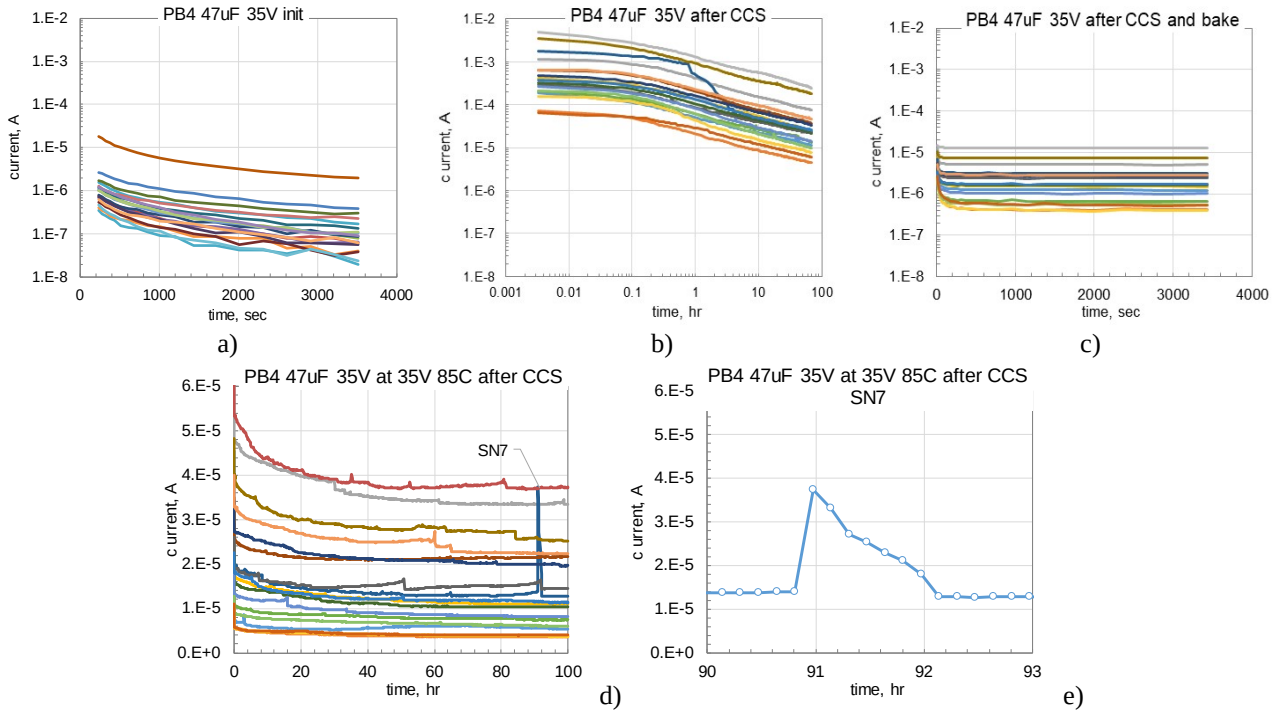

Fig. V.7. Leakage currents in polymer 47 μF 35 V capacitors at room temperature (a, b, c) and 85 ºC (d, e) before (a) and after (b-e) CCS testing. Fig. (e) shows a current spike at ~91 hour of testing in SN7. Note that the currents were scanned every 10 min, so the actual spike amplitude might be much greater.

The effect of scintillation breakdowns on leakage currents in low-voltage 6.3 V 330 μF and 10 V 100 μF polymer capacitors is illustrated on Fig. V.8. For these parts, leakage currents after CCS testing also increased substantially, by 2 to 3 orders of magnitude, but had a tendency of decreasing with time during 100 hours testing at room temperature and rated voltages.

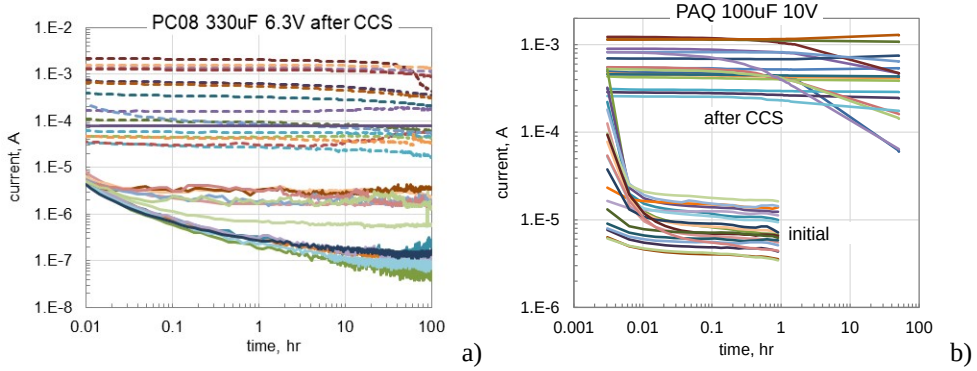

Fig. V.8. Initial and post scintillation testing leakage currents in polymer 330 μF 6.3 V (a) and 100 μF 10 V (b) capacitors at room temperature and rated voltages. Solid lines in (a) correspond to the initial, and dashed lines to post-CCS leakage currents.

Examples of *V-t* characteristics measured during CCS testing and the effect of testing on leakage currents in PC8 33 μF 25 V and PB4 220 μF 16 V capacitors are displayed in Fig. V.9 and V.10 respectively. The *V-t* characteristics are shown for samples that had minimal and maximal currents after the testing shown in Fig. V.9.d. Overall, similar to the previously discussed cases, leakage currents for both types of capacitors increased after scintillations by more than 2 orders of magnitude. Sample SN3 of PC8 capacitors at the end of CCS testing had leakage currents ~ 3 mA at 32 V (see Fig. V.9.a), which is consistent with ~1 mA current during post-CCS measurements at 25 V (Fig. V.9.d). Sample SN5 passed three scintillations with increasing slopes of *V-t* curves at voltages above 25 V thus indicating improvements in leakage currents. As a result, leakage currents in this sample after CCS were close to the initial (Fig. V.9.d). For SN9, improvements in leakage currents also occurred during test 1 and 2, but test 3 resulted in further

degradation (Fig. V.9.c). As a result, currents at 25 V increased compared to the initial by about an order of magnitude (Fig. V.9.d). These data show a correlation between currents assessed based on results of CCS testing and post-CCS direct measurements of leakage currents.

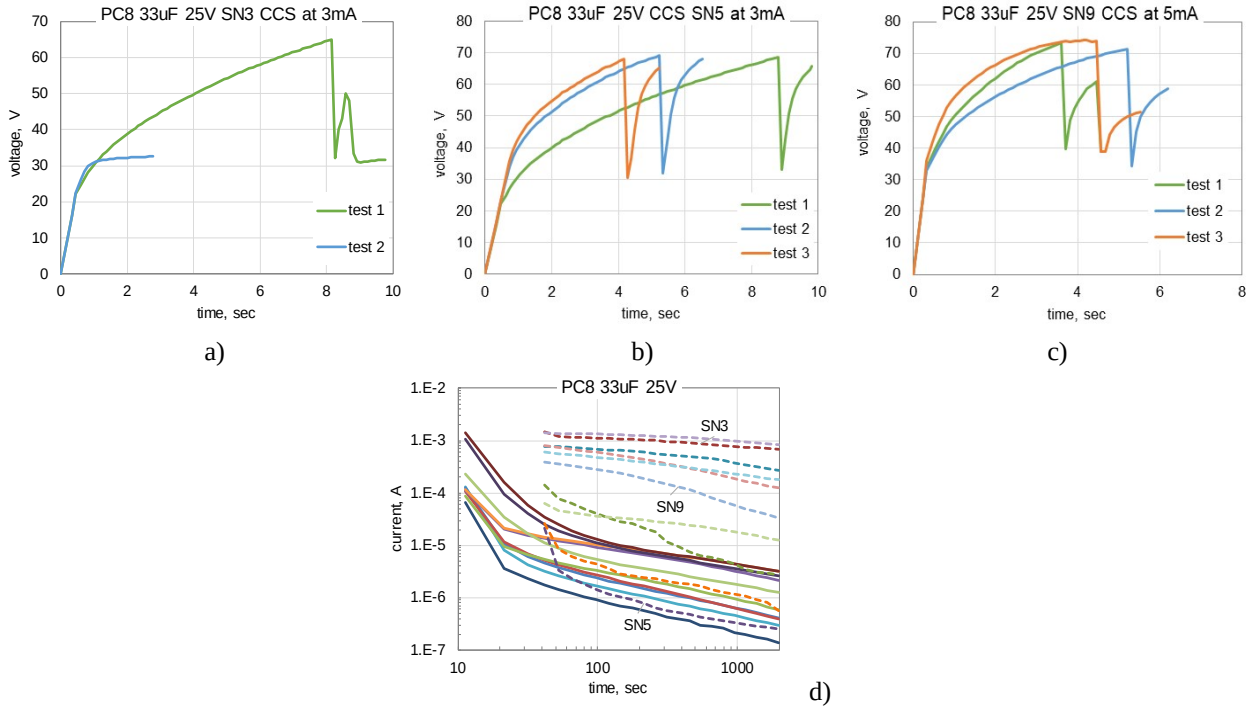

Fig. V.9. Results of CCS testing for SN3 (a), SN5 (b), and SN9 (c) of PC8 33 µF 25 V capacitors and relaxation of leakage currents for virgin (solid lines) and post-CCS testing (dashed lines) capacitors (d).

Contrary to PC8 type capacitors, no correlation between the level of damage detected during CCS testing and post-testing measurements of leakage currents was observed for PB4 capacitors (see Fig. V.10). Sample SN1 passed test 1, but increased leakage currents to ~ 10 mA at 16 V during test 2 (Fig.V.10.a). However, this sample had relatively low, ~ 1 µA currents after the testing (Fig. V.10.c). Sample SN5 had leakage currents ~ 5 mA at 16 V at the end of the first CCS test (Fig. V.10.b), but the currents decreased to below ~ 0.5 mA in several minutes of electrification after the testing (Fig. V.10.c). Sample SN7 that apparently passed three tests without degradation (Fig. V.10.b) had leakage currents more than an order of magnitude greater than initially (Fig. V.10.c). At 85 ºC and 16 V post-CCS test leakage currents initially were up to three orders of magnitude greater than for virgin capacitors but then gradually decreased more than an order of magnitude with time by 100 hour (Fig. V.10.d).

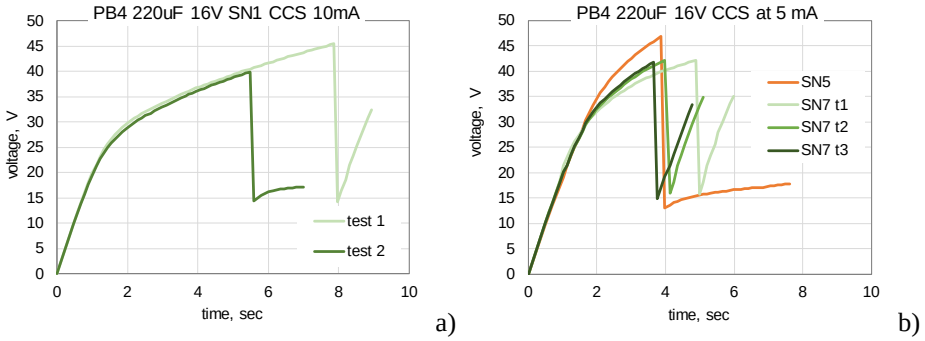

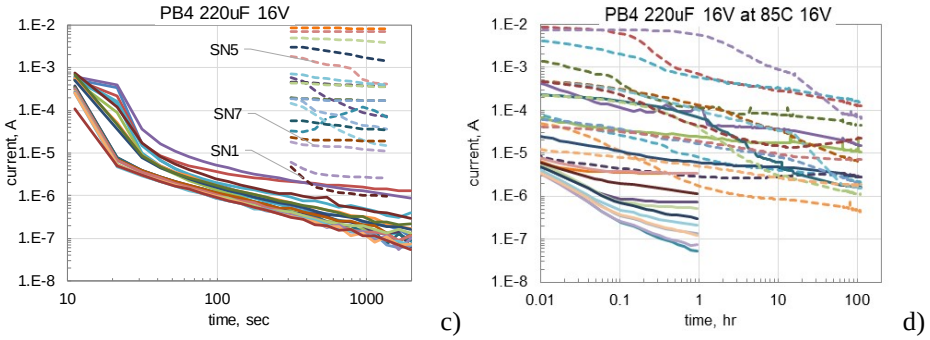

Fig. V.10. Results of CCS testing for SN1 (a) and SNs 5 and 7 (b) of PB4 220 µF 16 V capacitors. Figures (c) and (d) show variations of leakage currents with time at rated voltage and room temperature and 85 ºC respectively. Solid lines in figures (c, d) correspond to virgin and dashed lines to capacitors stressed by scintillation breakdown.

Fig. V.11 shows results of initial and post-CCS measurements of leakage current for polymer and MnO2 22 µF 35 V capacitors from the same manufacturer. Based on CCS results, 15 out of 20 polymer and 1 out of 20 MnO2 capacitors have been damaged by scintillation events. Leakage currents in all self-healed MnO2 and 7 polymer capacitors were monitored for 20 hours at room conditions and 35 V (see Fig. V.11.b). Similar to previous cases, DCL in MnO2 capacitors increased approximately an order of magnitude and had a tendency of further increasing with time under bias. Polymer capacitors had a more significant increase of DCL initially, but by 20 hours leakage currents in most parts reduced more than 2 orders of magnitude and were close to the level in unstressed parts. Even capacitors that failed CCS testing with resistances in the kiloohm range (dashed lines in Fig.V.11.b) reduced leakage currents with time substantially.

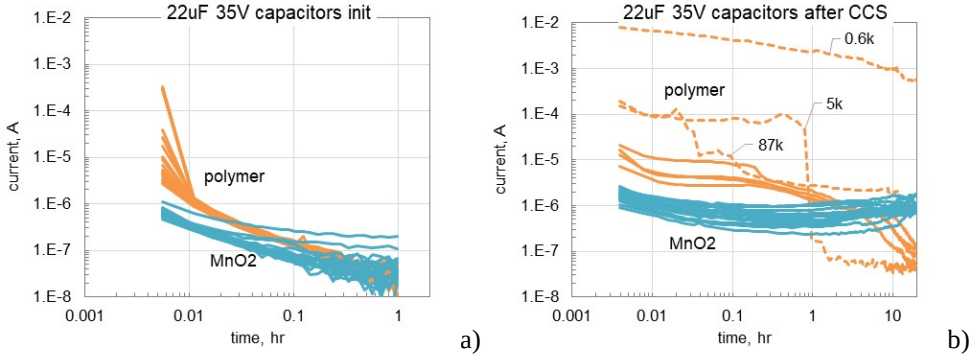

Fig. V.11. Initial (a) and post-CCS (b) leakage currents in MB5 and PB5 22 µF 35 V capacitors. Dashed lines in (b) correspond to capacitors that failed CCS test at the indicated resistances.

Results show that both types, polymer and MnO2, capacitors that appear self-healed during CCS testing have leakage currents significantly increased compared to the initial level. Overall, the increase of currents is greater for polymer than for MnO2 capacitors. However, contrary to MnO2 capacitors, that increase leakage currents with time under bias, polymer capacitors after CCS testing have a tendency of decreasing currents and recovery even after a significant degradation initially.

VI Failure analysis

Several samples of MnO2 and polymer capacitors damaged by CCS testing have been deprocessed by removing plastic case and cathode layers or cross-sectioned to reveal location and appearance of damaged sites. Before deprocessing or cross-sectioning, location of the damage was detected using a FLIR infra-red camera at a dissipating power in the range from 20 mW to 120 mW. Examples of hot spots in MnO2 and polymer capacitors are shown in Fig. VI.1.

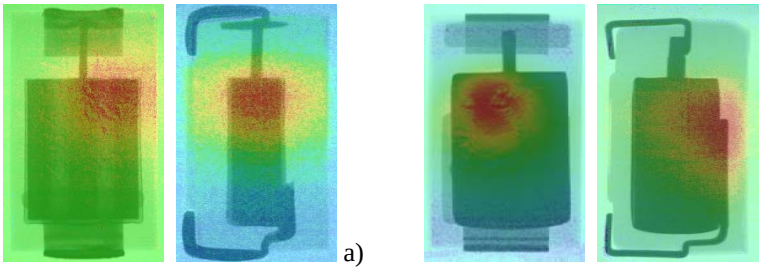

Fig. VI.1 Two side views of a 6.8 µF 35 V MnO2 capacitors SN 93 failed CSS testing at 40 ohm (a) and polymer PC8 33 µF 35V capacitor failed at 5.4 ohm (b). To get location of damage on the pellet, thermal images are overlaid with x-ray images.

VI.1. MnO2 capacitors.

Results of cross-sectioning of SN65 of 6.8 µF 35 V MnO2 capacitors that failed scintillation testing at 240 ohm are shown in Fig. VI.2. This part was designed using a flute-like shape of the pellet that allows for increasing of the surface area and thus reduction of ESR. The damaged site had a size of ~ 200 µm and was located on the surface of one of the groove as shown in the insert. The breakdown formed a void in the MnO2 and carbon layers and resulted in structural changes in the MnO2 and tantalum pellet. SEM and EDS analysis showed oxygen reduction in the manganese oxide and presence of fused tantalum oxide particles. The oxide areas comprised of a mixture of non-stoichiometric manganese and tantalum oxides.

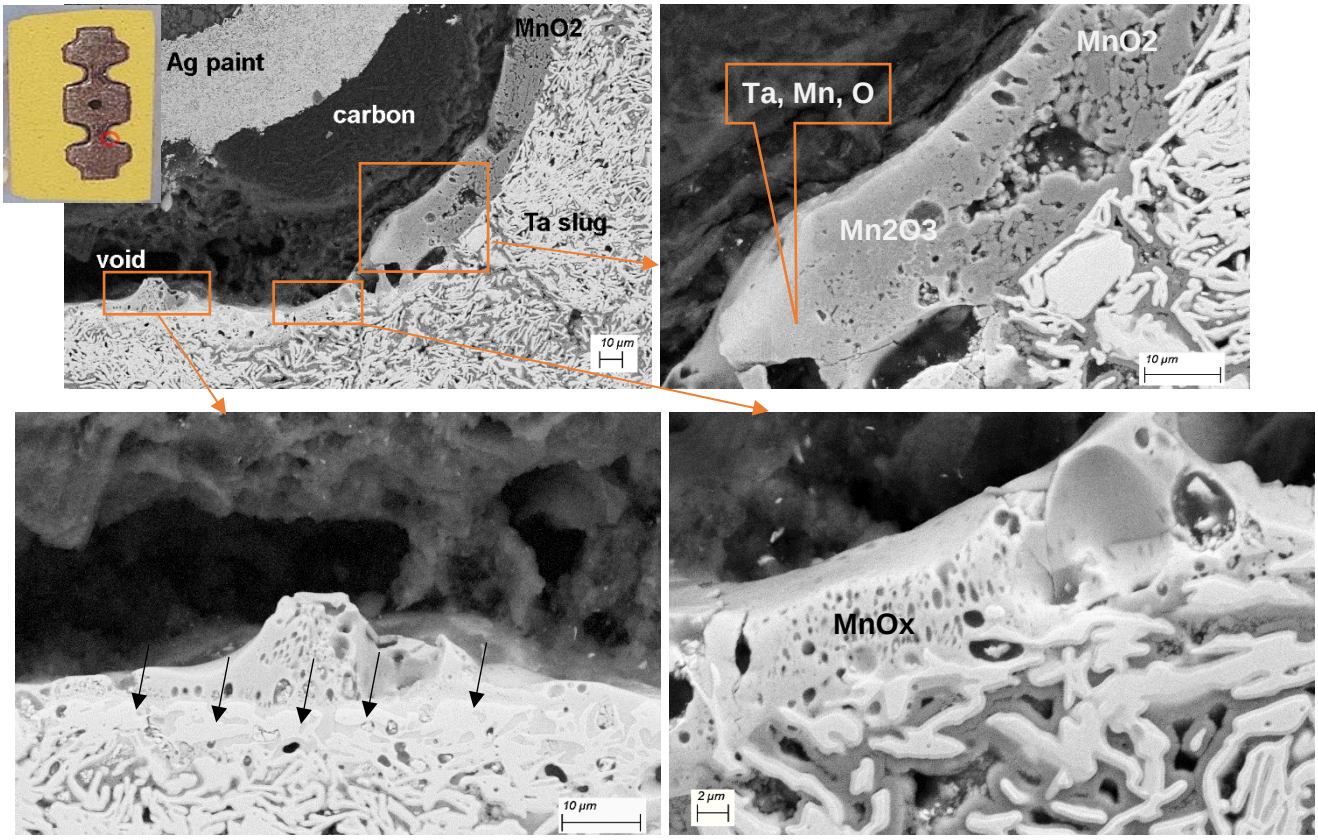

Fig. VI.2. Damaged site in a 6.8 µF 35 V capacitor that failed scintillation testing at 240 ohm. Here and below black arrows indicate areas of a tantalum pellet with fused particles and dissolved oxide.

Similar results, in particular voids and structural changes in the manganese oxide layer and the pellet, were observed during cross-sectioning of two other samples of 6.8 µF 35 V capacitors shown in Fig. VI.3 and VI.4. In both cases, damage was located on the surface of the pellet and had a size ~ 100 µm. Sample SN 93 in Fig. VI.3 had damage at the corner of the pellet (see insert) and was cross-sectioned along the groove. The damaged site in SN71 in Fig.VI.4

was cross-sectioned across the groove. Similar to the previous case, SEM and EDS analysis showed evidences of formation of areas with mixed TaOx/MnOx oxides.

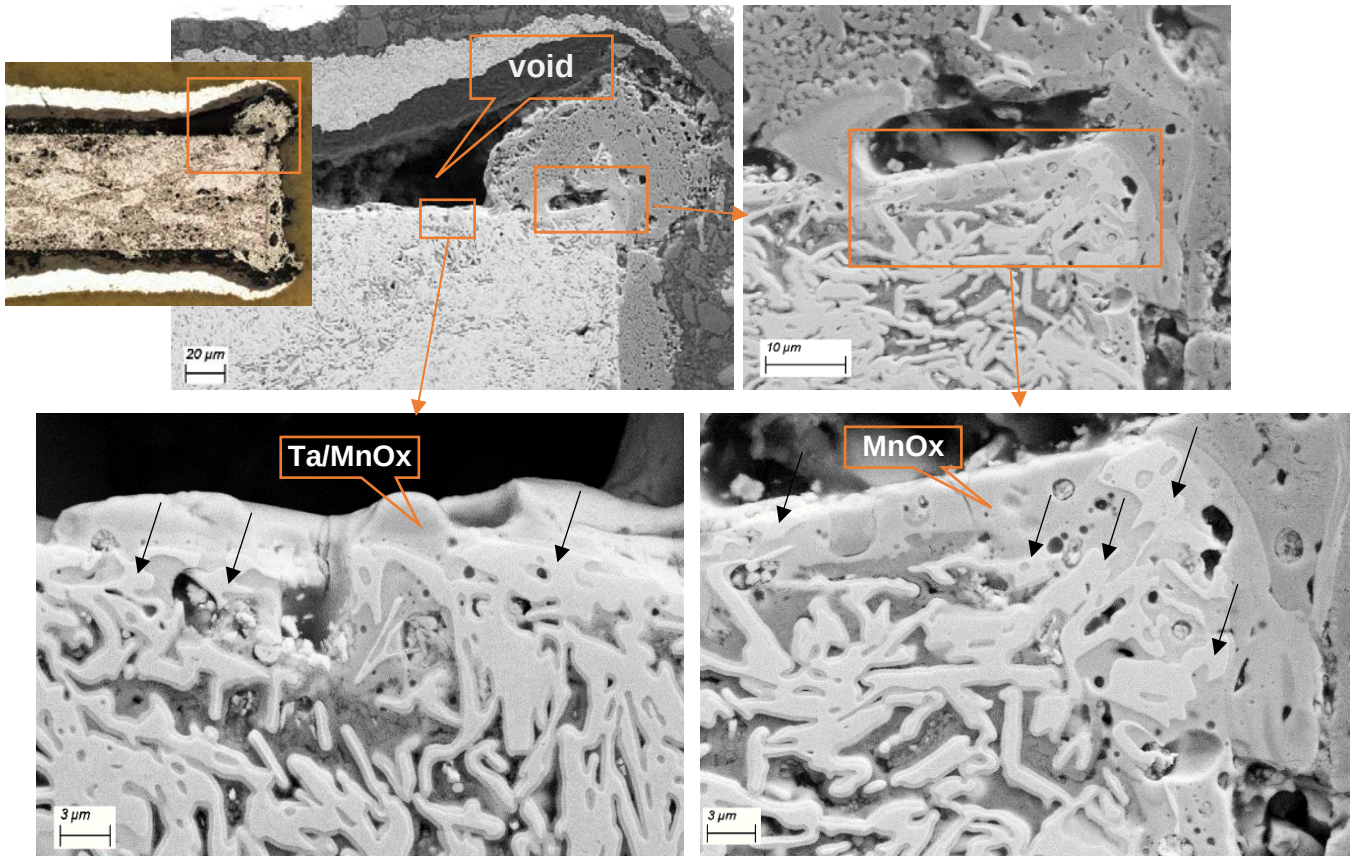

Fig. VI.3. Cross-sectioning of SN93 of MnO2 6.8 µF 35 V capacitors that failed the fifth scintillation test at 40 ohm.

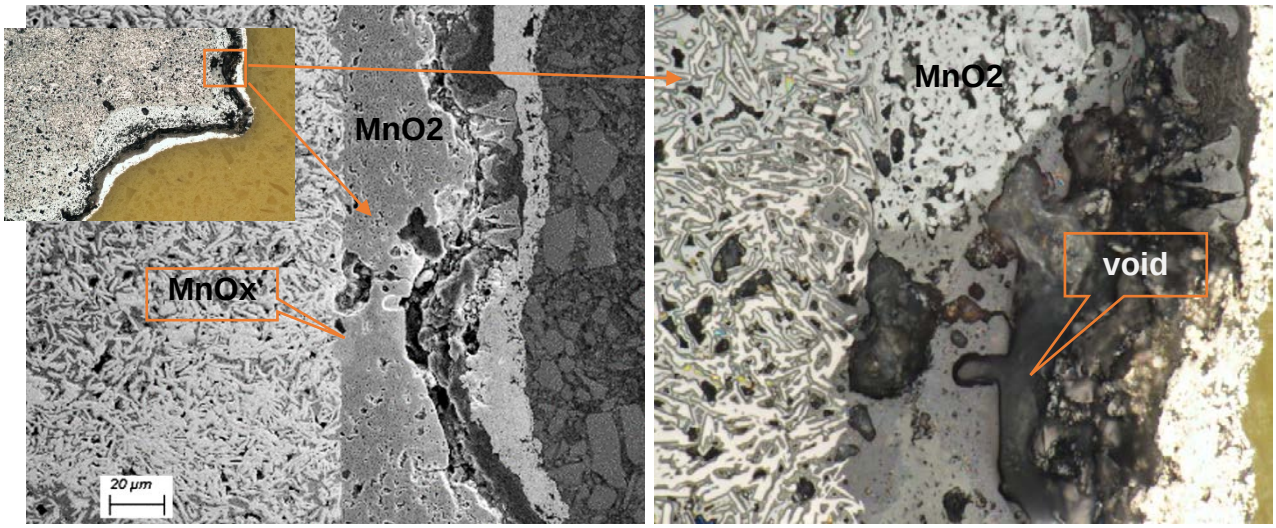

Fig. VI.4. Damaged site in MnO2 6.8 µF 35 V, SN71, that failed at 5k after the third scintillation tests. The left is an SEM and right an optical image of the same site. Note that darker manganese oxide areas in the optical image indicate oxygen reduction caused by the scintillation event.

Damaged sites in two other samples of MnO2 6.8 µF 35 V capacitors were revealed after chemical deprocessing (see Fig. VI.5 and VI.6). In these two cases, the damage was also located on the surface of the pellet and had a size ~ 100

μm. EDS analysis showed that the glassy layers on the surface of the damage consisted of tantalum and manganese oxides.

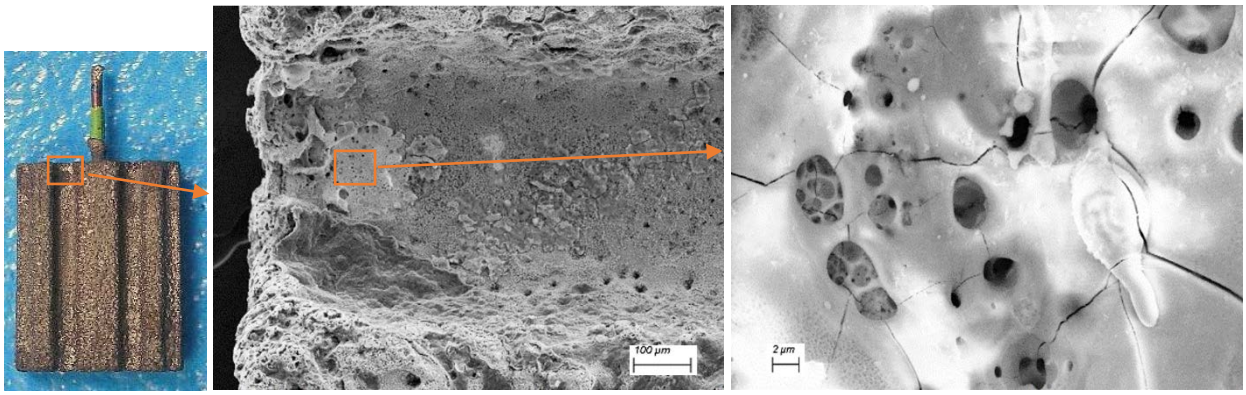

Fig. VI.5. Sample SN72 of 6.8 μF 35 V MnO2 capacitors failed at 26k after the second scintillation test.

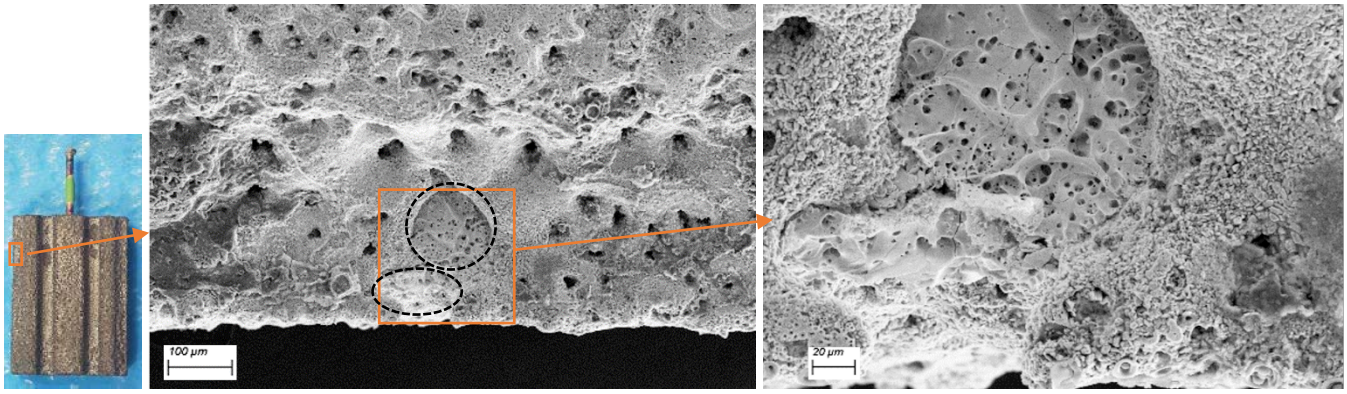

Fig. VI.6. Sample SN83 of 6.8 μF 35 V MnO2 capacitors failed at 17k after the first scintillation test. Dotted ovals indicate two damaged areas in the part.

A similar appearance had damage on the surface of a 10 μF 25 V CWR06 capacitor that had a chip-out during the second scintillation test, but did not fail short circuit (see Fig. VI.7).

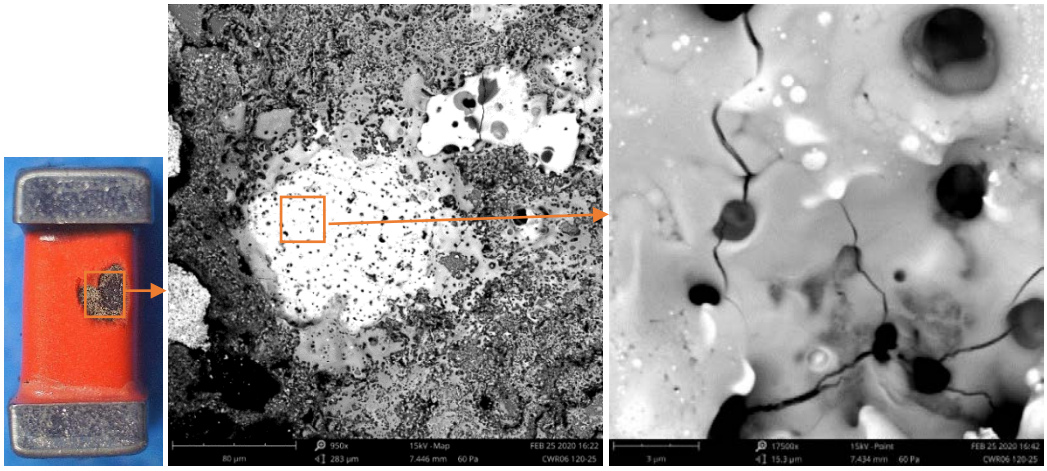

Fig. VI.7. Damage in a 10 μF 25 V CWR06 capacitor. This damage happened during the second scintillation test that created chip-out, but did not cause short circuit in the part.

Fig. VI.8 shows results of CCS testing and the following failure analysis of SN4 of 100 μF 10 V CWR29 capacitors that failed at 63 ohms. A relatively large current spike, up to 70A at a width of ~100 μsec (Fig. VI.8b) apparently consists of multiple, at least three, shorter duration spikes. Similar results were obtained for SN9 and 10 as shown in

Fig. VI.9 that failed in the kiloohms range. Note that the size of the damage for SN4 (~200 μm) was greater than for SN9 and 10.

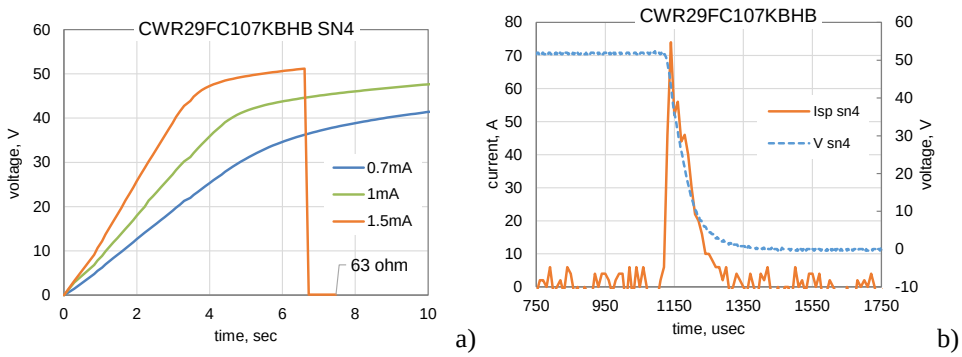

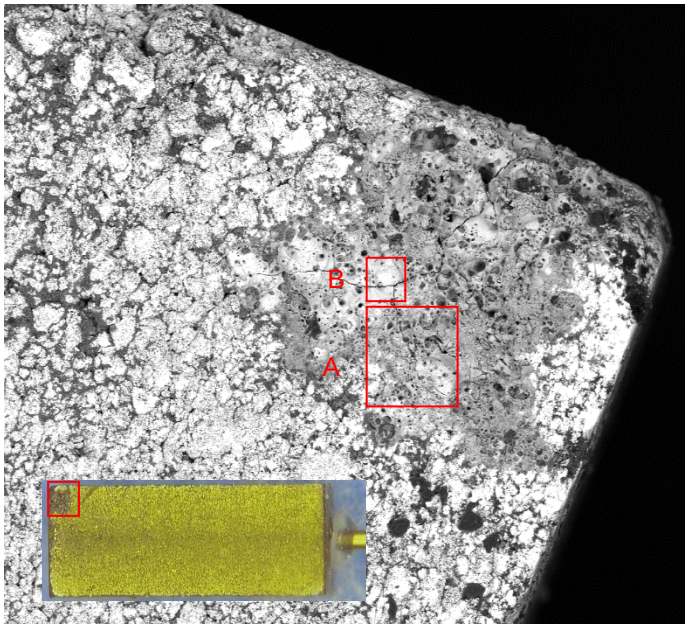

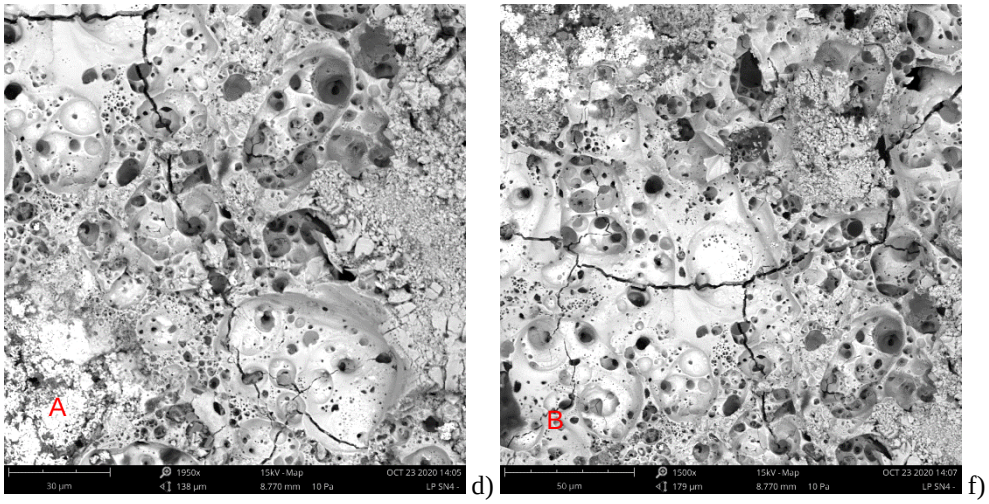

Fig. VI.8. Results of CCS testing (a, b) for SN4 of 100 μF 10 V CWR29 capacitor and an overall (c) and close-up SEM views of the damaged area showing multiple local breakdown sites.

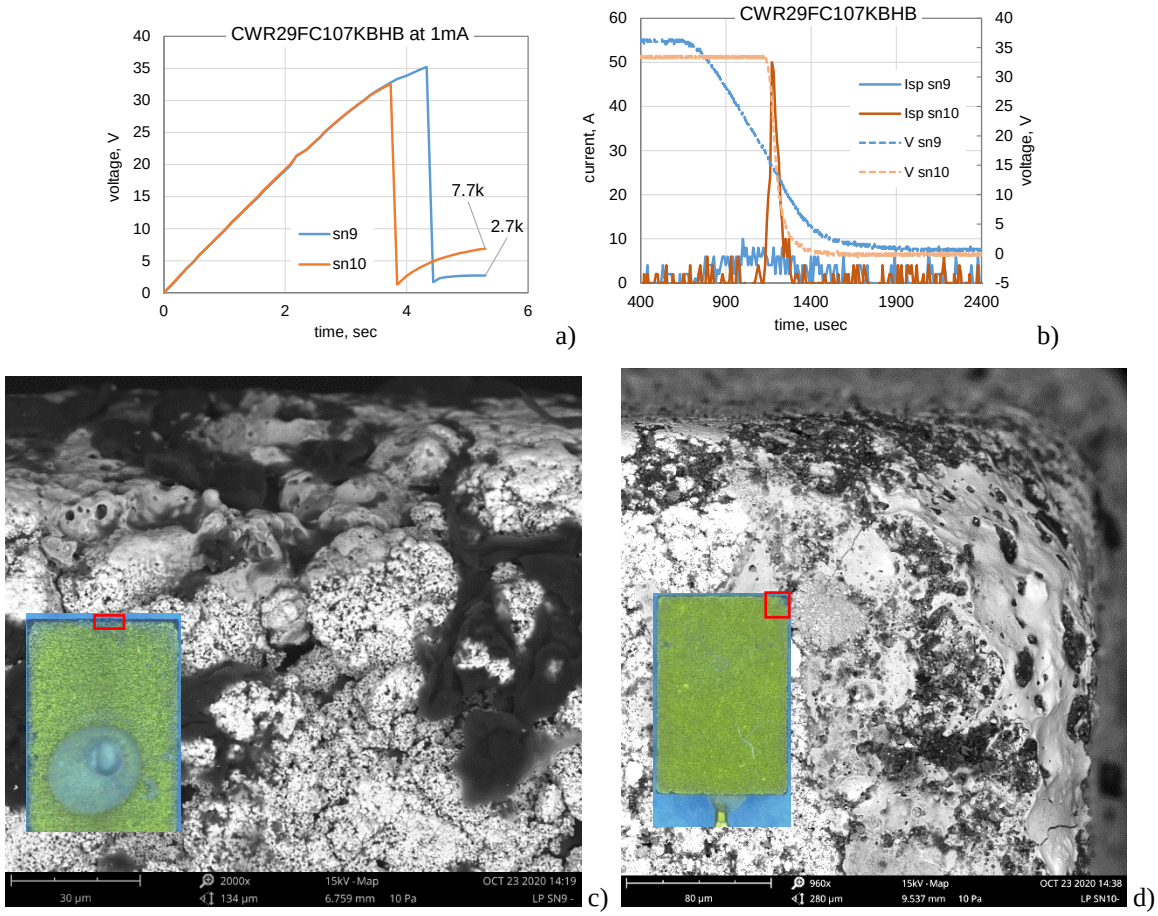

Fig. VI.9. Results of CCS testing (a, b) for SN9 and SN10 of 100 µF 10 V CWR29 capacitors and SEM views of the damaged sites (c-f). Inserts show edg (c) and corner (d) locations of breakdown.

Damaged sites in all cases were located on the surface of the slug and had sizes in the range from 100 to 200 µm. The damaged sites are often located at the edges or corners of the pellets. These sites experience greater mechanical stresses hence greater probability of damaging. For this reason, multi-anode capacitors might have a greater risk of failure compared to the single anode parts. However, this risk most likely will be lower compared to three single anode capacitors connected in parallel.

Evidences of the explosion-like damage caused by scintillation breakdown included formation of voids in the cathode materials (carbon and MnO2 layers) and molten and solidified mixture of tantalum and manganese oxides. Surface areas of the slug at the damage had fused tantalum particles with apparently fused Ta and Mn oxides. However, the sites had no evidences of molten tantalum. In agreement with the accepted self-healing model, elemental EDS analysis showed that the oxygen concentration in the manganese layers at the damaged sites was reduced indicating formation of high-resistive Mn2O3 and Mn3O4 oxides.

VI.2. Polymer capacitors.

Figure VI.10 displays scintillation events during CCS testing for two samples of PB4 47 µF 35 V capacitors that failed hard short circuit at 1 ohm (SN6) and 460 ohm (SN7). Optical and SEM images of the relevant damage sites revealed after chemical deprocessing are shown in Fig. VI.11 and VI.12. Similar to MnO2 capacitors, the damaged areas were located on the surface of the slugs and have a size of ~ 100 µm. Although sample SN6 failed after the first scintillation, it had multiple, at least 5 damaged sites as indicated in Fig. VI.11. Discharge currents in this sample (see Fig. VI.10.b) had at least two spikes, one at the beginning and another at the end of the scintillation process that might be associated with different locations of breakdown. EDS analysis showed the presence of tantalum oxide and traces of carbon and sulfur indicating remnants of the conductive polymer. Excessive amount of silver was detected at the site 5 that was likely due to the molten silver from the silver paint that mixed up with tantalum oxide during scintillation (Fig. VI.11). A similar presence of silver was detected also on the surface of the damage in sample SN7 (see Fig. VI.12).

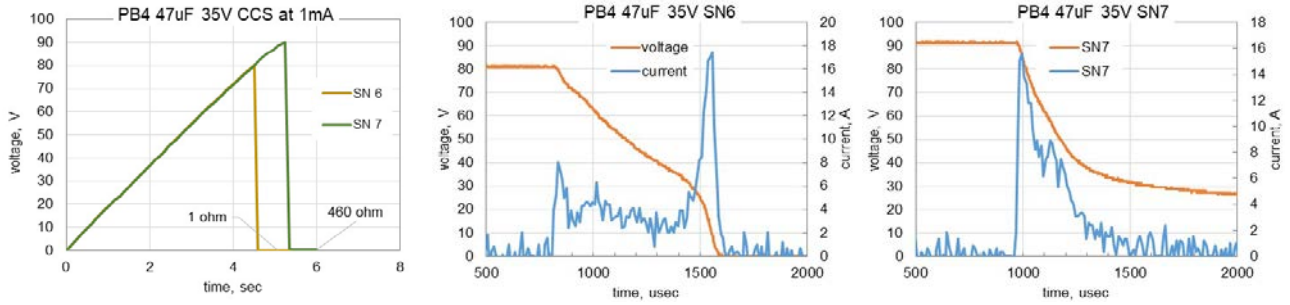

a) b) c)

Fig. VI.10. Results of CCS testing (a) and discharge currents and voltages during scintillation events in SN6 (b) and SN7 (c) of PB4 47 µF 35 V capacitors.

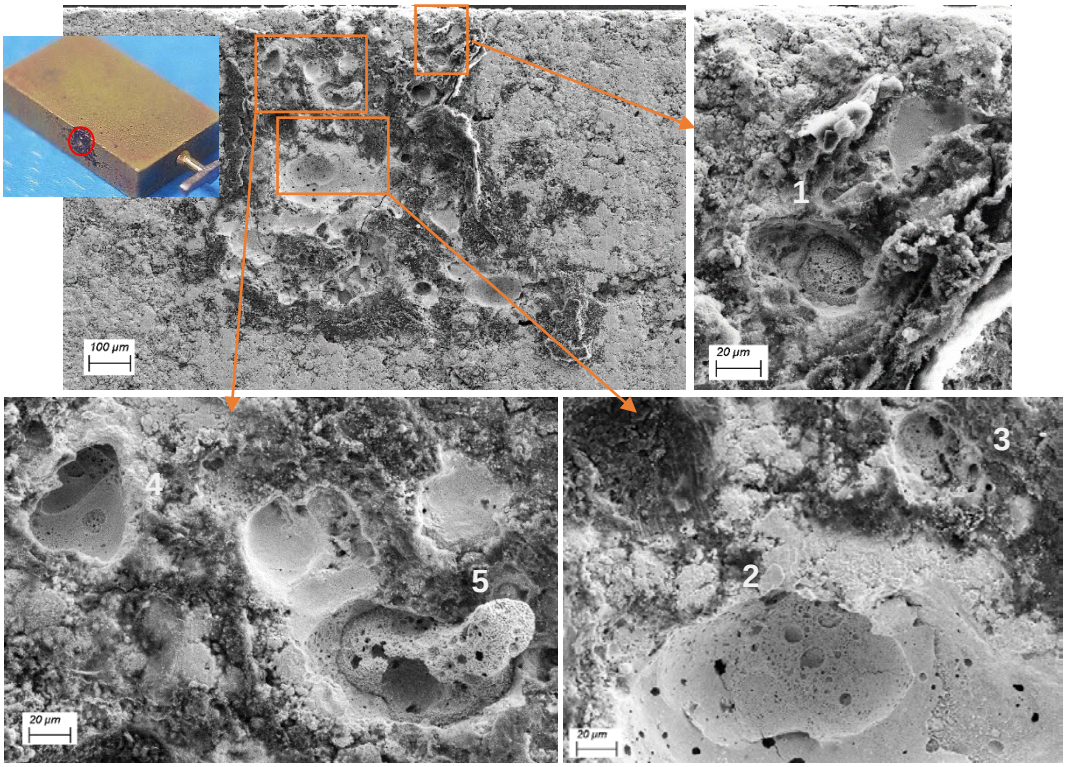

Fig.VI.11. Polymer PB4 47 µF 35 V capacitor SN6 that failed after the first scintillation event at 1ohm. Numbers indicate micro explosion areas that happened during the scintillation. Elemental analysis of area 5 revealed excessive amount of silver.

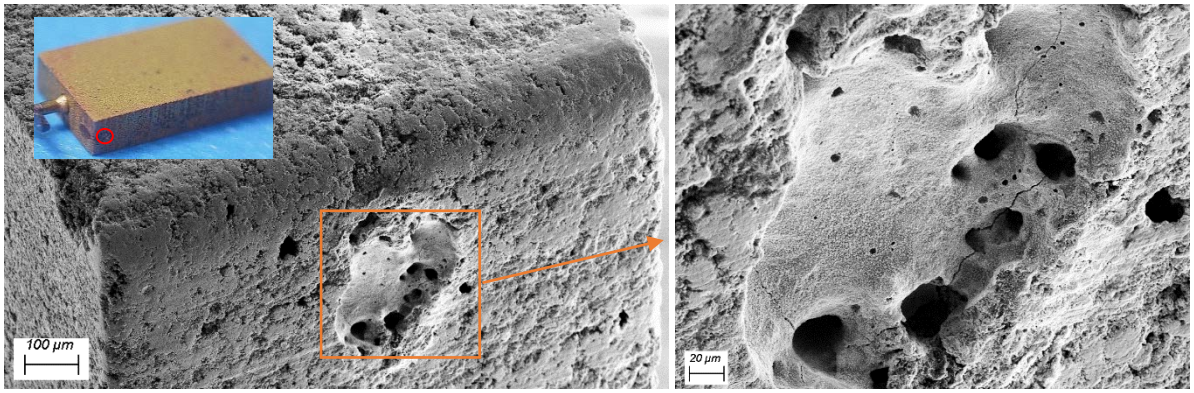

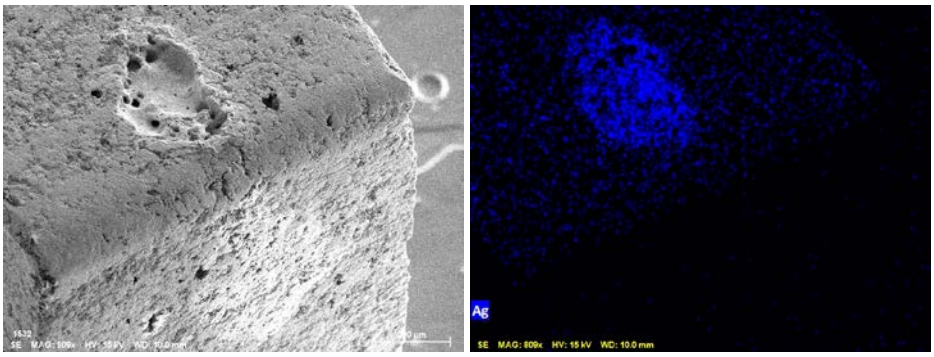

Fig.VI.12. Sample SN7 of polymer PB4 47 μF 35 V capacitors that failed after the first scintillation at 460 ohm. Note that the bottom SEM image and the relevant EDS mapping show the same site as the above images after rotation of the sample. A darkening area on the shoulder that can be seen on the insert corresponds to a lighter area on the bottom SEM image. This area indicates likely another damaged site in the part.

Two samples, SN2 and SN5, of polymer PC9 33 μF 35 V capacitors had increased leakage currents after scintillation testing but were able to reach the rated voltage at milliampere-level currents (see Fig. VI.13). Sample SN2 increased leakage currents to several hundred microamperes after the first test at 0.5 mA (Fig. VI.13.a) and appeared to recover after additional tests at higher charging currents. The scintillation events had durations ~ 1 msec, which is typical for CPTCs, and was associated with ~ 70 μsec discharge current spikes of a few amperes amplitude (Fig. VI.13.b). Sample SN5 also increased leakage currents after the first testing to hundreds microamperes and to milliamperes after the second test (see Fig. VI.13.c). Discharging during breakdown in this part was also similar to SN2 with somewhat greater current spikes reaching ~10 A.

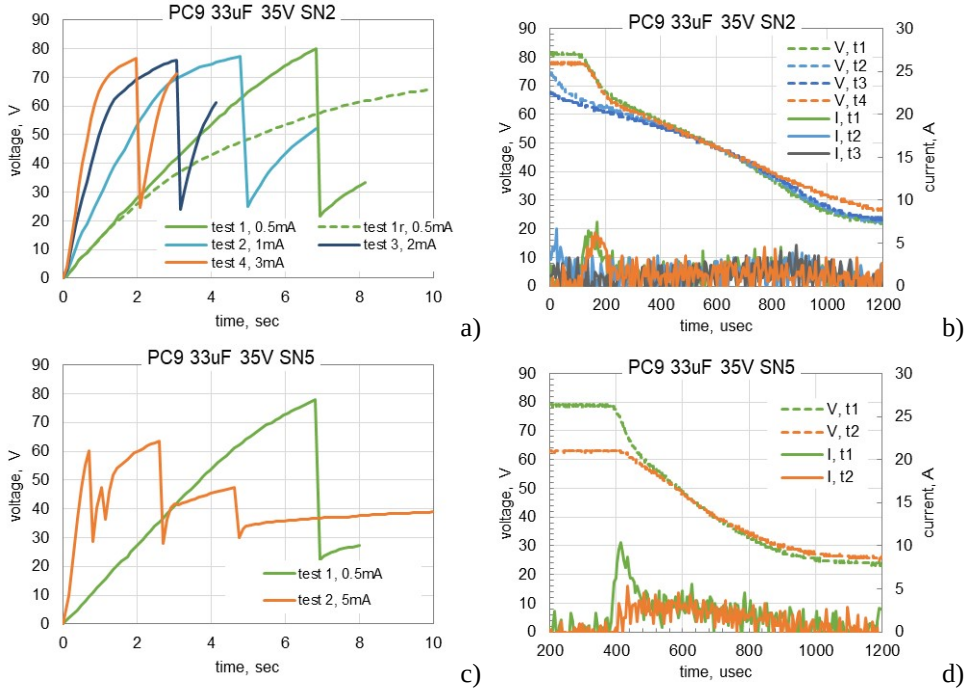

Fig. VI.13. Results of CCS testing for SN2 (a, b) and SN5 (c, d) of polymer PC9 33 μF 35 V capacitors.

Due to a relatively large post-CCS resistances in these samples, IR camera test failed to detect location of the damage. Optical examinations after chemical deprocessing revealed darkening areas as shown in Fig. VI.14 and 15. However, no significant structural defects were detected by SEM examinations.

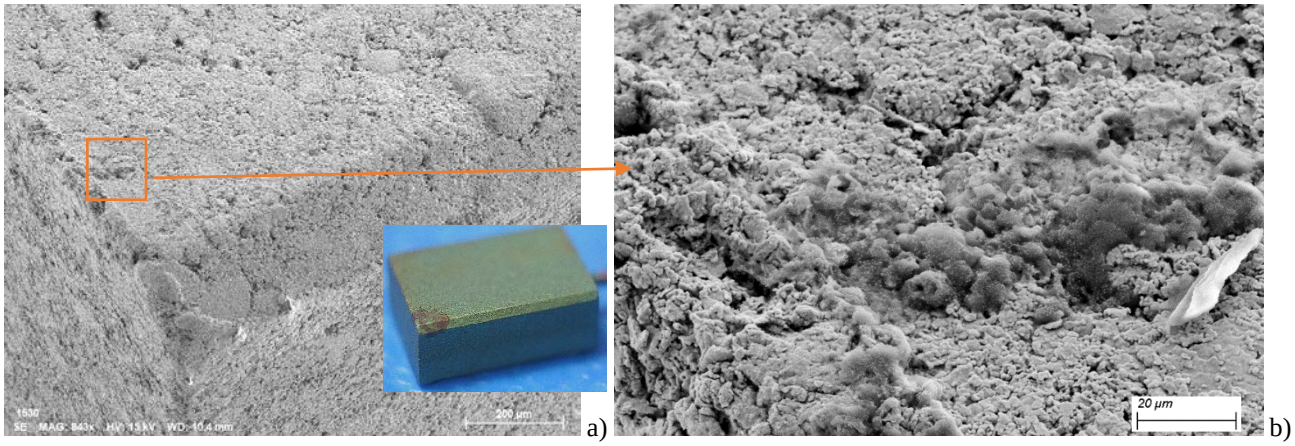

a) b)

Fig. VI.14. PC9 33 µF 35 V SN2 capacitor after deprocessing showing SEM images of the corner area that has darkening on the optical image (insert).

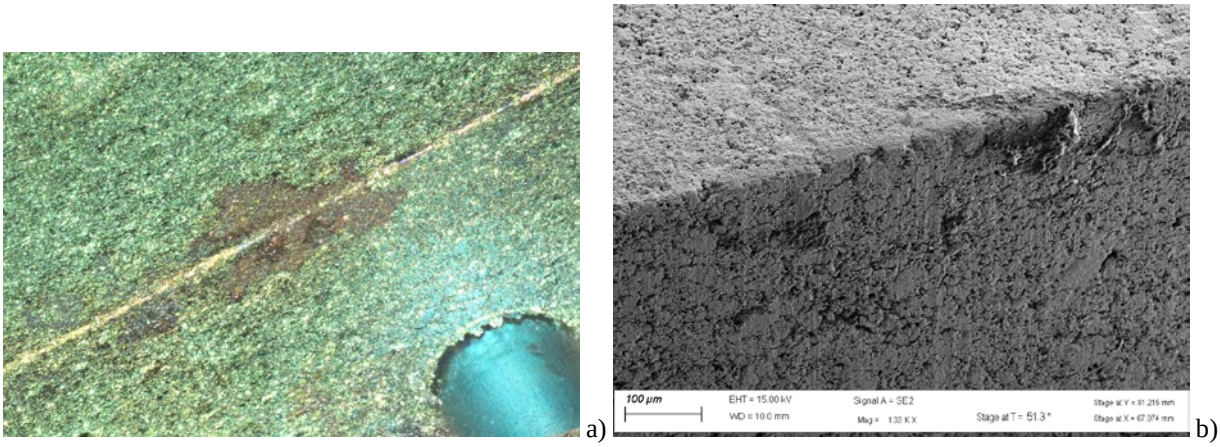

a) b)

Fig. VI.15. Optical (a) and SEM (b) views of PC9 33 µF 35 V SN5 capacitor after deprocessing.

A sample of another type of polymer capacitors, PCM SN4, had similar dark areas on the surface of the pellet after failing short circuit at 0.7 ohm (Fig. VI.16). This part passed the first test without substantial damage but failed the second test that resulted in a 25 A current spike by the end of the discharging process (Fig. VI.16.b). Deprocessing revealed damage at the corner of the slug (Fig.VI.16. c to e). Dark areas observed on this and other samples are apparently remnants of overheated and destructed PEDOT:PSS cathode layer as evident from the presence of sulfur and carbon revealed by EDS analysis (Fig.VI.16. g – h).

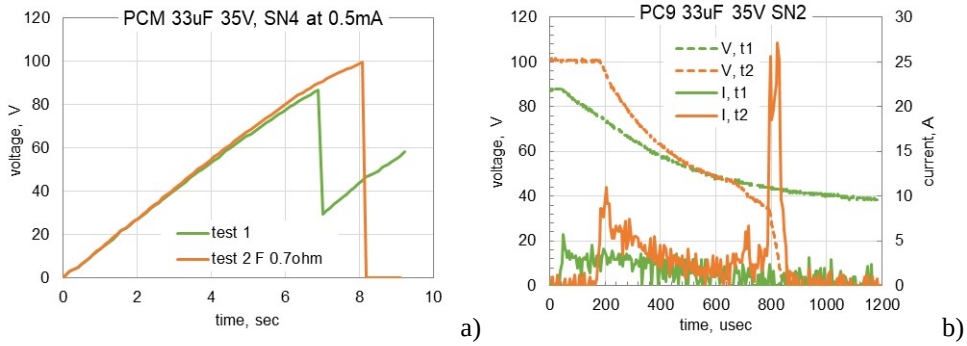

a) b)

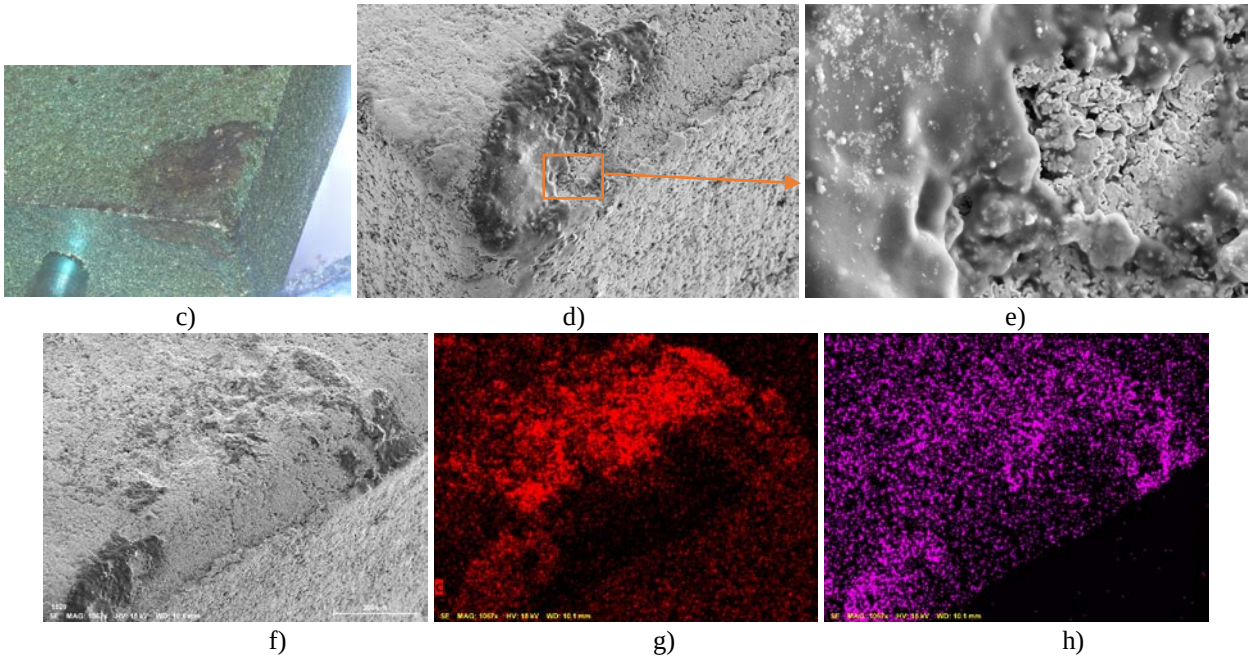

Fig. VI.16. Results of scintillation testing of PCM SN4 33 μF 35 V capacitor that failed shorted at 0.7 ohm after the second CCS test (a, b), optical (c) and SEM (d, e) views of the damaged area after deprocessing. EDS mapping (f - h) shows presence of remnants of a conductive polymer cathode layer.

A more powerful scintillation event with a discharge current spike of 90 A that resulted in a 5 ohm resistance happened in PAQ SN2 capacitor (Fig. VI.17. a, b). Deprocessing of this part revealed substantial damage at a corner of the slug (c, d, e) that also showed up as darkening on the surface of the pellet. The following SEM and EDS analysis revealed presence of sulfur and silver along the periphery of the damage. This indicates that similar to previous cases, a high-temperature event resulted in a destruction of conductive polymer and silver epoxy and fused some elements to the oxide on the surface of the part.

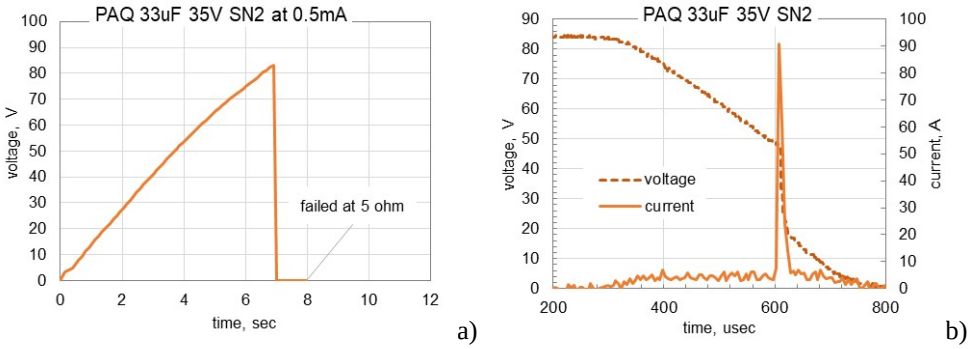

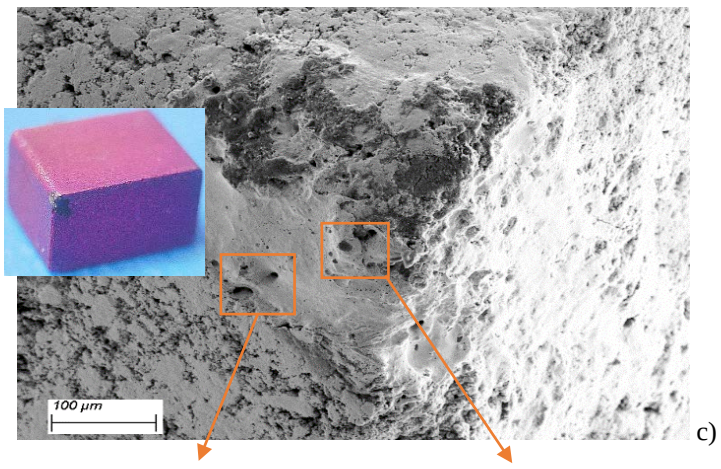

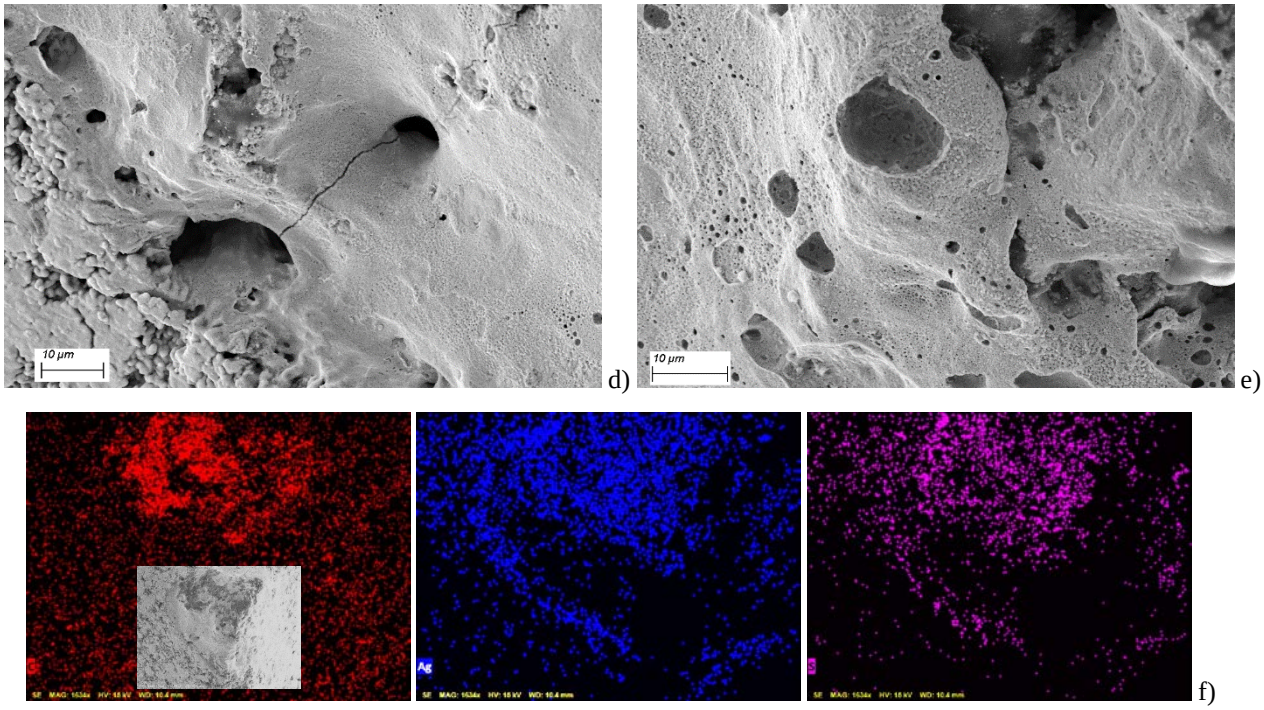

Fig. VI.17. A scintillation event in PAQ 33 µF 35 V, SN2 capacitor (a, b) that resulted in a substantial damage at the corner of the part (c to e). Figure (f) is EDS mapping of an area shown in the insert.

A similar scintillation event in another sample of PAQ capacitors, SN3, have resulted in a 1.7 ohm short as shown in Fig. VI.18. a, b. Following the hot spot detection, the part was cross-sectioned through the damaged site. Cross-sectioning revealed a relatively large, ~300 µm, damage on the surface of the pellet adjacent to a void in the conductive polymer. A comparison of the damaged area of the pellet (Fig. VI.18. e, f) with the bulk areas (Fig. VI.18. g, h) of the same sample suggests intensive oxide diffusion, fusion of the oxidized tantalum particles, and a substantial reduction of the size of pores between particles in the pellet. This fusion was caused by overheating during scintillation that likely resulted in oxide diffusion into tantalum and forming a non-stoichiometric tantalum oxide TaOx, x < 2.5, that might have substantially higher electrical conductivity compared to the stoichiometric Ta2O5 layers.

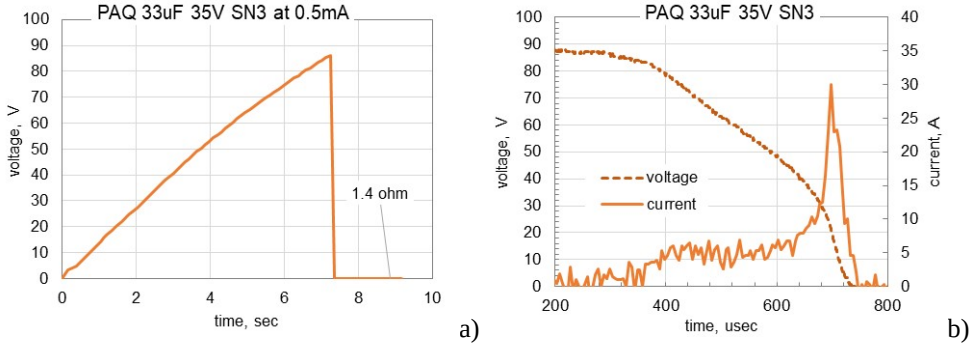

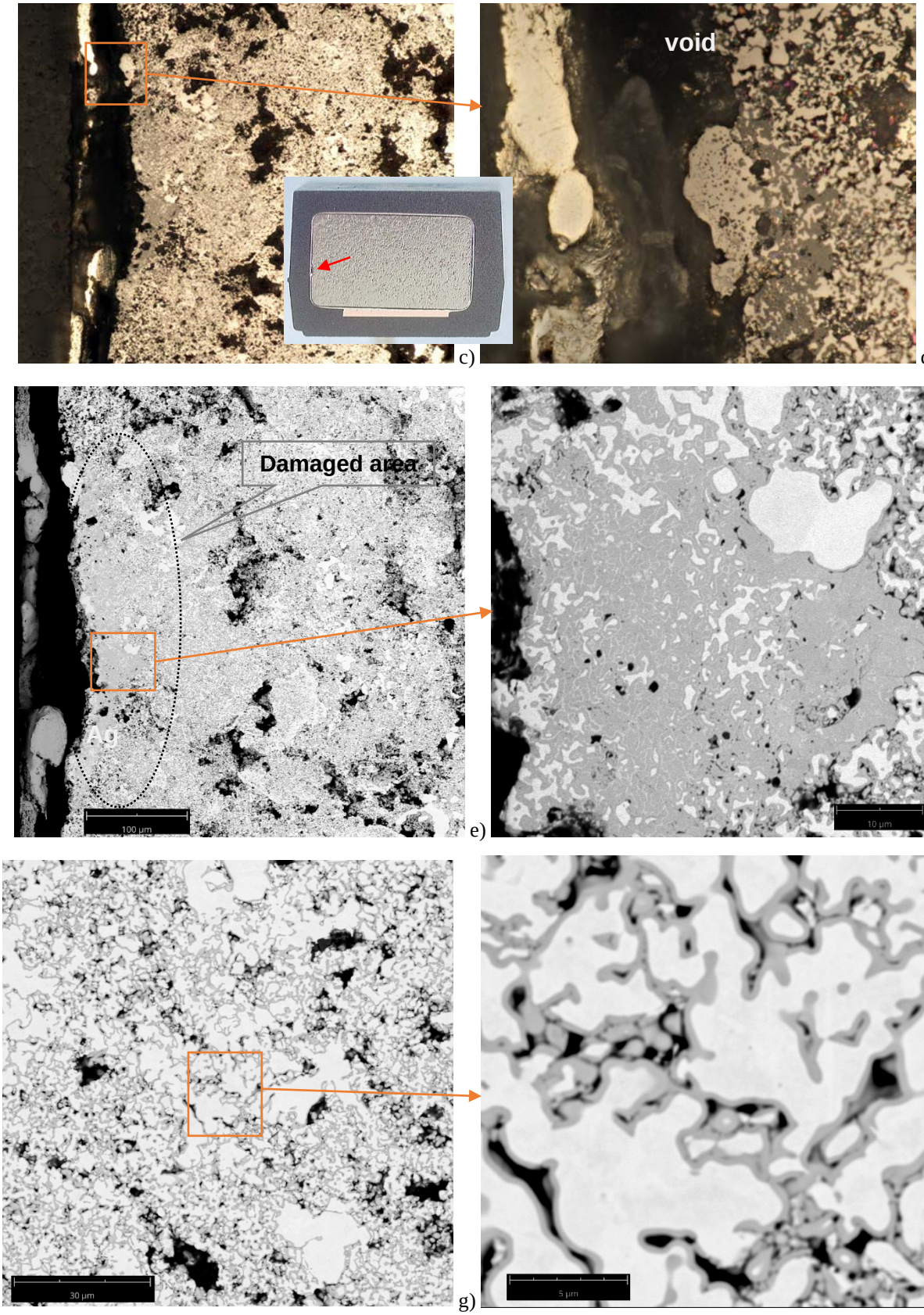

Fig. VI.18. A scintillation event in PAQ 33 µF 35 V SN3 capacitor (a, b), optical (c, d) and SEM (e, f) images of the cross-section across the damaged site. For comparison, figures (g, h) show internal, non-damaged areas of the part. The dark grey areas correspond to Ta2O5 dielectric and black areas are pores in the pellet.

Sample SN5 of PCM 33 µF 35 V capacitors failed at 120 ohm the second scintillation test (see Fig.VI.19. a, b) that resulted in a relatively large, ~0.6 msec discharge current spike with the amplitude in the range from 3 to 4 A. After CCS testing, in an attempt to get I-V characteristic of the damaged capacitor, the part was tested by a high dynamic current power supply at voltages increasing linearly within 3 sec to 35 V. During this testing (see Fig.VI.19. c, d), the currents increased linearly up to ~ 0.1 A at 3.3 V, that corresponds to ~ 33 ohm resistance, and then reduced to the milliampere range apparently due to a low-voltage scintillations and self-healing at the damaged site. As the voltage continued rising, the part experienced a few more scintillation events and finally failed short circuit at 0.4 ohm after ~10 A current spikes at 35 V with duration of dozens of milliseconds.

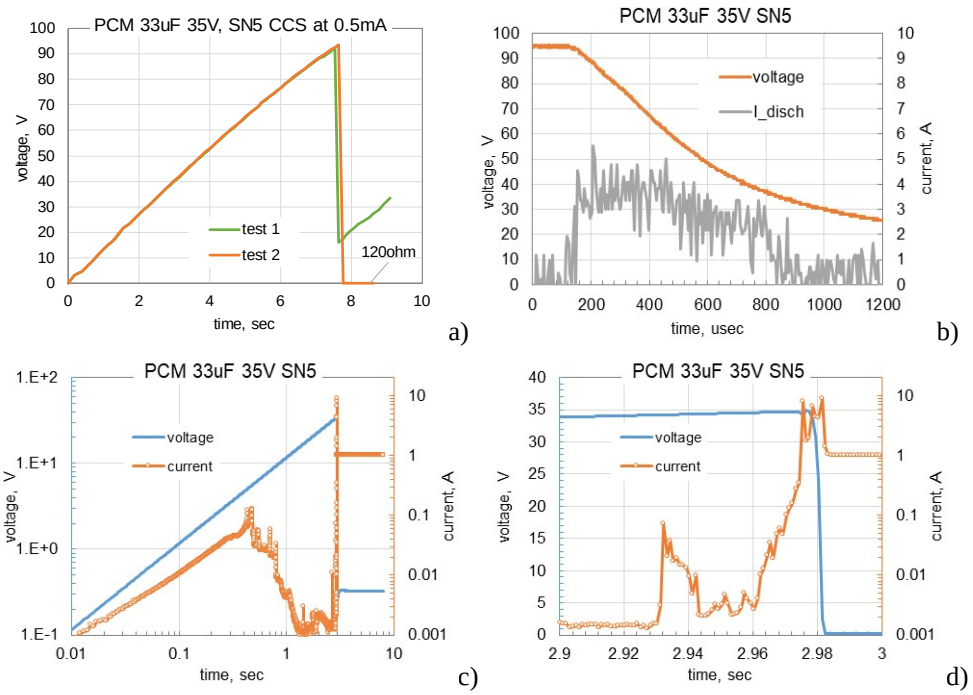

Fig. VI.19. Scintillation events in SN5 of 33 µF 35 V PCM capacitors (a, b) and variations of voltage and current during the following testing using a high dynamic current power supply (c, d). Note that figure (d) shows the same event at ~ 3 sec as figure (c), but with different scales.

IR camera was used successfully to locate the damaged site and Fig. VI.20 shows cross-sectional views of the damage. Similar to previous cases, the damage was located at the surface of the pellet and had a size of ~ 200 µm. SEM examinations revealed evidences of molten tantalum adjacent to large areas of Ta/TaOx mixture formed because of melting and solidification of multiple oxidized tantalum particles comprising the pellet.

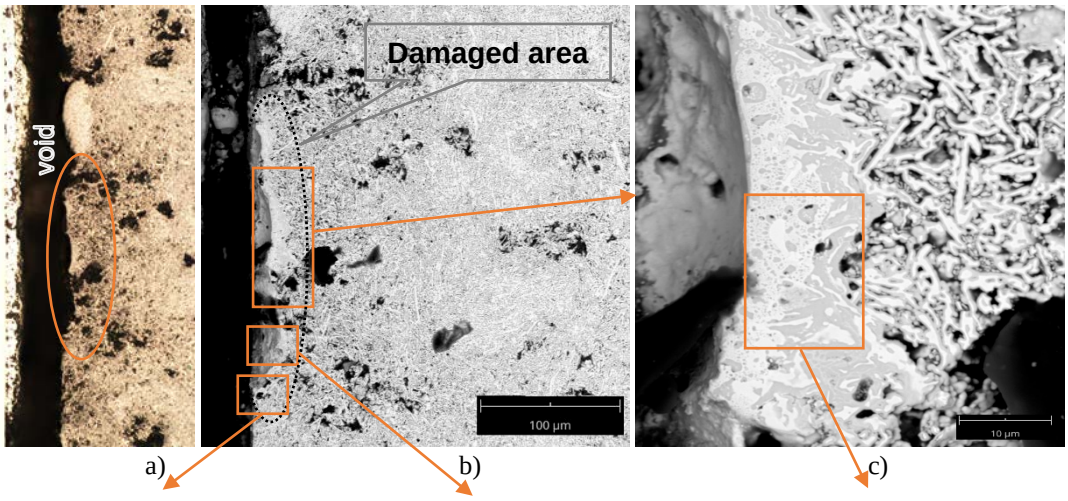

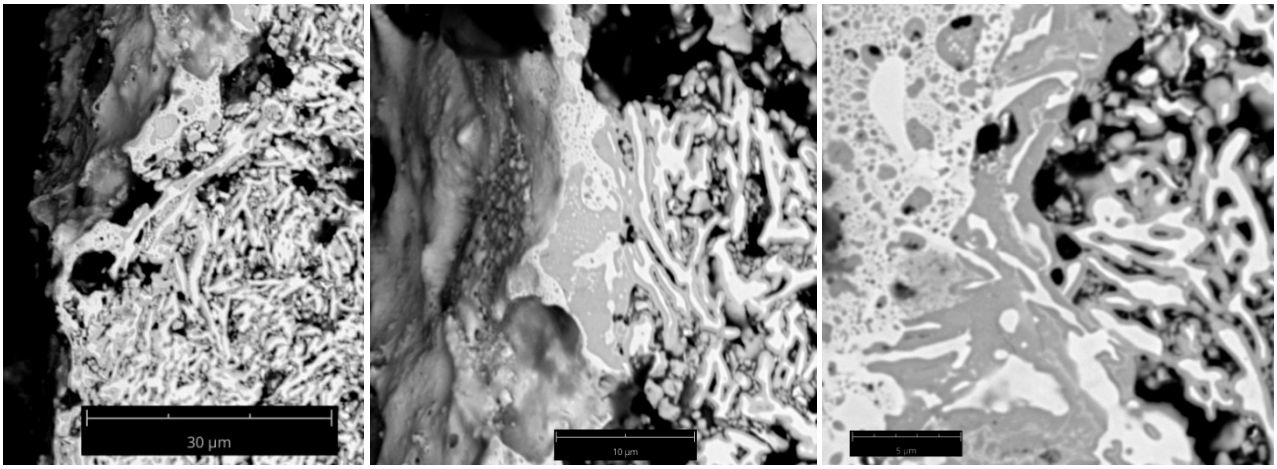

c) d) e)

Fig. VI.20. Cross-section of a 33 µF 35 V PCM capacitor, SN5, that failed short circuit at 0.4 ohm after CCS testing followed by I-V measurements using a high dynamic current power supply..

Results of failure analysis show that most damaged sites in capacitors that failed short circuit after scintillation breakdowns are located on the surface of the pellets. In MnO2 capacitors, reduction of oxygen in manganese layers, which is in agreement with the known self-healing mechanism, was confirmed by EDS analysis of damaged areas. In both types, polymer and MnO2, capacitors scintillations resulted in fusing of oxidized particles on the pellet, formation of large areas of non-stoichiometric tantalum (or Ta/Mn) oxides, and voids in the cathode layers.

VII Discussion

VII.1. Energy of scintillation events.

High current density associated with breakdown can cause local overheating and result in a physical damage to the structure. In case of tantalum capacitors, this might include local melting of tantalum, dissolving of tantalum pentoxide, or degradation/destruction of cathode layers.

The source of energy released during scintillation breakdown is the energy stored in the capacitor itself, E_C, and energy provided by the power supply, E_{PS}, that can be calculated as follows:

$$E_C = {}^{C}/_{2} \times (V_{BR}^2 - V_{min}^2), \quad \text{(VII.1)}$$

$$E_{PS} = \int_0^{W_{PS}} I(t)_{PS} \times V(t)_{BR} \times dt\ , \quad \text{(VII.2)}$$

where C is the capacitance, V_{BR} and V_{min} are maximum and minimum voltages during scintillation, $I(t)_{PS}$ and $V_{BR}(t)$ are the power supply current and voltage across the capacitor during breakdown, and W_{PS} is the width of PS spike.

For rough estimations, the energy delivered by the power supply can be estimated as:

$$E_{PS}' = I_{PS} \times V_{BR} \times W_{PS}\ , \quad \text{(VII.2.a)}$$

where I_{PS} is an average PS current during the spike.

As was shown in section III, breakdown voltages for both types of capacitors increase approximately proportionally to the rated voltage, $V_{BR} \approx 2.7 \times VR$. However, MnO2 capacitors are typically discharging by scintillations completely, so $V_{min} \approx 0$, whereas the minimal voltage for polymer capacitors increases with VR, $V_{min} \approx 0.5 \times VR$.

As was shown in section II, current spikes produced by a power supply source depend on its dynamic characteristics. For Keithley 2400 that was used in most experiments, the current spike amplitude was constant, I_{PS} = 0.22 A, and W_{PS} increased linearly with breakdown voltage: $W_{PS} = 1.56 \times VBR - 41.9 = 4.21 \times VR - 41.9$, where W_{PS} is in µsec.

Results of calculations of E_C and E_{PS}' for capacitors from 3.3 µF to 330 µF rated to different voltages are shown in Fig. VII.1. The energy of scintillation events varies from 0.1 mJ for 4 V 3.3 µF capacitors to more than 300 mJ for 330 µF 16 V capacitors. For the same rating, E_C for MnO2 capacitors is only ~ 4% greater than for polymer capacitors.

The energy of scintillation events that comes from discharging capacitors is orders of magnitude greater than from the power supply, and even for relatively low value, 3.3 μF capacitors rated to 4 V, it is more than an order of magnitude greater than E_{PS}.

The current in the damaged area is the sum of the internal, or discharge current of the capacitor and external current provided by the power supply. When the level of breakdown current is high enough, local overheating is substantial to trig extensive generation of oxygen from MnO2 cathode, start the exothermic reaction of tantalum oxidation and self-ignition. The latter is enhanced when the size of tantalum particles in the pellet is small. For this reason, large value (greater than 100 μF) MnO2 capacitors can ignite even when powered up with current limiting resistors or by a PS with low limiting currents (see examples in Fig. IV.8). In this regard, large CV value CPTCs are more reliable compared to MnO2 cathode capacitors.

The assessment of the possible damage size, *r*, caused by scintillation breakdown can be made for adiabatic conditions. At these conditions, the whole discharge energy goes for heating up of a certain volume of the pellet that can be represented by a sphere of radius *r*. Increasing temperature of this sphere by ΔT requires energy *Q*:

$$Q = v \times \rho \times c \times \Delta T \quad , \qquad \text{(VII.3a)}$$

where *v* is the volume of the sphere, ρ is the specific density, and *c* is the specific heat capacity of the pellet. When the temperature rise exceeds the melting point for tantalum, additional energy is required for fusing, and the heat energy can be calculated as:

$$Q = v \times \rho \times (c \times \Delta T + C_f) \quad , \qquad \text{(VII.3b)}$$

where C_f is the heat of fusion.

Characteristics of materials used for calculations per Eq.(VII.3) are shown in Table VII.1. The table shows also critical temperatures associated with different structural and phase changes in the materials: melting temperature of tantalum, 3017 ºC, melting of Ta2O5, 1870 ºC,which is close to the sintering temperature during formation of the pellet, decomposition or oxygen reduction of MnO2, 535 ºC, and decomposition of conductive polymer, 290 ºC. The latter value was determined in [20] using thermogravimetric analysis (TGA) and Differential scanning calorimetry (DSC) of different PEDOT-based compositions used as cathode materials in tantalum capacitors.

Estimations show that the amount of heat necessary to increase temperature of the dielectric and cathode layers is negligible compared to the one that is required to heat-up the tantalum.

Table VII.1. Characteristics of materials used

Characteristic	unit	Ta	Ta2O5	MnO2	polymer
specific heat capacity, *c*	J/(kg×K)	140		630	
specific density, ρ	g/cm^3	16.7	8.2	5	~1
heat of fusion, C_f	J/kg	175.6			
Thermal conductivity, *k*	W/(m×K)	58		0.2-0.5	~0.2
Critical temperature	ºC	3017	1870	535	290

The energy required to melt a sphere of tantalum of radius *r* (Q_Ta), reach the temperature that would cause melting of tantalum oxide (Q_TaO) or cause decomposition of manganese oxide (Q_MnO) or polymer (Q_polym) is shown in Fig. VII.1b. The energy required to reach melting point for tantalum is substantially greater than the additional energy necessary for melting, so Q_TaO is only ~40% less than Q_Ta. However, the energy required to reduce oxygen in MnO2 or damage conductive polymer is much less than the energy necessary to heat up the pellet to the melting point of tantalum. For MnO2 capacitors, it is 17% of Q_Ta and for polymer 9% of Q_Ta.

The energy dissipated during scintillation breakdowns is sufficient to damage a relatively large area of the pellet. A 33 μF 35 V capacitor can store ~150 mJ and bring a sphere of tantalum with a size of ~200 μm to the melting temperature. This energy is also sufficient to reach temperature necessary to reduce oxygen in MnO2 or destruct polymer cathode with a sphere of $r > 300$ μm. These estimations are in reasonable agreement with results of failure analysis in section VI, where in most cases, damages had a size in the range from 100 to 200 μm.

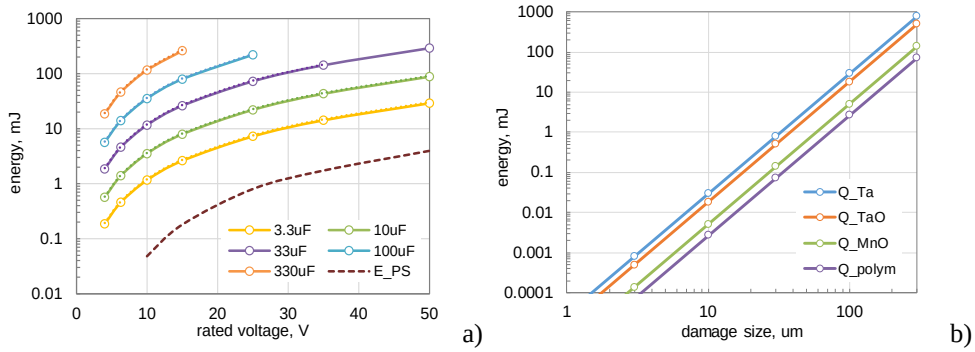

Fig.VII.1. Variations of the discharge energy for capacitors rated from 3.3 to 330 μF and voltages from 4 to 50 V (a) and relationship between the energy necessary to heat up damage to the critical temperature and the size of damage (b). The dashed line in figure (a) indicates the energy provided by Keythley 2400 power supply. Different lines in figure (b) correspond to energy required to melt tantalum (Q_Ta), melt oxide (Q_TaO), reduce oxygen in MnO2 (Q_MnO), or decompose conductive polymer (Q_polym).

VII.2. Discharge times during scintillations.

Due to energy losses, the size of the damage can be substantially less than estimated above. Apparently, the faster the voltage discharge during scintillation the closer thermal processes to adiabatic conditions. The rate of capacitors' discharge can be estimated based on the value of ESR. A charged capacitor shorted externally will decrease voltage with time exponentially with the characteristic time $\tau = C \times ESR$. Considering that the same value polymer capacitors have much lower ESR compared to MnO2 capacitors, the characteristic times will reduce respectively. For example, median ESR values for 10 μF to 47 μF capacitors rated to 35 V used in this study are within 20 to 30 mohms for polymer and from 100 to 200 mohms for MnO2 types. Respectively, the range of τ is ~ 0.2 to 1 μsec for polymer and ~ 2 to 10 μsec for MnO2 capacitors. However, measurements of the discharge width were 2 to 3 orders of magnitude greater than τ. More than that, these values for polymer were substantially greater than for MnO2 capacitors.

This discrepancy can be explained considering difference in discharge conditions for a capacitor shorted externally, and internally, as in the case of breakdown. Schematics in Fig. VII.2 illustrate these two cases. For a capacitor shorted externally, the discharge occurs in all areas of the pellet and the current is accumulated along the whole surface in the cathode layers. In this case, the transient currents flow is similar to AC currents and the effective resistance is determined by ESR. During breakdown, the current flow is restricted by a small area of the damaged site and R_{disch} is significantly greater than ESR, hence the duration of the scintillation events, $Wid = C \times R_{disch}$, is substantially larger than the discharge time, τ.

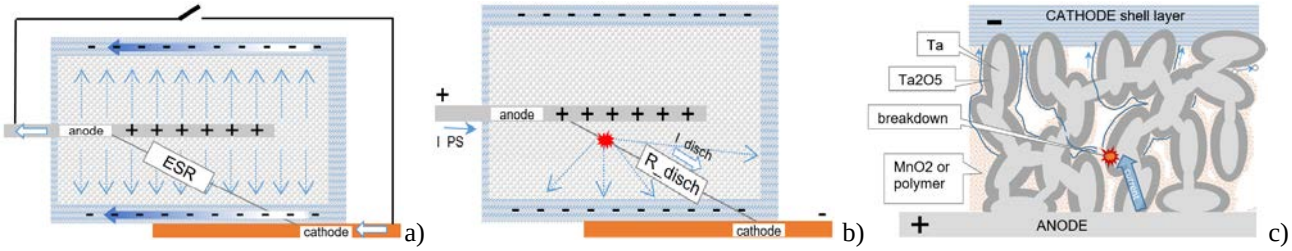

Fig. VII.2. Discharge in a tantalum capacitor during an external (a) and internal (b) shorts. Figure (c) illustrates currents flowing along the cathode layers inside a capacitor during breakdown.

The discharge resistance, R_{disch}, can be estimated as a constriction electrical contact resistance of a circular area between two contacting semi-infinite materials: tantalum on the one side and MnO2 or conductive polymer on another. For small contact sizes, r, the constriction resistance can be calculated using a modified Holm's equation:

$$R_{disch} = \frac{1}{4r}\left[\frac{\rho_{Ta}}{(1-\gamma)} + \frac{\rho_{cat}}{\gamma}\right], \qquad \text{(VII.4)}$$

where ρ_{Ta} and ρ_{cat} are specific resistances of the tantalum and cathode materials, and γ is the porosity of the pellet. The resistivity of tantalum, $\rho_{\_Ta}$ = 1.3E-5 ohm_cm, is more than 4 to 5 orders of magnitude below the cathode

materials, $\rho_{\_cat}$ = 1 to 10 ohm_cm for MnO2 capacitors and 0.1 to 1 ohm_cm for polymer capacitors. Considering that γ is typically ~0.5, the contribution of tantalum resistance to R_{disch} can be neglected.

Variations of R_{disch} calculated per Eq.(VII.4) at γ = 0.5 with the damage size are shown in Fig. VII.3. Values of R_{disch} for micrometer size damage are relatively large, in the range from 0.5 to 50 kiloohm. This means that a substantial portion of the discharge energy will be lost for heating of areas outside the breakdown site. For this reason, formation of small size damage with r < ~ 10 μm in the bulk of the pellet during scintillation events, is unlikely.

Analysis of possible damage size was done in an assumption of adiabatic conditions. This assumption might be reasonable at fast enough events when a time for the temperature spreading over the region is comparable with the duration of the event. The characteristic time of heat diffusion across a sphere of radius r can be estimated as:

$$\theta = {r^2}/{\alpha}\,, \qquad \text{(VII.5)}$$

where $\alpha = {k}/{\rho \times c}$ is the thermal diffusivity. This characteristic indicates the rate at which a temperature variation propagates through the material. Based on estimations for composite materials [21], the value of α for a tantalum pellet with the porosity γ = 0.5, *is* ~ 1.2E-5 m^2/sec. Variations of θ with r (see Fig. VII.3) show that scintillation events in the range from 0.1 to 1 msec might result in adiabatic heating for the damage size in the range from 50 to 100 μm, which is close to the sizes of damages revealed by failure analysis. This confirms that adiabatic conditions can be used for analysis of thermal processes for scintillation events.

Assuming that pores of the slug are completely filled with cathode materials and γ = 0.5, variations of R_{disch} with the size of damage calculated per Eq.(VII.4) are shown in Fig. VII.3. Based on the duration of scintillations for 33 μF 35 V capacitors (*Wid* ~1 msec for polymer and ~0.1 msec for MnO2 capacitors), the value of R_{disch} is ~ 30 ohm for polymer and 3 ohm for MnO2 capacitors. This corresponds to the damage size of 15 to 150 μm for polymer and more than 1 mm for MnO2 capacitors. The latter size is comparable with the size of the slug and is not realistic. Also, according to these estimations, R_{disch} , hence duration of the scintillation events for MnO2 should be greater than for polymer capacitors, which does not agree with experimental data.

Equation VII.4 is applicable in the assumption of a contact between two semi-infinite materials. This assumption might be used if pores in the slug are filled with cathode materials, MnO2 or conductive polymer. In a case when cathode layers inside the pores are thin, the current will flow along the surface of the pores as shown in Fig. VII.2.c, and actual resistance will be much greater than the one estimated per Eq.(VII.4). To explain this discrepancy, we need to consider actual internal structure of the capacitors.

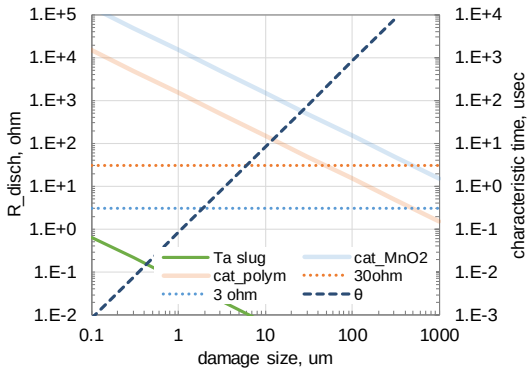

Fig. VII.3. Calculated per Eq.(VII.4) discharge resistance at different damage sizes. The dotted lines corresponds to the resistance values calculated for 33 μF 35 V capacitors based on typical durations of the scintillation events. The dashed line is the characteristic time of heat diffusion calculated per Eq. (VII.5).

VII.3. Internal structure of the pellet in MnO2 and polymer capacitors.

Examples of internal views of cross-sectioned MnO2 and polymer capacitors are shown in Fig. VII.4 and V.II.5. Apparently, the thickness of cathode layers covering pores of the pellets is much greater for MnO2 than for polymer capacitors. For this reason, the assumption that the cathode material fills pores completely might be reasonable for MnO2, but is not realistic for polymer capacitors. At the size of pores of a few micrometers and the thickness of

polymer coating below 0.1 μm, the effective resistivity of the cathode material in pores will be 10 to 100 times greater than the resistivity of PEDOT:PSS (0.1 to 1 ohm_cm). At these conditions, the value of R_{disch} for polymer will increase above the one for MnO2 capacitors. This explains one of the reasons for greater discharge times of scintillation events for polymer than for MnO2 capacitors.

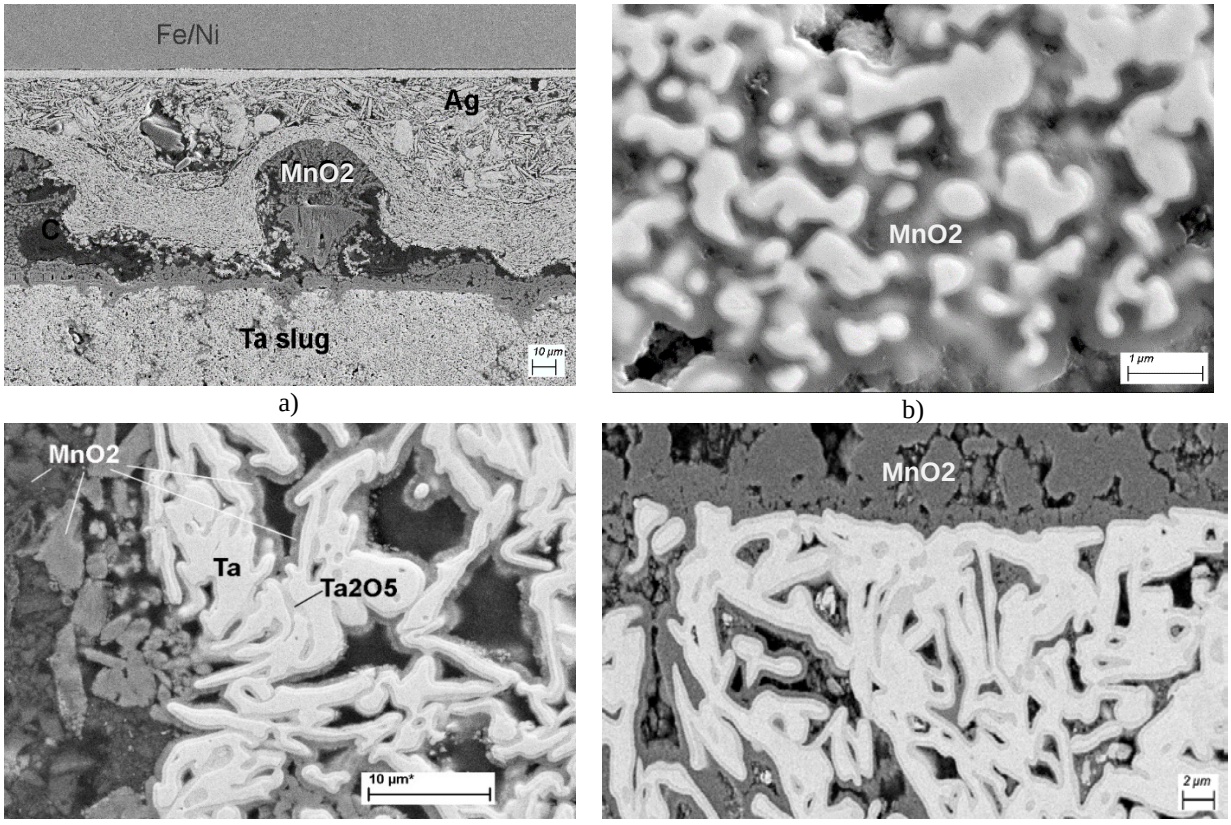

Fig. VII.4. Cross-sectional views of MnO2 capacitors showing that pores in the pellet are almost completely filled with the cathode material. (a, b) 220 μF 10 V, Mfr.B; (c) 10 μF 35 V, Mfr.A; (d), 6.8 μF 35 V, Mfr.C. The thickness of MnO2 layers in the pores is typically ~0.5 to 1 μm.

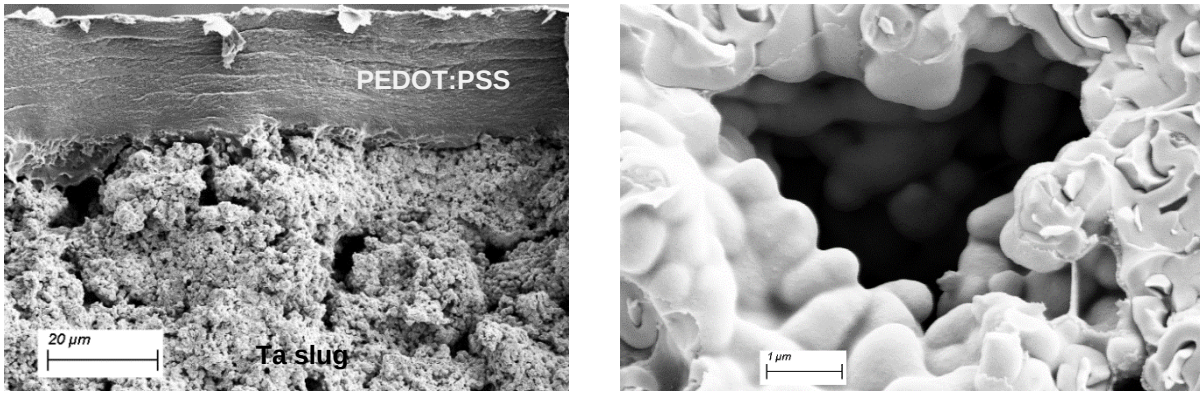

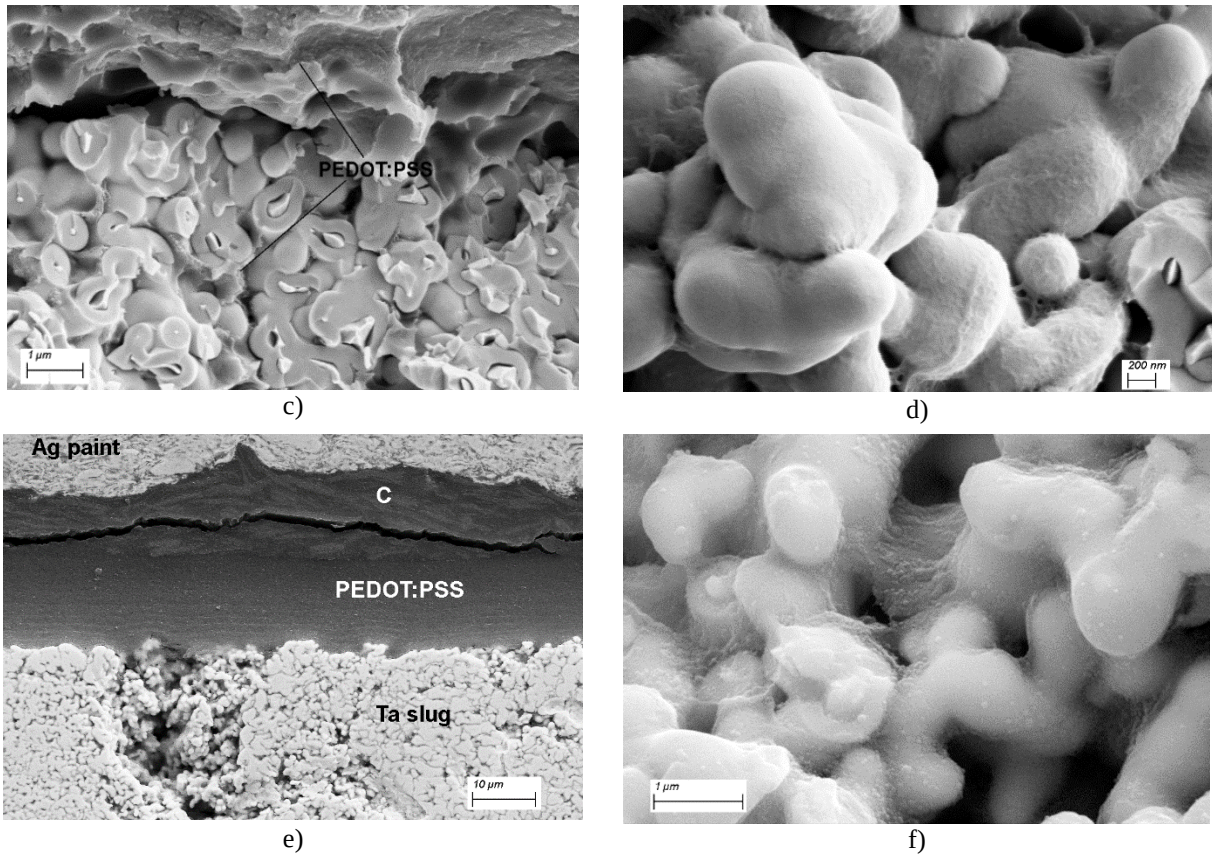

c) d) e) f)

Fig. VII.5. Internal views of 33 μF 35 V from Mfr.C (a – d) and 15 μF 35 V from Mfr.A (e, f) polymer capacitors showing that the thickness of conductive polymer in pores is below ~ 0.1 μm.

VII.4. Power of scintillation events.

The severity of the damage depends on the temperature rise in the breakdown site that in turn is controlled by the power dissipated during the scintillation. The power of scintillation is a product of the discharge current and voltage across the capacitor that was detected experimentally by oscillograms of the events:

$$P(t) = C \times V(t) \times \frac{dV(t)}{dt}. \qquad \text{(VII.6)}$$

Results of these calculations for several types of MnO2 and polymer capacitors are shown in Fig. VII.6. As discussed before, damaging scintillations are often associated with a sharp voltage decrease resulting in high current spikes. The amplitudes of power during these spikes vary from hundreds of watts to dozens of kilowatts, and their duration is in the range from 2 to 5 μsec. The less powerful spikes that did not cause shorting failures had typically amplitudes below a few hundreds of watts and durations from 10 to 100 μsec.

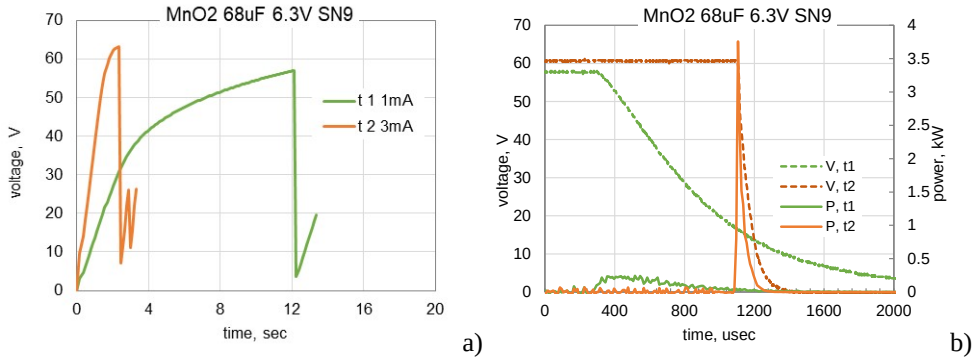

a) b)

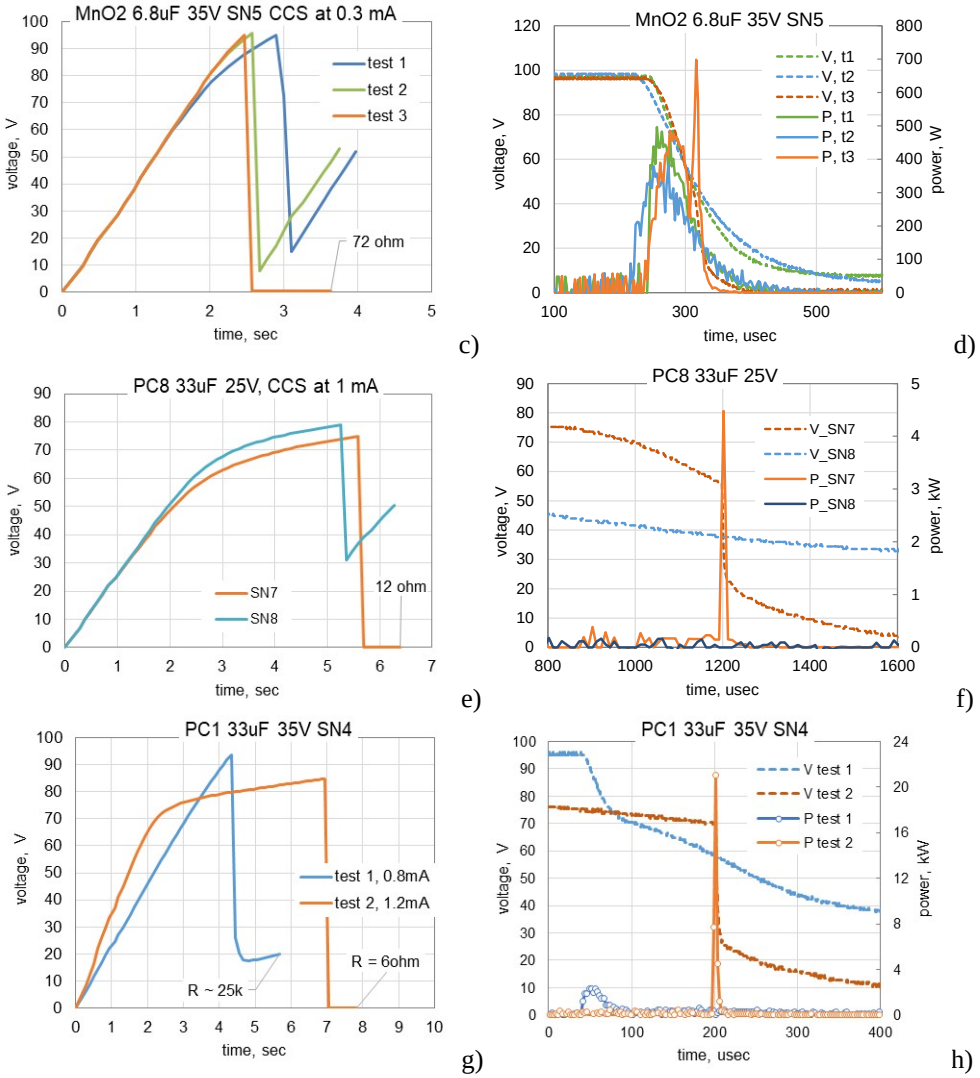

Fig. VII.6. Examples of CCS testing (left charts) and variations of voltage and power during scintillation events (right charts) for different MnO2 (a to d) and polymer (e to h) tantalum capacitors.

A simple one-dimensional model allows for the assessment of temperature on the surface of a sample that experienced an instant energy pulse. For a power pulse amplitude P_0 and duration Δt, the peak temperature rise of the surface of in adiabatic conditions is [22]:

$$\Delta T = \frac{P_0 \Delta t^{0.5}}{\pi r^2 (\gamma \pi k \rho c)^{0.5}}, \qquad \text{(VII.7)}$$

At the porosity $\gamma = 0.5$ and materials' characteristics for tantalum shown in Table VII.1, results of ΔT calculations for different power of scintillation breakdown and damage size are shown in Fig. VII.7. For a given size of the damage, same energy spikes ($P \times \Delta t = const$) result in substantially greater temperatures for shorter spikes. For example, one kilowatt 3 μsec spike can increase temperature of a 100 μm site up to 4000 ºC, whereas for a spike of 100 W with duration of 30 μsec the temperature rise will be ~ 1000 ºC. Melting of tantalum can be expected in the first case, whereas only reduction of oxygen in MnO2 or decomposition of polymer can be expected in the second case. Also, longer spikes allow for more energy losses and make adiabatic conditions, hence applicability of Eq.(VII.7), less acceptable.

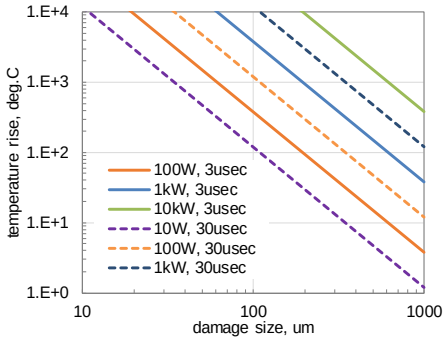

Fig. VII.7. Maximum temperature at the damaged site on the surface of the pellet for power spikes with different amplitudes and durations.

As was discussed above, the in-bulk location of damage will have a large constriction resistance that would limit the power dissipated at the breakdown site substantially, thus making damage very unlikely. Obviously, defect sites at the surface of the pellet would have much lesser constriction resistances. This explains results of failure analysis showing that in all cases the damage was located at the surface of the pellet. At a thickness of the cathode shell layers from 10 to 20 μm and resistivity of the cathode material from 0.1 to 10 ohm_cm, the constriction resistance of a 100 to 200 μm damage will be from 0.3 to 300 ohm. This is more than an order of magnitude lower than for the bulk location of the damage.

Obviously, total resistance of a damaged capacitor is a sum of the constriction resistance and the resistance of the damage site itself. Considering increasing resistance of the damaged site after oxygen reduction in MnO2, this additional resistance might be large enough for MnO2 capacitors. A substantial increase of the resistance might occur in both MnO2 and polymer capacitors if a decomposition of the cathode layers results in a large enough void capping damaged.

VII.5. Mechanism of breakdown.

Processes of polymer cathodes formation occur at much lower temperatures (≥ 180 ºC) compared to MnO2 cathodes that are formed by pyrolysis of manganese nitrate at temperatures in the range from 250 to 350 ºC. At high temperatures required for MnO2 formation, significant concentration of oxygen vacancies at the Ta/Ta2O5 interface is generated. Also, high-temperature processes create greater mechanical stresses, hence generate more defects in the Ta2O5 dielectric compared to polymer cathodes. This might explain tighter distributions of breakdown voltages in CPTCs compared to MnO2 capacitors. A higher concentration of defects and oxygen vacancies in MnO2 than in polymer capacitors, hence greater concentration and size of the filaments, explain a faster, more powerful, and more complete ($V_{min} \approx 0$) discharge in MnO2 capacitors during scintillation events.

Based on results of section V, all scintillation events in both types of capacitors, including those that passed CCS testing without damage, resulted in increased leakage currents. This behavior can be explained considering processes in Ta2O5 dielectric layers at high, close to breakdown voltages. At high electric fields, an intensive growth of conductive filaments in the Ta2O5 dielectric of both types of tantalum capacitors occurs. This process is similar to the one responsible for switching and operation of the resistive elements formed by thin tantalum oxide structures that have been extensively studied for the last decade for development of high-efficiency redox-based resistive random access memory (ReRAM) microcircuits [23-26]. It is commonly accepted that the switching behavior in these structures is related to reversible formation and rupture of nano-size filaments composed of oxygen vacancies (V_O).

Typically, ReRAM elements are prepared by means of atomic layer deposition, chemical vapor deposition, or reactive sputtering of tantalum in oxygen containing atmosphere that results information of nanometer size layers of tantalum oxide structures [24]. Elements with thicker tantalum oxide layers have been shown also to have a similar switching behavior. In [27], 100 nm Ta2O5 layers were deposited via radio frequency(RF) sputtering to produce Ag/Ta2O5/Pt switching elements. In these structures, silver ions in addition to V_O participated in the formation of the filaments that were directly observed by the transmission electron microscopy (TEM), energy dispersive spectrometry (EDS) and electron energy loss spectroscopy (EELS) techniques. High humidity enhanced migration of silver ions allowing formation of conductive filaments at lower voltages. A review of high-spatial resolution spectroscopic techniques

that have been used to get insights into the filament formation and the corresponding structural and chemical changes in different types of filamentary-switching oxides, including Ta2O5 are described in [28].

Structures with a relatively thick, 20 to 40 nm Ta2O5 layers operating at voltages from 10 to 20 V were formed by anodic oxidation of tantalum in [29]. Results of this work suggest that processes in tantalum capacitors and ReRAM elements using Ta2O5 dielectric are similar. However, electrochemically grown Ta2O5 layers are more dense and less porous compared to the sputtered films and are less sensitive to the presence of moisture.

In a simplified form, the mechanism of filament formation and operation of ReRAM elements can be described as follows. At a positive bias on tantalum, oxygen ions are dragged to the anode leaving oxygen vacancies in the oxide. As a result, vacancies start accumulating at some locations at the cathode surface forming sites from which conductive filaments are growing. At a negative bias on tantalum, oxygen ions move back and recombine with the vacancies thus resetting the element and switching it from a low- to a high-resistive mode. In thin Ta2O5 oxide layers, the filament growth occurs within dozens of nano-seconds at a few volts bias. In particular, devices based on the electrochemically grown tantalum oxide show the SET switching times of 20 ns and RESET times of 165 ns [29]. In general, switching times in different types of ReRAM elements decrease exponentially with the set or reset voltage [30].

The formation of filaments is a stochastic process and multiple filaments in Ta2O5 elements with different diameters are likely formed [31]. The switching can also occur at the same polarity of the bias as the setting process if the applied voltage is high enough to generate sufficient amount of joule heating and destruct the filaments thermally [32].

Simple Ta/Ta2O5/Me structures do not endure multiple switching cycles because oxygen ions can move deep into tantalum and the reversibility of the processes in such elements is poor. A substantial improvement in reliability was achieved by introducing thin, nanometer-size layers of oxides that play a role of a buffer zone capable to easily accumulate or release oxygen ions. These layers can be formed by non-stoichiometric oxides of Ti [24], Hf [24, 33], Ta [23, 25, 31], and Mn [34, 35].

Processes in the dielectric during scintillation breakdowns in tantalum capacitors can be explained by formation and destruction of conductive filaments at high electric fields similar to operation of ReRAMs. Fig.VII.8 gives a schematic illustrating the process of the filaments' formation and rupture during breakdown. The filaments are forming along the whole surface of the dielectric in a capacitor but their concentration and size is uneven and in some areas, likely at the defects in tantalum, concentration of the vacancies and filaments might be much greater than in others. When one of the filaments grows large enough, a micro-scintillation event occurs. This event has a short, in the range of dozens of nanoseconds, duration and is terminated by a thermal destruction, and similar to resetting of ReRAMs elements does not damage structure of the anode material (pellet for tantalum capacitors). Due to a short duration and small size, micro-scintillations discharge capacitors only partially and locally, so the process continues until multiple events occur (progressive breakdown [36]) to create a macro-scintillation that is detected experimentally during CCS testing.

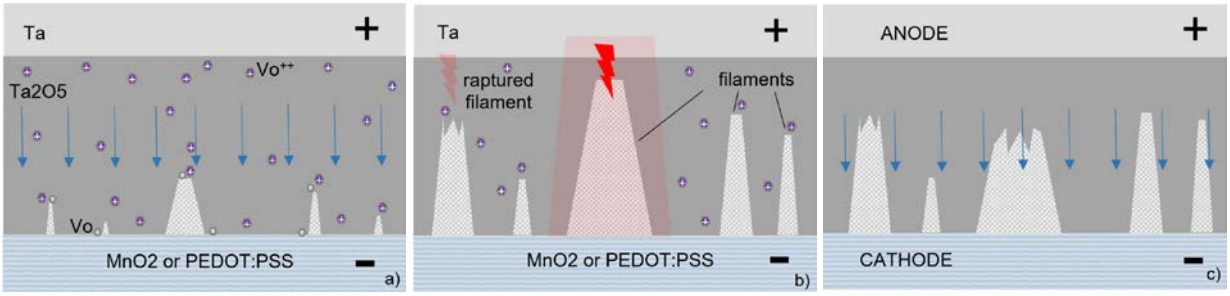

Fig. VII.8. A schematic showing formation and growth of conductive filaments (a), thermal micro-scintillation breakdown resulting in a rupture of the filaments (b) and remnants of the filaments that increase local electric field and thus leakage current after breakdown (c).

The initial micro-scintillation facilitates discharging at the close-by filaments due to increased temperature in the area that decreases breakdown voltages in tantalum capacitors [37]. In addition, micro-scintillations generate electrical oscillations along the surface of the dielectric that might increase voltage and facilitate additional micro-breakdowns. These oscillations occur because at sub-microsecond times of the pulses, the dielectric can be presented as a distributed capacitance and inductance ladder. As a result of progressive micro-scintillations, a relatively soft breakdown with duration from 0.1 to 1 msec occurs, but the structure of the pellet remains intact.

After such a breakdown, capacitors have normal characteristics and can be considered self-healed. However, the destruction of the filaments occurs only partially, so the remnants of filaments increase local electric fields in capacitors under bias as shown in Fig. VII.9.c. This rises injection of electrons from the cathode and increases post-CCS leakage currents in the parts.

At rated voltages, the filaments continue growing, although at a much lower rate than at pre-breakdown voltages. This growth increases further the electric field and conduction through the dielectric with time under bias, which is consistent with the results of section V. Another factor increasing the rate of degradation is generation/activation of oxygen vacancies during scintillation events that enhance redistribution of the charged vacancies, Vo^{++}, and reduce the barrier at the cathode/Ta2O5 interface [38]. The increased rate of degradation of leakage currents indicates that reliability of the self-healed capacitors can be compromised; however, capacitors with relatively low concentration of oxygen vacancies might have stable, although increased leakage currents and endure long-term operation.

VII.6. Mechanisms of self-healing.

Destruction of the filaments in tantalum capacitors occurs ether thermally by the joule heating, or by recombination with oxygen generated at the cathode. The first process occurs in both types, polymer and MnO2 capacitors, whereas the second one can occur in MnO2 capacitors only. The latter is due to the capability of MnO2 to generate oxygen under heating and also to provide oxygen for solid state anodic oxidation in MnO2/metal structures under bias [39]. For this reason, a better self-healing in MnO2 capacitors is due not only to the transformation of MnO2 into a less conductive Mn2O3 or Mn3O4 compositions, but also to a more efficient and faster destruction of the filaments.

Due to a smaller constriction resistance for damage sites on the surface of the pellet compared to the bulk areas, damaging scintillations were associated with defects at the surface of the slug. For this reason, the uniformity and thickness of the cathode shell layers plays an important role in the self-healing process. Sufficiently thick and dense MnO2 layers on the surface of the Ta2O5 dielectric improve the self-healing capability of tantalum capacitors [11]. A relatively poor reproducibility of cathode shell layers that is intrinsic to the MnO2 technology might be one of the reasons of significant lot-to-lot variations of the proportion of damaging scintillations. In general, the uniformity of the polymer cathode shell layers is substantially better than of MnO2 cathodes.

In many cases, discharging during scintillation events that typically last for 0.2 to a few milliseconds occur not smoothly, but exhibit one or several short, a few microseconds, high-power spikes. This behavior can be explained assuming that the concentration of filaments in different areas of the dielectric varies substantially and the process of their growth continues after breakdown process at other micro-scintillation sites has started. At a certain moment, simultaneous, within a few microseconds, micro-scintillations at several adjacent filaments occur as shown in see Fig. VII.9. As a result, the scintillation breakdown is powerful enough to cause damage to the structure of the pellet including fusion of the oxidized tantalum particles, and changing the composition of oxides and creating voids in cathode layers.

Contrary to MnO2, leakage currents in polymer capacitors after scintillation events decrease with time under bias. Also, some CPTCs can recover after repeat exposure to high voltages during CCS testing. Apparently, self-healing in polymer capacitors is not only less effective than in MnO2 capacitors but occurs differently.

Large leakage currents in CPTCs after scintillation events can be explained assuming that these events are associated with overheating and moisture release from polymer cathode layers. Assessments of the Joule heating and temperature of conductive filaments during reset switching of NiO elements [40] showed that the critical temperature for destruction of the filament is ~350 ºC and the effective size of the heated area is ~ 80 nm. Obviously, thermal destruction of multiple filaments might result in formation of a relatively large area with substantially increased conductivity of the Ta2O5 dielectric.

The effect of increasing leakage currents in dry polymer capacitors by orders of magnitude is known and is the major reason of the anomalous transients phenomena observed in these parts [16]. Conduction in discharged dry polymer capacitors rises exponentially with voltage [19], so leakage currents after the first scintillation might be comparable or even greater than the charging currents during CCS testing. With time under bias, these currents decrease gradually (hours to dozens of hours) and the parts can recover (self-heal). Conduction of Ta2O5 dielectrics in these capacitors reduces with time by orders of magnitude due to electron trapping at the states in the PEDOT:PSS polymers that increases the work function of the cathode and reduces electron injection. The process of trapping occurs faster at high electric fields/high currents thus explaining recovery of the parts after repeat scintillation tests.

A significant increase of leakage currents in dry polymer capacitors explains also the effect of moisture on breakdown voltages that has been shown in section III of this report. Contrary to MnO2 capacitors, the presence of moisture in CPTCs reduces leakage currents by several orders of magnitude [19] and thus reduces the probability of breakdown.

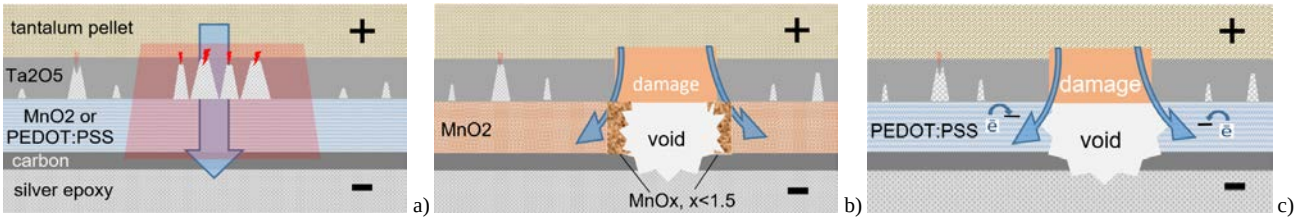

Fig. VII.9. Illustrations of a multiple micro-scintillation event resulting in damage to the surface of the pellet (a), self-healing in MnO2 (b) and polymer (c) tantalum capacitors.

Self-healing in MnO2 and polymer capacitors is due to combination of different mechanisms. These mechanisms involve (i) thermo-oxidative destruction of the conductive filaments, (ii) conversion of MnO2 areas at the damaged site into high-resistive oxides, and (iii) formation of voids in the cathode layers as illustrated in Fig. VII.9.b. Self-healing in polymer capacitors is due to (i) thermal destruction of the filaments, (ii) formation of voids in the cathode layers, and (iii) trapping of electrons into states in conductive polymers (see Fig. VII.9.c).

Different processes have different efficiency and require different times to recover capacitors from a short circuit to a condition with an acceptable level of leakage currents. Destruction of the filaments occurs fast, within dozens of nanoseconds, and due to recombination with oxygen generated in MnO2 is more effective for MnO2 than for polymer capacitors. Oxygen reduction of MnO2 that forms high-resistive oxides and isolates the damage requires from 0.1 to 1 msec. The time necessary for formation of the voids is difficult to assess, but based on results of monitoring of PS current spikes, it is likely within a few milliseconds. It is possible that similar to self-healing in polymer film capacitors [41], the probability of void formation in tantalum capacitors depends on the mechanical stresses in the part that are created during high-temperature curing (typically at 175 ºC) and cooling of the molding compound. The level of compression at the cathode layers surrounding the pellet affects the size of the voids and time of their formation.

Thermal destruction of the filaments in polymer tantalum capacitors happens also rather fast, within dozens of nanoseconds, and similar to MnO2 capacitors, void's formation happens within a few milliseconds. Reduction of the anomalous conduction of the Ta2O5 dielectric requires much longer time, and depending on the voltage and temperature, this process might take from seconds to hours.

VIII. Summary

Technique.

The constant current stress (CCS) technique has been modified to detect variations of voltage across capacitors (*V-t* curves) and power supply current spikes during breakdown events. Discharge currents and power during scintillations were calculated based on *V-t* data. This technique has been used to study specifics of scintillation processes in variety of MnO2 and polymer tantalum capacitors. Simulations of breakdown by external shorting and experiments with different power sources showed that PS current spikes depend on the dynamic characteristics of the power supply and do not reflect directly processes during scintillations.

Breakdown voltages and scintillation times.

Testing of 34 lots of MnO2 and 45 lots of polymer capacitors rated to voltages from 6.3 to 35 V showed that on average, breakdown voltages in polymer and MnO2 capacitors with the same ratings are close. However, polymer capacitors have tighter distributions and average values of the slope of Weibull distribution, β, are in the range from 13 to 20 for polymer and from 6 to 10 for MnO2 capacitors. This indicates a lesser concentration of defects in the dielectric in polymer capacitors, which is likely due to a lesser temperatures and mechanical stresses associated with formation of cathodes.

On average, breakdown voltages increase linearly with the rating: VBR ≈ 2.7×VR. However, the breakdown margin is much greater for low-voltage than for high-voltage capacitors. VBR ≈ 3.5×VR for 6.3 V capacitors and VBR ≈ 2.5×VR for 35 V capacitors.

The moisture content in MnO2 capacitors does not affect breakdown voltages significantly. However, in CPTCs VBR increased by ~ 21±14 % after 1 week in humidity chamber at 85%RH and 85 ºC compared to capacitors that had been dried-out at 125 ºC for 120 hours. This effect is yet another manifestation of anomalous transients in polymer capacitors.

Scintillation times are typically smaller for MnO2 (*Wid* ≈ 400 μsec) than for polymer (*Wid* ≈ 1 msec) capacitors and there is a trend of decreasing *Wid* with voltage rating for both types of capacitors. Although average discharge currents in polymer capacitors are several times lower than in MnO2 capacitors, several short current spikes with amplitudes up to dozens and hundreds of amperes and duration of a few microseconds might happen during a scintillation event. Similar spikes are causing damage and low-resistive shorts in capacitors.

Efficiency of self-healing.

In this study, a capacitor considered damaged by scintillations if it fails the first CCS test with a short circuit or has leakage currents close to the charging current. The proportion of damaged capacitors, *d*, was used to assess the effectiveness of the self-healing of a lot. Values of *d* for MnO2 capacitors varied from lot to lot substantially indicating that the self-healing capability is lot-related. The presence of pores in the cathode layers allowing silver penetration to the pellet and a relatively poor reproducibility of the shell layers in MnO2 capacitors might be one of the reasons of these variations.

Contrary, to MnO2, most polymer capacitors rated to 16 V and more, appear damaged after the first scintillation test. The average value of *d* for 5 lots of 35 V MnO2 capacitors was 11.5%, but it was substantially greater, 88.3%, for 11 lots of 35 V polymer capacitors thus indicating a less effective self-healing.

Some MnO2 capacitors were functional even after being physically damaged by breakdown that resulted in chip-outs in the case, destruction of a portion of the cathode layers, and exposing tantalum pellets. These parts did not fail short circuit and were able to sustain consecutive scintillation tests indicating high self-healing efficiency that can be provided by the MnO2 technology.

Repeat scintillation tests of MnO2 capacitors resulted in increasing breakdown voltages for approximately 50% of cases. Capacitors in these lots can sustain multiple breakdown events before failing short circuit. However, in some lots VBR changed erratically during consecutive tests. The first case is more likely for lots with low proportion of damaging scintillations, whereas lots with large values of *d* are more likely to have decreasing breakdown voltages. Apparently, in the first case, self-healing isolates damage reliably, and the next breakdown happens at a new site and requires higher voltage, whereas in the latter case, repeat scintillations are likely happening near the same damaged site.

Several MnO2 330 μF and 470 μF capacitors ignited during CCS testing and their burning lasted for several seconds, much longer after the test was terminated. This indicates that the energy stored in large value capacitors might be sufficient for a scintillation event to trig ignition even when parts are used in high impedance circuits with a limited current from the power supply. In this regard, large CV value CPTCs are more reliable compared to MnO2 cathode capacitors.

Distributions of post-scintillation resistances in most types of polymer capacitors stretched widely, from ohms to hundreds of kiloohms. However, behavior of these parts is often unstable for both, MnO2 and polymer capacitors and their resistances can change after repeat testing. In some cases, shorted MnO2 capacitors could be healed at relatively low voltages after a powerful enough current surge. However, these parts have a greater chance to turn into shorts with even lower resistance.

Effect of scintillations on characteristics of capacitors.

Capacitance and ESR for both, polymer and MnO2 tantalum capacitors did not change significantly after CCS testing, which can be explained considering that the damaged area after scintillation breakdown is relatively small. However, depending on the severity of damage, dissipation factors might increase several times or up to several orders of magnitude. Due to a large margin, capacitors after scintillations might have DF values within the specified limits. Considering that reliability of these parts can be compromised, to select the best quality capacitors for space applications, the out-of-family samples should be screened out, for example, using the 3-sigma criterion.

Both types, polymer and MnO2 capacitors that appeared self-healed during CCS testing have leakage currents significantly increased compared to the initial level and in this regard all scintillation events degrade tantalum capacitors. Overall, the increase of currents is greater for polymer than for MnO2 capacitors. However, contrary to

MnO2 capacitors, where leakage currents increase with time under bias, polymer capacitors after CCS testing have a tendency of decreasing currents and recovery even after a significant degradation initially.

In some cases, leakage currents at rated voltages in capacitors that passed CCS testing have erratic behavior indicating occurrence of additional scintillations after hours of operation at relatively low voltages. This behavior is consistent with the TDDB model of failures in capacitors that have breakdown voltages reduced by previous scintillation events.

Appearance of damaged sites.

Results of failure analysis show that damaged sites in capacitors that failed after scintillation breakdowns are located on the surface of the pellet. In MnO2 capacitors, reduction of oxygen in manganese layers was revealed by EDS analysis of damaged areas. This confirms the known self-healing mechanism in these parts. In both types, polymer and MnO2 capacitors, scintillations resulted in fusing of oxidized particles in the pellet, formation of large areas of non-stoichiometric tantalum (or Ta/Mn) oxide, and voids in the cathode layers.

Analysis of energy transformations in the parts during breakdown shows that the energy stored in capacitors is sufficient to create damaged area in the range from 100 to 200 μm, which is in agreement with results of failure analysis. The surface location of damaged sites is due to much lower constriction resistances for discharge currents at the surface than in the bulk of the pellet.

The power during scintillation events vary from hundreds of watts to dozens of kilowatts, and the duration of high-power spikes is in the range from 2 to 5 μsec. Calculations based on the amplitude and width of the power spikes show that short high-power spikes can increase temperature of a 100-200 μm size surface area of the pellet to above 2000 ºC, which is sufficient to fuse oxidized particles of the pellet and change composition of the oxides. Less powerful spikes with amplitudes of dozens of watts and durations from 10 to 100 μsec can increase temperature by several hundreds of degree Celsius, which is sufficient to damage or transform cathode layers without causing catastrophic failures. In some cases, several high-power short spikes occur during breakdown resulting in multiple locations of damaged sites on the surface of the pellet.

Mechanisms of breakdown and self-healing.

Breakdown in tantalum capacitors is due to the growth of conductive filaments in the Ta2O5 dielectric and occurs when the filaments are large enough. The process of filaments formation and growth is similar to the one responsible for switching and operation of resistive elements in redox-based random access memory (ReRAM) microcircuits. The filaments have submicrometer sizes and are formed as a result of migration of oxygen vacancies. Destruction of the filaments occurs during micro-scintillation events that have duration of dozens of nanoseconds and is due to the Joule heating and/or generation of oxygen that compensates vacancies in case of MnO2 cathodes.

Consecutive micro-scintillations result in a relatively large discharge times in capacitors that typically last hundreds of microseconds for MnO2 and up to a few milliseconds for polymer capacitors. One of the reasons for a shorter duration of scintillations in MnO2 capacitors is a more efficient destruction of the filaments that occurs mostly due to compensation of vacancies with oxygen generated by MnO2.

When the process of progressive micro-scintillations reaches a defect site on the surface of the pellet, their intensity increases resulting in a powerful, up to dozens of kilowatt, breakdown that lasts for a few microseconds and causes damage to the part. The damage includes structural changes in the pellet, oxygen reduction in MnO2 or thermal/thermal-oxidative destruction of conductive polymers, and formation of voids in cathode layers.

Several mechanisms with different efficiency and time frame occur to recover capacitors from a short circuit to a condition with an acceptable level of leakage currents. For MnO2 capacitors, these mechanisms include (i) thermo-oxidative destruction of the conductive filaments, (ii) conversion of MnO2 at the damaged site into high-resistive oxides, and (iii) formation of voids in the cathode layers. Self-healing in polymer capacitors involves (i) thermal rupture of the filaments, (ii) formation of voids in the cathode layers, and (iii) charge trapping in the polymer cathode that decreases anomalous currents caused by drying and discharging associated with the initial scintillation.

Destruction of the filaments occurs fast, within a few microseconds, transformation of MnO2 into high-resistive forms of oxides that isolates the damaged area requires from 0.1 to 1 msec, and the time necessary to create a void is likely a few milliseconds. The longest process that depending on voltage and temperature might take from seconds to hours is reduction of the anomalous conduction of the dielectric in polymer capacitors.

IX. Acknowledgment

This work was sponsored by the NASA Electronic Parts and Packaging (NEPP) program. The author is thankful to Peter Majewicz, NEPP Program manager and Jonathan Pellish, NEPP program deputy manager for support of this task, and Bruce Meinhold, SSAI, chief staff engineer, for a review and discussions. My sincere appreciation to manufacturers of tantalum capacitors for providing samples for this study.

X. References

[1] L. W. McPherson, J. Kim, A. Shanware, H. Mogul, and J. Rodriguez, "Proposed universal relationship between dielectric breakdown and dielectric constant," in *Digest. International Electron Devices Meeting, IEDM '02*, 2002, 8-11 Dec., pp. 633 - 636.

[2] A. Teverovsky, "Scintillation Breakdowns and Reliability of Solid Tantalum Capacitors," *IEEE Transactions on device and materials reliability*, vol. 9, pp. 318-324, 2009

[3] Y. Freeman and P. Lessner, "High Reliability Principles and Verifications in Solid Tantalum Capacitors. Capacitor Manufacturing Processes," in *CARTS International*, Santa Clara, CA, 2014, March 31- April 3.

[4] A. Teverovsky, "Screening and Qualification Testing of Chip Tantalum Capacitors for Space Applications," in *CARTS USA*, New Orleans, LA, 2010, March 15-18. https://escies.org/download/webDocumentFile?id=62198

[5] A. Teverovsky, "Effect of Preconditioning and Soldering on Failures of Chip Tantalum Capacitors," in *NEPP Report*. Greenbelt, MD NASA/GSFC, 2014, https://ntrs.nasa.gov/archive/nasa/casi.ntrs.nasa.gov/20140017366.pdf.

[6] B. Long, M. Prevallet, and J. D. Prymak, "Reliability Effects with Proofing of Tantalum Capacitors," in *The 25th Symposium for Passive Components, CARTS'05*, Palm Springs, California, 2005, March 21-24, 2005, pp. 167-172.

[7] T. Fritzler, M. H. Azarian, and M. G. Pecht, "Scintillation Conditioning of Tantalum Capacitors With Manganese Dioxide Cathodes," *IEEE Transactions on Device and Materials Reliability*, vol. 14, pp. 630-638, 2014

[8] A. Teverovsky, "Effect of Surge Current Testing on Reliability of Solid Tantalum Capacitors," in *The 28th Symposium for Passive Components, CARTS'08*, Newport Beach, CA, 2008, March 17-20, pp. 293-310.

[9] J. D. Prymak and M. Prevallet, "Scintillation Testing of Solid Electrolytic Capacitors," in *The 26th symposium for passive components, CARTS'06*, Orlando, FL, 2006, April 3-6, 2006, pp. 395-406.

[10] T. Zedníček. New Tantalum Capacitor Technologies Polymer and NbO. *AVX Technical information*. 2007, Available: https://www.avx.com/docs/techinfo/New_Tantalum_Technologies.pdf

[11] Y. Freeman, *Tantalum and Niobium-Based Capacitors: Science, Technology, and Applications*: Springer, 2017.

[12] A. Teverovsky, "Evaluation of Polymer Hermetically Sealed Tantalum Capacitors," NASA/GSFC, Greenbelt, MD 2014, https://nepp.nasa.gov/files/26468/2015-562-Teverovsky-Sealed-Final-Pres-NEPPWeb-TN19013.pdf

[13] A. Teverovsky, "Advanced Wet Tantalum Capacitors: Design, Specifications and Performance," in *20th annual International conference "Commercialization of Military and Space Electronics"*, Los Angeles, CA, 2016, March 6-9. https://nepp.nasa.gov/

[14] H. Domingos, J. Scaturro, and L. J. Hayes, "Breakdown Voltage of Discrete Capacitors Under Single-Pulse Conditions," *IEEE transactions on components, hybrids, and manufacturing technology*, vol. CHMT-4, pp. 545-552, December 1981

[15] A. Teverovsky, "Effect of Moisture on AC Characteristics of Chip Polymer Tantalum Capacitors," *IEEE Transactions on Components, Packaging and Manufacturing Technology*, vol. 9, pp. 2282-2289, 2019

[16] A. Teverovsky, "Anomalous Transients in Chip Polymer Tantalum Capacitors," presented at the ESA 3rd International Symposium - Space Passive Component Days, Noordwijk, The Netherlands, 2018. https://www.spcd.space/

[17] A. Teverovsky, "Degradation and ESR Failures in MnO2 Chip Tantalum Capacitors," in *Components for Military and Space Electronics, CMSE'17*, Los Angeles, CA, 2017, April 11-13. https://ntrs.nasa.gov/archive/nasa/casi.ntrs.nasa.gov/20170003492.pdf

[18] A. Teverovsky, "Effect of Environmental Stresses on Breakdown Voltages in Chip Tantalum Capacitor.," in *The 28th Symposium for Passive Components, CARTS'09*, Jacksonville, FL, 2009, March 30-April 2, pp. 293-310.

[19] A. Teverovsky, "Reliability Issues with Polymer and MnO2 Tantalum Capacitors for Space Applications," presented at the 2020 Annual Electronic Technology Workshop, NEPP ETW, Greenbelt, MD, 2020. https://nepp.nasa.gov/workshops/etw2020/talks/17-JUN-WED/1530-Teverovsky-NEPP-ETW-20205002788-Tantalum-Capacitors.pdf

[20] Y. Jin, Q. Chen, and P. Lessner, "Thermal Stability Investigation of PEDOT Films from Chemical Oxidation and Prepolymerized Dispersion," *Electrochemistry*, vol. 81, pp. 801-803, 2013

[21] A.Salazar, "On thermal diffusivity," *EUROPEAN JOURNAL OF PHYSICS*, vol. 24, pp. 351-358, 2003

[22] J. H. Yu, G. De Temmerman, R. P. Doerner, R. A. Pitts, and M. A. van den Berg, "The effect of transient temporal pulse shape on surface temperature and tungsten damage," *Nuclear fusion*, vol. 55, p. 93027, 2015
[23] C. M. M. Rosário, B. Thöner, A. Schönhals, S. Menzel, A. Meledin, N. P. Barradas, *et al.*, "Metallic filamentary conduction in valence change-based resistive switching devices: the case of TaOx thin film with x ∼ 1," *Nanoscale*, vol. 11, pp. 16978-16990, 2019 http://dx.doi.org/10.1039/C9NR05285B
[24] Y. Wang, Y. Yan, C. Wang, Y. Chen, J. Li, J. Zhao, *et al.*, "Controlling the thin interfacial buffer layer for improving the reliability of the Ta/Ta2O5/Pt resistive switching memory," *Applied Physics Letters*, vol. 113, p. 072902, 2018 https://aip.scitation.org/doi/abs/10.1063/1.5040430
[25] J.-H. Hur and D.-K. Kim, "A study on mechanism of resistance distribution characteristics of oxide-based resistive memory," *Scientific reports*, vol. 9, pp. 302-8, 2019
[26] D. Lelmini and R. Waser, *Resistive Switching: From Fundamentals of Nanoionic Redox Processes to Memristive Device Applications*: Wiley-VCH Verlag GmbH & Co. KGaA 2016.
[27] C.-F. Chang, J.-Y. Chen, C.-W. Huang, C.-H. Chiu, T.-Y. Lin, P.-H. Yeh, *et al.*, "Direct Observation of Dual-Filament Switching Behaviors in Ta2O5-Based Memristors," *Small*, vol. 13, p. 1603116, 2017
[28] C. Lenser, R. Dittmann, and J. P. Strachan, "Valence Change Observed by Nanospectroscopy and Spectromicroscopy," in *Resistive Switching: From Fundamentals of Nanoionic Redox Processes to Memristive Device Applications*, D. Lelmini and R. Waser, Eds., ed: Wiley-VCH Verlag GmbH & Co. KGaA 2016, pp. 437-455.
[29] A. Zaffora, D.-Y. Cho, K.-S. Lee, F. Di Quarto, R. Waser, M. Santamaria, *et al.*, "Electrochemical Tantalum Oxide for Resistive Switching Memories," *Advanced Materials*, vol. 29, p. 1703357, 2017
[30] L. Goux and S. Spiga, "Universal Switching Behavior," in *Resistive Switching: From Fundamentals of Nanoionic Redox Processes to Memristive Device Applications*, D. Lelmini and S. Menzel, Eds., ed: Wiley-VCH Verlag GmbH & Co. KGaA 2016, pp. 317-340.
[31] H.Chee, T.Kumar, and H.Almurib, "Electrical model of multi-level bipolar Ta2O5/TaOx Bi-layered ReRAM," *Microelectronics Journal*, vol. 93, p. 104616, 2019
[32] X. X. Zhang, Ling; Zhang, Hui; Liu, Jian; Tan Dingwen, "Effect of Joule Heating on Resistive Switching Characteristic in AlOx Cells Made by Thermal Oxidation Formation," *Nanoscale Research Letters*, vol. 15, 2020
[33] W. Sun, B. Gao, M. Chi, Q. Xia, J. J. Yang, H. Qian, *et al.*, "Understanding memristive switching via in situ characterization and device modeling," *Nature communications*, vol. 10, pp. 3453-13, 2019
[34] N. J. Lee, "Tri-state resistive switching characteristics of MnO/Ta2O5 resistive random access memory device by a controllable reset process " *Journal of physics. D, Applied physics* vol. 51, p. 225102 (7pp), 2018
[35] Q. Hu, Y. Abbas, H. Abbas, M. R. Park, T.-S. Yoon, and C. J. Kang, "Resistive switching characteristics in manganese oxide and tantalum oxide devices," *Microelectronic Engineering*, vol. 160, pp. 49-53, 2016/07/01/ 2016
[36] J. Suñé, N. Raghavan, and K. L. Pey, "Dielectric Breakdown Processes," in *Resistive Switching: From Fundamentals of Nanoionic Redox Processes to Memristive Device Applications*, D. Lelmini and R. Waser, Eds., ed: Wiley-VCH Verlag GmbH & Co. KGaA 2016, pp. 225-251.
[37] A. Teverovsky, "Scintillation and Surge Current Breakdown Voltages in Solid Tantalum Capacitors," *IEEE Transactions on Dielectrics and Electrical Insulation*, vol. 16, pp. 1134-1142, 2009
[38] A. Teverovsky, "Degradation of leakage currents in solid tantalum capacitors under steady-state bias conditions," in *Electronic Components and Technology Conference (ECTC), 2010 Proceedings 60th*, 2010, 1-4 June 2010, pp. 752-757.
[39] D.Smith, "Solid-State Anodic Oxidation of Tantalum," *Journal of the Electrochemical Society, 1966, Volume: 113 Issue: 1 Page: 19*, vol. 113, pp. 19-25, 1966
[40] L. Goux and S. Spiga, "Introduction to Unipolar Resistive Switching," in *Resistive Switching: From Fundamentals of Nanoionic Redox Processes to Memristive Device Applications*, D. Lelmini and R. Waser, Eds., ed: Wiley-VCH Verlag GmbH & Co. KGaA 2016, pp. 363-392.
[41] C. W. Reed and S. W. Cichanowskil, "The fundamentals of aging in HV polymer-film capacitors," *IEEE Transactions on Dielectrics and Electrical Insulation*, vol. 1, pp. 904-922, 1994